ADVANCES IN PHYSICS, 2002, VOL. 51, NO. 4, 1189–1257

Intersonic shear cracks and fault ruptures

ARES J. ROSAKIS*
Aeronautics and Mechanical Engineering, California Institute of Technology, Pasadena, CA 91125, USA

[Received 10 October 2001; revision received 19 October 2001; accepted 29 November 2001]

Abstract

Recent experimental observations of intersonic shear rupture events that occur in a variety of material systems have rekindled interest in the intersonic failure phenomenon. Since the early 1990s, engineers and scientists working in all length scales, from the atomistic, the structural, all the way up to the scale of the earth's deformation processes, have undertaken joint efforts to study this unexplored area of fracture mechanics. The analysis in the present article emphasizes the cooperative and complementary manner in which experimental observations and analytical and numerical developments have proceeded. The article first reviews early contributions to the theoretical literature of dynamic subsonic and intersonic fracture and highlights the significant differences between tensile and shear cracks. The article then uses direct laboratory observations as a framework for discussing the physics of intersonic shear rupture occurring in constitutively homogeneous (isotropic and anisotropic) as well as in inhomogeneous systems, all containing preferable crack paths or faults. Experiments, models, and field evidence at a variety of length scales (from the atomistic, the continuum, and up to the scale of geological ruptures) are used to discuss processes such as (1) shock wave formation, (2) large-scale frictional contact and sliding at the rupture faces, and (3) maximum attainable rupture speeds and rupture speed stability. Particular emphasis is given to geophysical field evidence and to the exploration of the possibility of intersonic fault rupture during shallow crustal earthquake events.

Contents

* e-mail: rosakis@atlantis.caltech.edu

Advances in Physics ISSN 0001–8732 print/ISSN 1460–6976 online
http://www.tandf.co.uk/journals
DOI: 10.1080/00018730210122328

1. Introduction

1.1. *Basic terminology*

Supersonic aircraft are part of our everyday experience as perhaps are other objects moving fast in air, such as rockets, shooting stars or common handgun bullets. When a moving object's speed exceeds the speed of sound (the speed of pressure waves) in air, which is approximately $340\,\mathrm{m\,s^{-1}}$, we refer to the object as being 'supersonic'. It is called 'sonic' if its speed equals the speed of sound and is referred to as 'subsonic' if its speed is less than that of sound.

When supersonically moving objects travel in air, or in other gases, they form pairs of pressure shock waves. These jumps are often visualized as sets of V-shaped lines, which are attached to the moving object's leading and trailing edges or tips. The V-shaped structures of the shock waves are called 'Mach cones' and represent envelopes within which wave information caused by the moving object can travel. A particle of air outside the shock wave receives no information indicating that the object is approaching until the Mach cone sweeps across the particle producing a supersonic boom, that is an audible sudden jump in pressure.

Supersonically propagating objects or entities in solids are perhaps much less common to our everyday cognition since such objects are too fast for unaided human observation. Examples of potentially supersonic entities in solids are dynamically propagating cracks. Such displacement discontinuities (opening and/or shear) result in the rapid creation of new surfaces by the breaking of bonds in a previously undamaged material. To see whether a crack tip (leading edge of a spreading displacement discontinuity) is supersonic, intersonic, subsonic or simply subRayleigh, its speed should be compared with the speeds of stress waves in the rupturing solid which are typically an order of magnitude higher than in air. Indeed, for the simple cases of isotropic linear elastic solids, in a manner equivalent to an object moving in a gas, a supersonic crack tip is defined as a crack tip that moves faster than the dilatational (or pressure) wave speed c_ℓ of the solid. Dilatational stress waves are equivalent to pressure waves in a gas and feature material particle vibrations along the direction of travel of the wave. Similarly, an 'intersonic' crack is defined as a crack whose speed lies in the open interval between the dilatational wave speed c_ℓ and the shear wave speed c_S of the solid, while a 'subsonic' crack has a speed of less than c_S. Shear waves feature particle motion perpendicular to their direction of travel and their speed c_S is typically less than twice the pressure wave speed. The exact ratio between c_S and c_ℓ depends on the Poisson ratio of the linear elastic solid [1]. In this article, cracks propagating at exactly the dilatational wave speed will be referred to as 'pressure-sonic' (p-sonic), while cracks that move at exactly c_S will be called 'shear-sonic' (s-sonic).

Since moving cracks result in the creation of new surfaces (free or otherwise) it is perhaps not surprising that Rayleigh waves or other types of surface waves, such as Stonely waves or generalized Rayleigh waves [1], become important in their analysis.

Rayleigh waves are constrained to propagate along free surfaces with a speed c_R, which is typically equal to 87–95% of the shear wave speed of an isotropic linear elastic material. In this article, cracks propagating at speed c_R will be referred to as 'Rayleigh cracks' while cracks propagating at below speed c_R will be referred to as 'subRayleigh'. Finally, the terminology 'superRayleigh/subshear' will be used to describe cracks that propagate in the small speed interval between c_R and c_S.

1.2. *Two perspectives: engineering and geophysics*

Dynamic fracture mechanics is the study of stress wave induced failure phenomena such as sudden crack nucleation initiation and growth in the presence of high local strain rates. A common characteristic of these failure phenomena is the rapid loss of stress carrying capability. This loss may occur either in such time scales that local (near tip) inertial and/or material rate sensitivity effects are important, or in time scales that are comparable with the characteristic wave transit times in a structure. The ultimate physical demonstration of dynamic failure in a solid is the fast nucleation and rapid growth of individual cracks or fractures. These in turn, as it has already been stated, are displacement discontinuities spreading in an otherwise intact material. On the basis of the nature of the displacement discontinuity near an advancing crack edge or tip, three distinct fracture modes can be defined:

- mode-I, the in-plane opening mode resulting from normal separation of the crack faces (opening displacement discontinuities activated by tensile stresses);
- mode-II, the in-plane shearing mode resulting from relative sliding of crack faces perpendicular to the crack edge (sliding displacement discontinuities activated by in-plane shear stresses); and
- mode-III, the antiplane shearing mode resulting from the relative out-of-plane sliding of the crack faces (tearing displacement discontinuities activated by out-of-plane shear stresses).

Stationary or growing cracks may be loaded in a variety of ways and may initiate or grow under a combination of modes. Such cracks are often called 'mixed mode' cracks.

As evident from Freund's exhaustive monograph on the subject [2], the past 50 years of dynamic fracture mechanics theories have provided enormous insight into the understanding of catastrophic failure of homogeneous (monolithic) brittle solids, a class of materials that exhibit a linear elastic constitutive response up to failure. Since its early days, fracture research has been driven mainly by engineering mechanics applications and was intimately linked to the need for the design of reliable structures spanning a variety of length scales. Early research work on dynamic fracture mechanics concentrated on materials and structures that are strictly homogeneous in nature. In other words, it has concentrated on materials that in addition to their homogeneous constitutive response also possess strictly homogeneous fracture toughness properties thus excluding the possibility of weak paths or bonds of varying cohesive characteristics. These are materials that are indeed truly homogeneous or 'monolithic'.

Let us first consider mode-I (opening) cracks propagating in homogeneous, monolithic, linear elastic solids under the action of remotely applied tractions on the boundaries. For simplicity, let us also restrict our discussion to isotropic solids. As the remotely applied loading is increased the crack tip is typically observed to accelerate to higher speeds and it does so rather smoothly up to a speed of about 30–

40% of c_R. The exact percentage will, in general, depend on the details of the material's microstructure. At about these speeds, a microbranching instability sets in whereby the crack tip speed tends to oscillate and the crack follows a wavy path producing, as it attempts to branch, increasingly rough fracture surfaces. The wavy crack path, as well as the microbranching attempts, are intimately linked to a dramatic increase in the size of the process region, the region of microdamage near the moving crack tip. This increase in microcrack population indicates a strong increase in fracture energy which is required to sustain propagation at these speeds [3–9]. Eventually the initial mode-I crack tip branches to two or more crack paths at speeds that in a laboratory setting have never been observed to exceed $0.65c_R$. A high-speed snapshot of two branched crack tips propagating in a bulk metallic glass plate captured just after branching is shown in figure 1. Metallic glasses are brittle amorphous metallic materials that are produced by rapid quenching of melts. These materials offer perhaps the closet approximation to homogeneous isotropic linear elastic behaviour available [10]. The two crack tips are visible by the intense

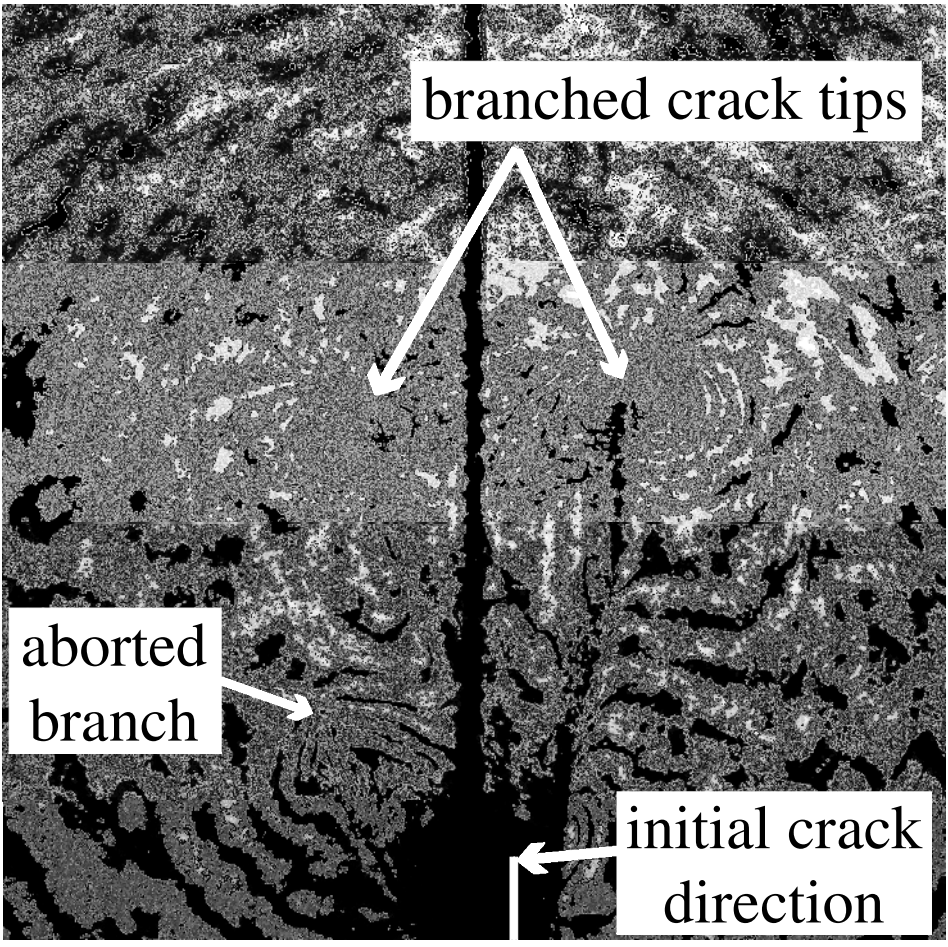

Figure 1. Dynamic crack branches propagating (from bottom to top) in a bulk metallic glass plate. Visualization through CGS interferometry.

concentration of fringes that correspond to surface out-of-plane displacement gradient contours and are obtained through coherent gradient sensing (CGS) interferomentry [11]. The resulting branched crack tips are also purely mode-I (opening) and they propagate at speeds slightly above the speed of the original crack just before branching. A further increase in loading, not shown here, results in further branching of the first two branches, a process that is repeated sequentially and eventually leads to the complete fragmentation of the metallic glass plate [10]. This process resembles the way that a silica glass window pane would fragment if hit by a heavy object. As the experiments clearly show, the speed limit of mode-I crack growth, in purely homogeneous solids, is well below the material's Rayleigh wave speed. The reason for that is the branching instability.

As summarized by Freund [2] and Broberg [12], early theories of mode-I crack growth have also wrestled with questions of limiting crack tip speeds within the context of homogeneous linear elasticity. By assuming that an opening crack will propagate along a perfectly straight crack path, these workers have examined the crack's behaviour as the crack tip increases its speed. As the crack tip speed increases, the energy flux into the crack tip decreases monotonically and eventually it vanishes at c_R. At even higher speeds no analytical solution can be found with finite and positive energy flux into the tip, making superRayleigh crack growth unattainable within the confines of linear elastodynamics and singular dynamic crack growth models [2, 12–14]†. Indeed, positive energy flux into the crack tip is required to sustain cracking since crack growth involves material separation, which is inherently an energy consuming process. Hence, a necessary condition for crack growth is that energy should be supplied from the outer stress field to the crack tip region. These theoretical studies therefore conclude that the limiting crack tip speed for remotely loaded mode-I cracks in brittle solids is c_R. Such a prediction is substantially higher than the practical speed limit set by the onset of the branching instability.

The discrepancy is perhaps not so surprising if one takes a closer look at a particularly restrictive assumption that is inherent in all theoretical treatments of the subject. As has already been mentioned, all the theoretical models so far have restricted the path of the crack tip. They prescribe a predetermined straight-line path and in so doing they disregard the physical crack's natural tendency to oscillate and eventually to branch at a specific propagation speed. Thus, the analytical models approximate a very interesting, but nevertheless very different physical situation; a situation that mimics the existence of a weak plane of lower fracture toughness within the otherwise homogeneous linear elastic solid. Along this path the crack is trapped and can propagate without the possibility of activating the energy consuming process of microdamage creation, without the freedom to follow a wavy

† When the crack is 'analytically' forced to propagate within the intersonic regime the lowest order singular solution features a speed dependent singularity exponent that varies between 1/2 and 1. This solution still satisfies the physical requirements of bounded displacements at the growing tip. However, the order of singularity implies that an infinite supply of energy (energy flux) is provided into the tip. Furthermore, close examination of the predicted stresses and displacement gradients show that this flux also is negative. The prediction of 'negative infinity' for the energy flux is clearly physically unacceptable. The next, lower, order of singularity features bounded stresses and displacement gradients throughout the intersonic regime. This implies a zero energy flux into the tip which is also bothersome from a physical point of view.

path, and without the eventual possibility of branching. The existence of such a plane (or line in a two-dimensional setting) suppresses branching and, in essence, it allows the crack to approach c_R, which is predicted by the theory.

The above interpretation of the discrepancy has clear experimental support. Specifically, Washabaugh and Knauss [15] fabricated weak planes in an otherwise homogeneous material by bonding two identical plates of a brittle polymer and then drove remotely loading mode-I cracks along the weak bond. They reported mode-I crack tip speeds approaching the polymer's Rayleigh wave speed in the limit of vanishing bond strength thus verifying the theoretical prediction.

The existence of weak fracture paths within solids significantly alters the initial theoretical assumption of strict material homogeneity and makes such systems very different from strictly monolithic solids. Although such materials are still homogeneous regarding their constitutive properties, they are not homogeneous regarding their fracture resistance or their fracture toughness response. This is a very important distinction to bear in mind and will become even more important in the discussions throughout this article. In fact, as we have already seen for mode-I crack growth, the limiting crack tip speed for a strictly homogeneous (monolithic) solid is $0.65c_R$ or less, whereas for a solid that contains weak crack growth paths this speed is the theoretically predicted value of c_R. The differences regarding the failure of these two distinct classes of materials become even more enhanced when the possibility of shear dominated mode-II failure is considered.

Let us now consider the situation of a strictly homogeneous elastic body subjected to asymmetric dynamic loading conditions. A pre-existing stationary crack in such a body, generally speaking, would develop mixed-mode characteristics, which evolve up to the time of crack extension. The ratio of mode-I to mode-II up to that time will depend on the time history of loading and on the geometry [2]. At the instant of crack initiation, the time at which the crack tip ensues its movement throughout the body, the newly generated moving crack tip will not grow straight ahead of the initial stationary mixed-mode crack. Instead, the predominant theoretical belief is that it will kink and propagate at an angle to the initial crack plane, an angle that depends on the relative amount of the mode mix (ratio of mode-II or mode-I) of its stationary predecessor. What makes this process relevant to the present discussion is the realization that this angle is also chosen to be such that the growing crack tip always maintains purely tensile (mode-I) conditions at its tip [16–18]. Indeed, the newly created crack tip will curve continuously and, if necessary, it will again kink abruptly to ensure that it remains a locally mode-I crack as it decoheres the homogeneous materials in local tension. Figure 2 illustrates such a situation. A pre-existing fatigue crack in a metallic glass plate crack, shown here as a small vertical line at the bottom of the figure, is initiated dynamically under the combination of symmetric and asymmetric far-field loading. Figure 2(a) shows the early stages of crack growth following the emission of unloading stress waves, which are still visible as a semicircular arch in the centre of the field of view. Following these waves, a kinked crack is clearly visible. 5 μm later the same crack has propagated following a curving crack path chosen in such a way as to ensure locally mode-I conditions at the growing tip. Experimental analysis of the near tip fringe patterns indeed confirms the absence of a mode-II deformation component during continuous crack growth.

The natural tendency of growing cracks to propagate under strictly mode-I conditions in homogeneous monolithic solids explains the lack of interest of early

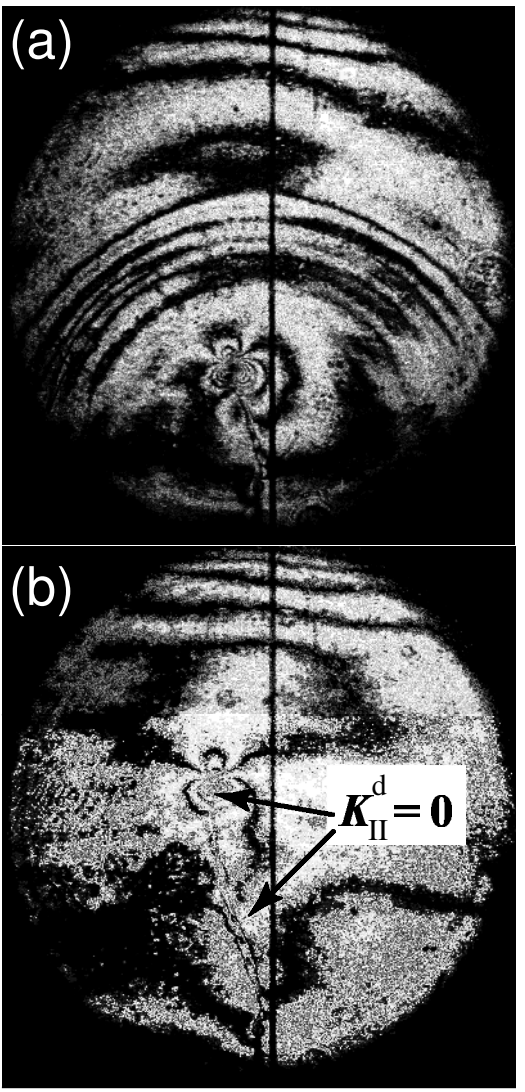

Figure 2. Dynamic crack growth under asymmetric loading conditions. The crack chooses the path that would ensure locally tensile conditions at its tip ($K_{II}^{d} = 0$).

engineering researchers in mixed mode, or mode-II, dynamic crack growth. In recent years this situation has changed drastically since there is an increasing demand for specialized lightweight, high-strength structures made from inhomogeneous (heterogeneous) solids. Such solids include structural composite sandwich structures, bonded layered materials, as well as continuously graded solids. Many of these materials are composed of brittle constituents possessing substantial mismatch in wave speeds and are bonded together with weak interfaces, which frequently serve as sites for catastrophic failure. Indeed, many of these solids are designed for applications involving either anticipated or accidental impact loading. The existence of interfaces in this new generation of structural materials has refocused the attention of engineers on the problem of dynamic crack growth along predetermined

crack paths that are often identified as the boundaries between the phases of heterogeneous solids. Forcing a crack to propagate dynamically along a specific path and thus removing its freedom to choose a path that will allow it to remain locally mode-I, results in a number of very interesting phenomena, some of which will be discussed in this article. In fact, mixed mode or mode-II growing cracks in inhomogeneous solids exhibit behaviours that are very different from their mode-I counterparts. As we shall see in the following sections, such behaviours include the possibility of intersonic and even supersonic crack tip speeds, as well as the likelihood of large-scale dynamic frictional contact and dissipation of the crack faces. Finally, these behaviours often feature the radiation of shock-wave-like discontinuities from the crack tips and from the ends of the contact zones.

On a scale that is entirely different from that of engineering structures (length scale difference of over seven orders of magnitude), geophysicists have studied dynamic fault ruptures for at least as many years as engineers have studied dynamic fracture in structural materials. The earth's crust contains weak interfaces in the form of earthquake faults and as such can be viewed as an inhomogeneous solid. Depending on the local topography and the geological age of a fault, the material's properties and, therefore, the wave speeds across a fault may vary. For example, some geologically young crustal faults may feature very small differences in wave speeds across the fault line. Consequently, the earth's crust in such locations may be approximated as a constitutively homogeneous solid containing an inhomogeneity in shear fracture toughness or rupture resistance. Such inhomogeneity in shear strength models the fault as a mathematical line along which shear displacement jumps, mode-II cracks or ruptures may dynamically propagate. In most cases of mature faults the elastic material properties do vary substantially across the fault and the shear wave speeds may differ by as much as 30% [19, 20]. This is due to the active faulting, which in turn brings into contact rock bodies of different properties that were originally widely separated. In such cases, the solid containing the fault may be viewed as a bimaterial system and the fault as a plane of lower rupture resistance at the interface between the two dissimilar, individually homogeneous, constituents. The entire system is now conceived as being inhomogeneous both in the constitutive and in the fracture toughness sense of the word. In both cases, fault ruptures occurring along the bimaterial interface may be approximated as dynamically growing (mode-II and mode-III) cracks propagating in the presence of high ambient compressive and shear pre-stresses.

In the present article, the reader's attention is focused on shear dominated cracks or fault ruptures forced to propagate along weak planes at the interface between linear elastic solids. For simplicity, the article's point of view, theoretical or experimental, will remain a two-dimensional one. A brief review of the theoretical literature on the subject will first be presented. Then, the article will concentrate on the question of the attainability of intersonic rupture speeds. The discussion will revolve around the presentation and analysis of laboratory evidence of intersonic crack growth in different material systems involving similar isotropic or anisotropic constituents that are separated by weak interfaces. In addition, recent field evidence of intersonic rupture that occurred during the 1999 Izmit and Düzce earthquakes in Turkey will be presented. Such evidence will then be discussed within the context of the laboratory observations and the available theoretical modes. The discussion will not follow the proper chronological order of research discoveries. Rather, it will centre around two distinct classes of bonded material systems: one involving

identical isotropic constituent solids and the other involving simple anisotropic solids. A brief discussion of bimaterial systems involving highly dissimilar constituents will also be presented.

2. Rupture of constitutively homogeneous systems containing weak planes: isotropic materials

Much of the work on dynamic mode-II crack growth in linear elastic systems can be found in the geophysics literature. This is perhaps not very surprising since a majority of shallow earthquakes are caused by sudden rupturing of the earth's crust along pre-existing fault planes under the action of high ambient compressive and shear pre-stresses. Rice [19], Das [20], Dmowska and Rice [21], and Scholz [22] summarized the literature on dynamic shear crack propagation and its application to the modelling of earthquake source processes. As these point out, such processes involve a sudden slip or rupture in some local region along a crustal fault, mostly occurring at depths down to 50 km from the surface [23]. On the one hand, these local events are accompanied by a sudden stress drop over the slipping region and, on the other hand, by the associated emission of elastic waves that travel through the earth and are recorded at seismic stations on the surface. The elastic waves carry information regarding the initial location, nature, and subsequent movement of the earthquake source. Such information has allowed researchers to build realistic mechanics models and through them to reproduce and analyse the rupture history of seismic events.

Seismologists have never been able to directly observe the rupturing of the earth's interior. As a result, they have relied heavily on analytical and numerical models whose fidelity is ultimately judged on their capability of predicting the observed wave information collected at seismic stations. As eloquently described by Rice [19] there are two widely accepted classes of model that provide adequate approximations to source mechanics and have been widely used, through seismic inversion studies, to recover information about the speed of propagating ruptures [23, 24]. The oldest and most classical approach describes rupture through the use of elastodynamic shear crack models (enlarging shear cracks) [20, 21]. More recently, models that describe ruptures as 'self-healing' slip pulses have been introduced [25–32]. The question of whether ruptures assume a 'crack-like' or a 'pulse-like' mode and under what circumstances they do so is currently at the centre of fervent research activity [33–37] and will not be reviewed extensively here. However, some of the experimental observations described in later sections are clearly related to such an issue since they show evidence of laboratory rupture processes that have, under certain conditions, similarities to either description.

Let us now concentrate on the 'crack-like' view of rupture and focus on the question of favourable and maximum shear crack tip speeds. As mentioned before, dynamic mode-II crack models have been used extensively in conjunction with radiated elastic wave information, recorded by seismograms, to infer rupture front speeds. The average rupture speeds so inferred for most shallow crustal earthquakes range from 0.75–$0.95c_R$ where c_R is the average Rayleigh wave speed in the surrounding crustal rock body [23, 24]. As is evident from two-dimensional slip and slip velocity maps in crustal faults, fault ruptures are rather irregular processes. This reflects the heterogeneity of local fault strength and the local variations in elastic properties of the rock body along and across (bimaterial mismatch) a fault. As

a result of these heterogeneities, rupture propagation speed is often irregular and is expected to be very sensitive to such elastic property and fault strength variations. Indeed, in cases where the inferred average rupture speed was reported to be close to c_R it is plausible that for short durations rupture speed could be locally intersonic (on the portion of the rupture front where the slip is predominately in-plane shear). In fact, evidence supporting such a scenario in relation to a variety of earthquake events, at least over a portion of the fault, have recently been reported in the literature by Archuleta [38], Olsen *et al.* [39], Hernandez *et al.* [40], Ellsworth and Celebi [41], and Bouchon *et al.* [42, 43].

Until recently, these reports have been received by the wider geophysics community with great caution. Consequently, the concept of intersonic shear rupture was not universally accepted in the geophysics community. The hesitation of geophysicists to accept the existence of intersonically propagating fault ruptures is probably related to the complete lack of experimental observations of intersonic shear crack growth under controlled laboratory conditions. It is also related to the failure of early theoretical studies to provide conclusive statements regarding a mode-II crack's ability to enter the intersonic speed regime. The work to be discussed in this review article attempts to provide such unequivocal evidence.

2.1. *Early models of intersonic shear rupture*

Let us now turn our attention to the few early theoretical studies of intersonic shear rupture. In particular, let us first consider a semi-infinite mode-II crack propagating at a constant speed v along a predetermined straight-line crack path which models either a weak bond between two identical isotropic linear elastic solids or possibly a fault plane. This is a purely steady-state elastodynamic problem whose mode-I counterpart has already been discussed in the introduction. This problem was first analysed by Freund [44, 2] who concentrated on intersonic crack growth in linear elastic solids and commented on the remarkable changes that the asymptotic stress and particle velocity fields experience as the crack tip speed crosses different possible speed regimes. When the crack tip speed v is subRayleigh ($0 < v < c_R$) the asymptotic stress field is square root singular (as it is in the equivalent mode-I problem). The near tip stress components σ_{ij}, viewed from a local coordinate system which is propagating with the crack tip at speed v, have the following form†:

$$\sigma_{ij}(\eta_1, \eta_2) = K_{II}^{d} \frac{f_{ij}(\theta_\ell, \alpha_\ell, \alpha_S)}{r_\ell^{1/2}}, \tag{2.1}$$

where (η_1, η_2) are the coordinates of a point with respect to this moving Cartesian coordinate system (the η_1-axis lies along the direction of crack growth and the η_2-axis is perpendicular to the crack plane), $f_{ij}(.,.)$ are known functions of crack tip speed

† It should be noted here that linear elastic fracture mechanics involves assumptions that limit its applicability to the analysis of failure in a restricted class of solid usually referred to as 'brittle'. It is assumed that displacement gradients remain much smaller than unity and that the relation between stress and strain is reversible and linear. Both of these assumptions are clearly violated as the distance from the crack tip becomes small. Moreover, when crack problems are solved, only singular solutions that result in finite and positive energy flux into the crack tip are retained. Other mathematical solutions of the relevant boundary value problem that result in higher order singularities (singularity exponents higher than 1/2) are discarded on the basis of physical arguments.

and angular position, the indices ij have the range of 1,2,3, while the variables $r_\ell, \theta_\ell, \alpha_\ell$, and α_S are defined [2] as follows:

$$r_\ell(\eta_1^2 + \alpha_\ell^2\eta_2^2)^{1/2}, \quad \theta_\ell = \tan^{-1}\frac{\alpha_\ell\eta_2}{\eta_1}, \tag{2.2}$$

and

$$\alpha_\ell = \left(1 - \frac{v^2}{c_\ell^2}\right)^{1/2}, \quad \alpha_S = \left(1 - \frac{v^2}{c_S^2}\right)^{1/2}. \tag{2.3}$$

As it is evident from the general form of this solution, the six independent components of the stress tensor all feature a square root singularity with respect to r_ℓ and they all share a common amplitude factor K_{II}^d, which in turn is called the mode-II dynamic stress intensity factor and is itself expressible in the form:

$$K_{II}^d = k(v)K_{II}^S. \tag{2.4}$$

The factor $k(v)$ above is a universal function of crack tip speed and K_{II}^S is the stress intensity factor of an equivalent stationary crack at the same instantaneous location as the growing crack [2, 12]. K_{II}^S is independent of crack tip speed and it is an unknown function of external loading and geometry. The function $k(v)$, on the other hand, is known. When $v = 0$ the value of $k(v)$, is equal to 1, while it monotonically decreases to zero as $v = c_R$. The above asymptotic solution allows the evaluation of the dynamic energy release rate G, which represents the energy flux into the crack tip singularity per unit of new crack area (per unit of new area of sliding for mode-II cracks). This is given by:

$$G = A(v)\frac{(K_{II}^d)^2}{E'}, \tag{2.5}$$

where E' is an equivalent Young's modulus of the solid ($E' = E$ for plane stress, $E' = E/(1-\nu^2)$ for plane strain, where ν is Poisson's ratio) and $A(v)$ is an increasing function of speed such that $A(0) = 1$ and $A(v)\rightleftarrows\infty$ as $v\rightleftarrows c_R$ [2]. By substituting equation (2.4) into equation (2.5) the dynamic energy release rate G (energy supplied into the tip) can now be expressed in the following separable form:

$$G = g(v)\frac{(K_{II}^S)^2}{E'}, \tag{2.6}$$

where $g(v) = A(v)k^2(v)$ and is a function that exclusively depends on the crack tip speed and the elastic material properties. At this point it is very important to note that although $A(v)$ and $k(v)$ are monotonic functions that have opposite behaviour as $v\rightleftarrows c_R$ ($A(v)$ becomes unbounded while $k(v)$ vanishes) the combination $g(v) = A(v)k^2(v)$ nevertheless vanishes at this limit. In fact, $g(v)$ decreases almost linearly from 1 to 0 as the crack speed increases from 0 to c_R. The form of equation (2.6) and the properties of $g(v)$ have strong physical consequences. They imply that the energy supplied to the crack tip remains finite and positive throughout the subRayleigh regime and it vanishes only as the crack speed reaches c_R. The above provides a strong indication that subRayleigh cracks will have difficulty in propaging smoothly past c_R, unless some other mechanism is identified that allows for such a transition. Indeed, according to the steady-state model, if one now looks for crack growth solutions at the small speed interval between c_R and c_S, the energy supplied to the tip becomes negative thus excluding, in that interval, steady-state crack growth

[2, 14]. Obviously, transient crack growth past that interval is not excluded by the above discussion since so far the arguments are made on the basis of a strictly steady-state model. In fact, the cracks may conceivably jump discontinuously from one speed regime to the other without smoothly accelerating through the forbidden region. Cracks may also nucleate spontaneously and grow as intersonic cracks without ever being subsonic. Considering the above, the quest for intersonic possibilities is still justifiable.

Looking for solutions in the intersonic crack tip speed interval ($c_S < v < c_\ell$), Freund [44] was able to reveal the existence of a singular stress field that was drastically different from its subsonic counterpart. The mathematical reason for the difference is the change in the nature of the governing differential equations of two-dimensional plane elastodynamics, a change that occurs as the crack speed moves from the subsonic to the intersonic regime. Indeed, whereas in the subsonic case the steady-state problem involves two elliptic partial differential equations governing the two scalar elastic potential functions, in the intersonic regime it involves one elliptic equation and one hyperbolic equation. The elliptic equation governs the dilatational potential while the hyperbolic equation governs the shear potential. This allows for the possibility of 'characteristic' lines, somehow related to shear deformations. The physical meaning of such lines will become apparent in the following discussion.

If one follows the above conventions and notation in relation to the subsonic crack tip stress field, and if one employs a Cartesian coordinate system (η_1, η_2) translating with the crack tip and oriented as shown in figure 3, the intersonic asymptotic field for $c_S < v < c_\ell$ takes the form

$$\sigma_{ij}(\eta_1, \eta_2) = K_{II}^{*}\left\{\frac{l_{ij}(\theta_\ell, \alpha_\ell, \hat{\alpha}_S)}{r_\ell^q} - \frac{m_{ij}(\alpha_\ell, \hat{\alpha}_S)}{(-\eta_1 - \hat{\alpha}_S|\eta_2|)^q}\, H(-\eta_1 - \hat{\alpha}_S|\eta_2|)\right\}, \tag{2.7}$$

where $l_{ij}(.,.)$ is a known function of scaled angular position θ_ℓ and speed through the relativistic functions α_ℓ and $\hat{\alpha}_S$, and $m_{ij}(.,.)$ is a known function of only speed. $H(.)$ is the Heaviside step function and q is the singularity exponent, which is a function of crack tip speed given by

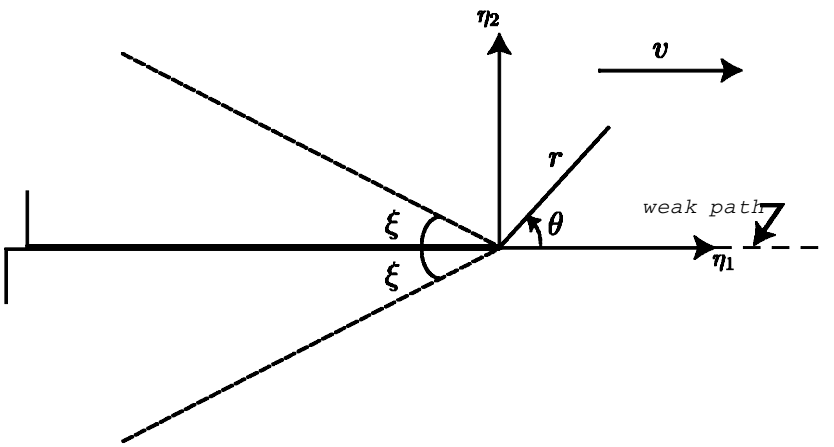

Figure 3. An intersonic mode-II crack confined to grow along a straight-line path in an isotropic solid. The illustration shows the crack tip coordinate system and two Mach lines radiating from the crack tip.

$$q(v) = \frac{1}{\pi} \tan^{-1} \frac{4\alpha_\ell \hat{\alpha}_S}{(1 - \hat{\alpha}_S^2)^2}. \tag{2.8}$$

The variables $r_\ell, \theta_\ell, \alpha_\ell$ are defined in equations (2.2) and (2.3) above while $\hat{\alpha}_S$ is given by

$$\hat{\alpha}_S = \left(\frac{v^2}{c_S^2} - 1 \right)^{1/2}. \tag{2.9}$$

The coefficient K_{II}^*, which represents a common amplitude factor to all stress components, is called the intersonic mode-II stress intensity factor and it is equivalent to K_{II}^d of the subsonic solution. This amplitude is not determined by the asymptotic solution. Rather it depends, in general, on the transient loading and on geometry [2].

From the Heaviside function that appears in equation (2.7) we clearly see that the asymptotic solution predicts two travelling stress discontinuities (Mach waves) attached to the shear crack tip and inclined at an angle $\xi = \sin^{-1}(c_S/v) = \tan^{-1}(1/\hat{\alpha}_S)$ to the crack faces as evident from by the argument of the step function. These stress discontinuities are schematically indicated in figure 3. The stresses are singular not only at the crack tip, but also along the two Mach fronts with the order of singularity the same as that of the crack tip. That means that the crack tip singularity is 'radiated' out along the Mach lines which are 'characteristics' arising from the hyperbolic nature of the partial differential equation that governs the shear elastic potential in the intersonic regime. Across the Mach front, the normal stress and the normal particle velocity perpendicular to the front are continuous, whereas the shear stress and tangential velocity suffer an infinite jump. Hence these fronts are shear Mach waves equivalent to the pressure Mach waves (shock waves) described briefly in relation to the supersonic gas dynamics problems in section 1.1. Another major difference of intersonic crack growth from the subRayleigh crack behaviour lies in the nature of the stress singularity exponent q. In the intersonic regime the singularity exponent is not equal to 1/2. Instead, it is a strong function of crack tip speed and its variation is plotted in figure 4 for both the plane stress and plane strain cases and for a value of Poisson's ratio ν of 0.34. The figure shows that q increases monotonically with speed from a value of 0 at c_S to a value of 1/2 at a speed of $\sqrt{2}c_S$ and thereafter, as the crack approaches the dilatational wave speed c_ℓ it decreases monotonically to 0. The fact that the strength of singularity is drastically reduced compared with the classical square root behaviour of the subRayleigh regime has direct consequences for the energetics of crack growth. In fact, the strongest consequence of that is the fact that dynamic energy release rate G, or equivalently the energy supplied to the shear crack tip per unit slip area increment, is identically zero in the intersonic interval except at one distinct crack tip speed. This speed is equal to $\sqrt{2}c_S$ and corresponds to a value $q = 1/2$. At that speed, the intersonic crack tip recovers its subsonic, square-root singular, nature and, as the functions $m_{ij}(\alpha_\ell, \hat{\alpha}_S)$ in equation (2.7) vanish, the shear Mach waves disappear. In addition, the energy supplied to the tip is no longer zero and has a positive finite value of

$$G = \frac{(K_{II}^*)^2}{4\mu\alpha_\ell}, \tag{2.10}$$

where μ is the shear modulus of the isotropic linear elastic solid [44].

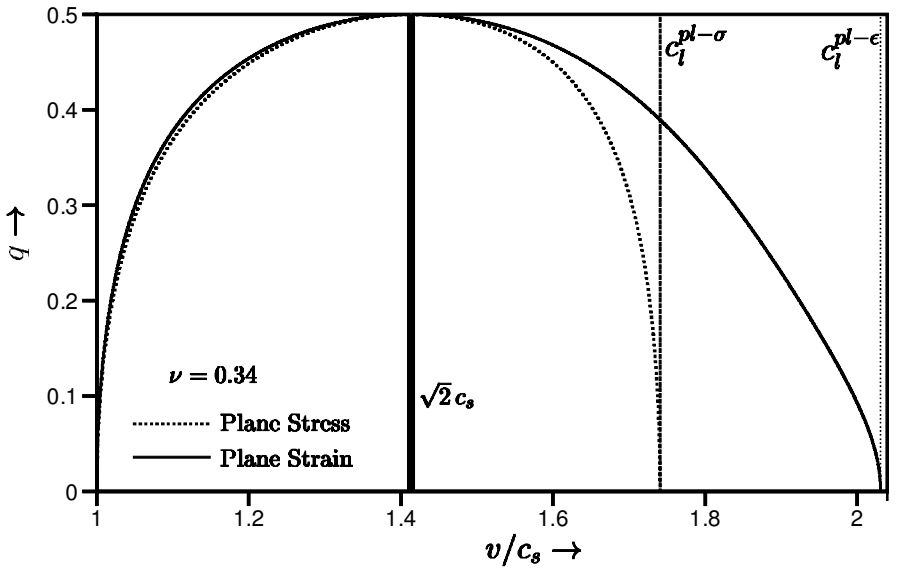

Figure 4. The variation of the mode-II crack tip singularity exponent with crack speed.

The implications of the above observations for the ability of a shear crack to propagate intersonically were first been discussed by Freund [44] and later by Broberg [13, 14]. As they point out, within the confines of the singular elastodynamic analysis discussed above, a shear crack can definitely propagate intersonically at the interesting crack tip speed of $\sqrt{2}c_S$, where finite and positive energy flux is available to it. At all other intersonic speeds the situation remains uncertain. At such speeds, G is identically zero which, although is not as prohibitive as is the negative value predicted for the superRayleigh/subsonic interval, it is, nevertheless, discouraging from the point of view of singular elastodynamics.

Following the above discussion, it is obvious that the theory does not exclude intersonic shear crack growth, as it clearly did for the mode-I discussed in the introduction. However, the theory is unable to conclusively predict whether the occurrence of such a phenomenon is likely or even possible. As emphasized by Broberg and Freund in most of their work on the subject [2, 12–14, 44–47], the idealization of the crack tip process zone to a point-size dissipative tip (the singular crack tip), results in a physically unrealistic situation whereby the requirement of a positive energy flux to the crack tip is met only at $\sqrt{2}c_S$. As a consequence, non-singular, cohesive zone models in which the crack tip region is permitted to assume a finite extent might allow for non-zero flux throughout the intersonic regime. In addition, the possibility of theoretically addressing the problem of the smooth crossing of the forbidden superRayleigh/subshear interval requires the relaxation of the steady-state assumption. In so doing, there is some hope that a transient mechanism which would facilitate the transition from subRayleigh to intersonic, could be identified. Obviously, the possibility of achieving both such goals analytically is slim, whereas early numerical studies have indeed managed to provide us with the means of analysing such issues.

In perhaps the first transient analytical study of shear rupture ever reported, Burridge [48] employed a simple form of cohesive zone model to analyse the problem

of a mode-II crack-like entity propagating along an interface between two identical half spaces. The rupture was allowed to grow in a self-similar manner from zero initial length along the interface. The two half spaces were subjected to uniform normal and shear tractions and were held together by Coulomb friction. In effect, this problem represents the limiting case of a shear crack of zero cohesive energy together with a finite fault strength limit and hence it mimics a 'propagating stress drop'.

For stress drop ruptures propagating with high subRayleigh speeds, Burridge was able to identify a peak in shear stress propagating ahead of the main rupture. This peak was observed to increase in magnitude as the main rupture speed approached c_R. He then postulated that if this stress peak exceeds the limiting static friction then a secondary microrupture may nucleate and may grow ahead of the main stress drop. The main rupture may continue to move at the Rayleigh wave speed, provided that the fault strength is sufficiently high. Otherwise it joins up with the microrupture and the resulting combination may accelerate and propagate at a speed close to c_ℓ. By using a finite difference scheme, Andrews [49] analysed the transient problem of the symmetric expansion of a mode-II crack propagating along a prescribed path under the action of a uniformly applied remote shear stress. Rupture at the crack faces was resisted by a slip weakening cohesive zone of the type described by Ida [50], and by Palmer and Rice [51]. Andrews corroborated Burridge's analytical prediction and he found that the expanding shear crack accelerates to speeds close to c_R and induces the nucleation of a secondary slip region propagating just in front of it. This was found to be possible provided that the limiting static friction (measure of fault strength) was not too high. This secondary rupture zone coalesces with the main rupture and the combination was found to propagate at about speeds 1.5 c_S, a value that is surprisingly close to the special speed of $\sqrt{2}c_S$ described by Freund's analysis [44]. Andrews' numerical observations together with the study by Burridge [48] describe one possible mechanism that would allow a subsonic rupture to cross the forbidden speed regime between c_R and c_S. For the remainder of this article this mechanism will be referred to as the 'Burridge–Andrews mechanism'.

Andrews [49] pointed out that for intersonic cracks, where the crack tip singularity is less than 1/2, a non-zero fracture energy is supported only when the stress drop is not abrupt, that is when the crack tip region is allowed to have a finite extent. Das and Aki [52] used a boundary integral method to study transient mode-II crack expansion in an infinite, linear elastic isotropic solid subjected to remote shear stress. The crack tip in this study was modelled as a structureless point and dynamic friction was assumed to act along the crack faces. Using a critical stress criterion, they confirmed the numerical results of Andrews [49]. The subsequent numerical studies by Day [53] and Johnson [54], who examined various aspects of intersonic rupture, also confirmed the importance of the stress peak travelling with the shear wave speed in facilitating the subRayleigh to intersonic transition. The Burridge–Andrews mechanism was found to be activated in a variety of situations and thus became a widely accepted interpretation. The stability of a semi-infinite steady-state mode-II crack, confined to propagate along a straight-line path under the action of a point load at a finite distance from the crack tip was first studied by Burridge *et al.* [55]. This work assumed the presence of a slip-weakening cohesive zone resisting crack advance and concluded that the crack is inherently unstable in the entire subRayleigh regime. When propagating intersonically, the crack was found to be

unstable in the open speed interval between c_S and $\sqrt{2}c_S$ and stable when v lies in the closed interval between $\sqrt{2}c_S$ and c_ℓ. The open speed interval between c_ℓ and c_S was confirmed to be forbidden.

Extensive analytical contributions into the cohesive modelling of shear rupture have been presented by Broberg [45, 56]. He considered the problem of a self-similar intersonic mode-II crack expanding symmetrically from zero initial length under the action of a remote uniform shear stress. By assuming a Barenblatt process region he was able to show that the energy G supplied to the crack tip remains positive and finite during intersonic crack growth. At the same time, he was able to demonstrate that G depends on the extent of the process zone as

$$G = f(v)(\tau_\infty^2 a/\mu)(L/a)^{1-2q}, \tag{2.11}$$

where L is the length of the process zone, a is the crack length, $f(v)$ is a complicated function of a rupture speed and $q(v)$ is the speed dependent crack tip singularity exponent shown in figure 4. The dependence of G on L/a, for the limit of a vanishing normalized process zone length, $L/a \rightleftarrows 0$, shows that the energy supplied to the crack tip vanishes at all intersonic speeds with the exception of $v = \sqrt{2}c_S$ which is the speed for which $q = 1/2$. This observation is consistent with the results of the purely singular (structureless) analysis of Freund [44] who predicted G to be identically zero at all speeds with the exception of $v = \sqrt{2}c_S$ where G remained finite and positive. For cases when the process zone length may not be neglected, numerical evaluation of equation (2.11) reveals that the energy flux increases from zero at $v = c_S$ to a maximum value at a speed somewhat lower than $\sqrt{2}c_S$ and then vanishes again at $v = c_\ell$. The exact location of this maximum is dependent on L/a and moves to $\sqrt{2}c_S$ as $L/a \rightleftarrows 0$. In expanding the above analysis, Broberg also considered the requirement of a constant critical fracture energy G_C (or fault rupture strength) balancing the available energy flux. In so doing, he effectively imposed a criterion for intersonic growth. He showed that under these conditions the crack would accelerate from a speed close to that corresponding to the maximum value of G all the way up to the dilatational wave speed c_ℓ. In a later contribution he also solved the transient problem of an accelerating semi-infinite intersonic mode-II crack [47].

2.2. *Laboratory evidence of intersonic shear rupture: bonded isotropic solids*

The experimental results of this section can be better understood with the above discussion in mind. The theoretical models of intersonic shear rupture presented in section 2.1 illuminate the crucial points that are central to our understanding of the experimental observations.

The first point involves the identification of 'permissible' and 'forbidden' rupture speed regimes during dynamic shear rupture. In this regard, the small speed regime between c_R and c_S is identified as being forbidden while purely subsonic and intersonic rupture is theoretically plausible.

The second point is related to the identification of a mechanism that could allow an intersonic crack to transit through the forbidden regime. Here two possibilities seem to emerge. A subsonic crack may induce secondary intersonic rupture by using the Burridge–Andrews mechanism or may be 'born' as intersonic. In both cases the crack circumvents the issue of having to cross the forbidden zone as a single entity.

The third point is related to the significance of the curious speed of $\sqrt{2}c_S$ that seems to repeatedly appear in many of the models discussed above. This speed is

related to the energy supply (or flux) into the crack tip and has been linked to issues of favourable crack growth speeds and crack tip stability within the intersonic regime. It is also the speed at which conditions near the crack tip assume a pseudo subsonic square root singular form. Although the special significance of this speed is somehow de-emphasized by Broberg's introduction of cohesive strength (introduction of structure into the tip), this speed nevertheless persistently re-appears in relation to the laboratory and field observations to be described later. It is also present in relation to more recent edge dislocation and shear crack studies that will be summarized below.

The first conclusive evidence of intersonic shear crack growth in a laboratory setting was reported a few years ago by Rosakis *et al.* [57]. These experiments were designed to mimic the primary assumptions featured by all of the theoretical models described in section 2.1. Their basic purpose was to investigate whether intersonic crack growth can be observed in a highly controlled environment thus resolving, once and for all, the debate concerning the attainability of intersonic shear rupture speeds. For this purpose, a straight-line weak path was introduced ahead of a prefabricated notch tip in the form of a bond between two identical pieces of homogeneous isotropic material. The bonding process was carefully chosen so that the constitutive properties of the bond were very close to those of the bulk material and so that the bond width was less than 30 μm [57]. A material system was thus constructed which, although not strictly homogeneous or monolithic, was homogeneous with regard to its linear elastic constitutive properties. However, the fracture toughness or rupture strength of the bond line was kept lower than the constituent pieces so that the material was inhomogeneous with regard to its fracture properties. The functionality of the weak bond was there to ensure the directional stability of a propagating shear crack tip, following its initiation from the asymmetrically loaded prenotch. As the issues discussed in the introduction clearly suggest, the bond is there to also mimic the theoretical assumption of a predetermined straight-line fracture path (or fault) inherent in all models previously mentioned.

The geometry and relative dimensions of the specimen are shown in figure 5. Dynamic photoelasticity was chosen as a diagnostic method for capturing the stress field near the propagating fracture because of its sensitivity to maximum shear stresses. At this point it should be recalled that according to Freund's asymptotic solution (see equation (2.7)), shock waves featuring strong shear stress discontinuities are anticipated if a crack is captured to propagate intersonically. Two identical plates of Homalite-100, a brittle polyester resin that exhibits stress induced birefringence, were bonded together and the notch was machined at one edge along the bond line. In certain cases the bonding agent was polymerized *in situ* and cured appropriately to produce variable bond strengths, whereas in other cases, the bond was created by temperature-enhanced surface sintering. This later procedure does not involve any bonding agent. With such a method, there was no ambiguity regarding the constitutive homogeneity of the resulting bonded structure. The dilatational wave speed of Homalite-100 is $c_\ell = 2187\,\mathrm{m\,s^{-1}}$, the shear wave speed is $c_S = 1255\,\mathrm{m\,s^{-1}}$, while $c_R = 1155\,\mathrm{m\,s^{-1}}$. It should be noted that Homalite-100 is mildly rate sensitive and that these numbers correspond to a strain rate of $10^3\,\mathrm{s^{-1}}$. The equivalent quasi-static values for the wave speeds are approximately 15% lower. The tensile strength of bulk Homalite-100 is approximately 35 MPa, while the shear strength τ_0 of the bond was approximately 14 MPa.

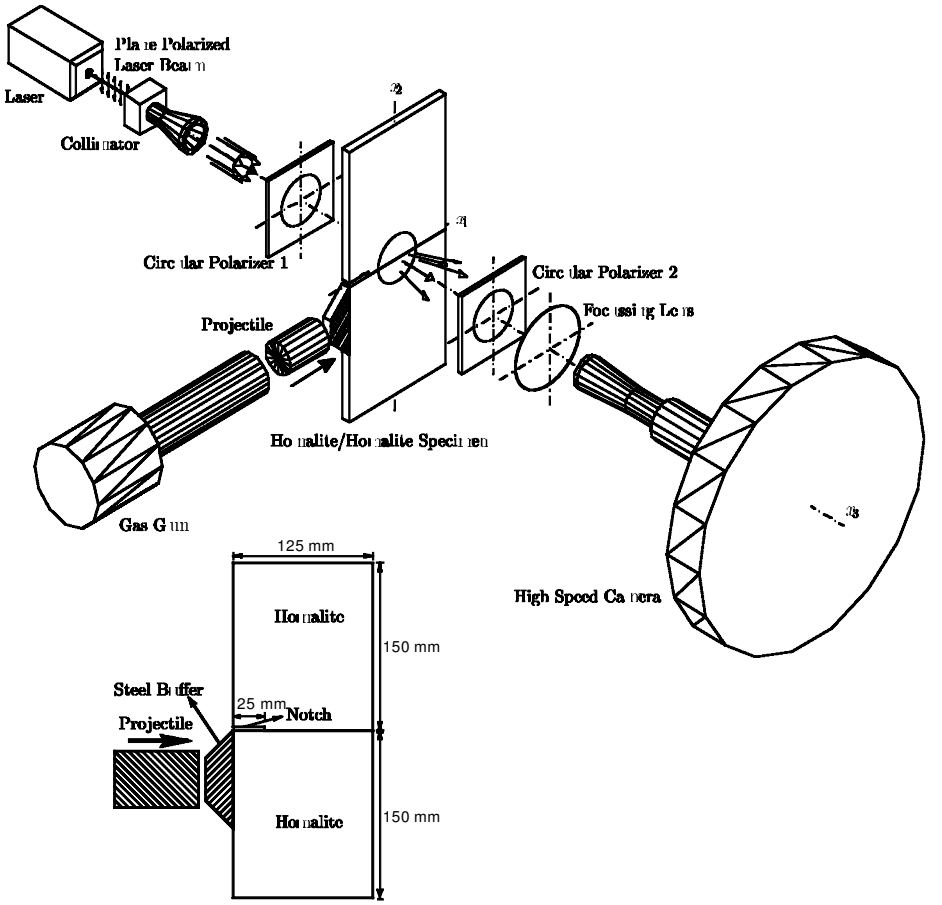

Figure 5. The dynamic photoelasticity set-up. A bonded Homalite/Homalite specimen is photographed by a high-speed camera (2×10^6 frames s^{-1}) as it is subjected to asymmetric impact by a projectile fired by a gas gun.

The specimen was subjected to asymmetric impact loading through a cylindrical steel projectile whose speed ranged from 8 m s^{-1} to 40 m s^{-1}. A steel buffer was bonded to the specimen at the impact site to prevent shattering and to induce a planar loading wave front into the Homalite plate. The compressive longitudinal wave loads the notch which is initially in a predominantly shear mode provided that it is wide enough to prevent the transmission of stress waves into the top half. It is exactly for that reason that a notch was inserted into the specimen edge. If, instead, the specimen was hit directly below the bond line, a substantial opening component would be introduced, potentially decohering the interface in a mixed-mode fashion. The dynamic stress field produced by the impact was recorded by high-speed photography used in conjunction with a classical photoelastic set-up as shown in figure 5. The resulting high-speed sequence of photoelastic fringe patterns shows contours of constant maximum in-plane shear stress $\tau_{\max}$ governed by the stress optical law

$$2\tau_{\max} = \sigma_1 - \sigma_2 = nF_\sigma/h, \tag{2.12}$$

where F_σ is the material's stress optical coefficient, h is the specimen thickness, σ_1, σ_2 are the principal stresses and n is the isochromatic fringe order. For Homalite-100, $F_\sigma = 22.6\,\mathrm{kN\,m^{-1}}$.

The first experiments discussed in this article correspond to low projectile impact speeds of 20m/s. Figure 6 is a high-speed sequence of isochromatic images showing the crack initiation process. The notch is visible on the left side of the circular field of view while the prefabricated weak plane is shown as the horizontal dark line. Following the impact, the initial loading waves produce a predominately shear

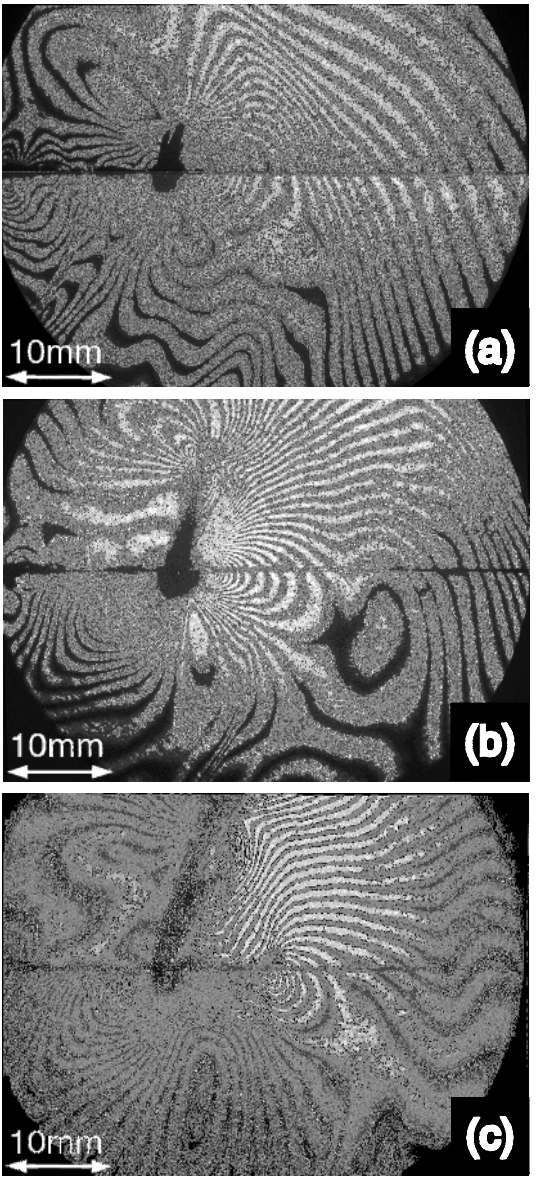

Figure 6. A sequence of isochromatic fringe patterns showing the progression of failure in a bonded Homalite/Homalite specimen subjected to low speed impact. A kinked mode-I crack is shown propagating at 72° off the horizontal weak bond.

loading state that spreads throughout the specimen. Prior to these waves reflecting from the specimen boundaries and arriving back at the notch tip, a kinked crack is observed to initiate from the notch and to propagate along a straight-line path at approximately 70° to the weak plane. The kinked crack is a mode-I crack, which follows the path that would ensure that local crack tip deformations remain symmetric as the crack grows into the upper half of the specimen. Indeed, as discussed in section 1.1, this is an expected behaviour when a notch within a strictly homogeneous solid is subjected to pure mode-II loading. For such a case, the analysis by Hutchinson and Suo [18] predicts a kink angle of 72°, which is very close to the experimental observation. Such a result, however, is still puzzling. The solid is not strictly homogeneous since it contains a weak horizontal path that is placed there intentionally in order to capture and guide the fracture thus preventing it from kinking off to an angle. The existence of such a bond is obviously ignored by the failure sequence in this experiment and so the question remains of whether it is ever possible to propagate a shear crack under such conditions. There are three obvious ways to encourage the crack to initiate in shear and to propagate along the bond line. The most obvious is to intentionally decrease the bond strength even more. The second is to impose a far-field hydrostatic stress state that would tend to discourage any mode-I opening cracks from forming. The final, and perhaps the simplest to implement, is to increase the amplitude of the dynamically applied shear loading by simply increasing the impact speed of the projectile.

Figure 7 shows what happens when the impact speed is increased from 20 m s^{-1} to 27 m s^{-1}, which, at first glance, seems to be a moderate change. The bond strength was left unchanged. The time elapsed after impact, as well as the crack tip speed, is shown in each frame. This selected sequence of images is drawn from two nominally

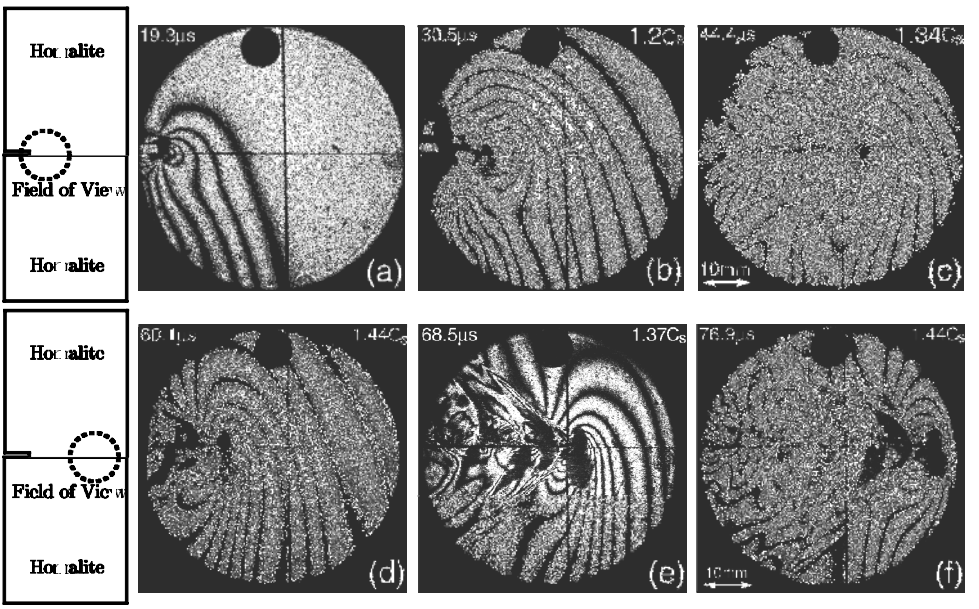

Figure 7. Isochromatic fringe pattern around a shear crack initiating from a notch and propagating along a weak plane in Homalite-100. (a)–(c) Field of view centred 20 mm ahead of the notch tip. (d)–(f) Field of view centred 63 mm ahead of the field of view.

identical experiments differing only by the position of the field of view. In frames (a)–(c), the field of view of 50 mm in diameter is centred on the weak plane 20 mm ahead of the notch tip. In figure 7(a), the stress waves that result from the impact site and diffract around the notch tip can be observed. As they do so they simultaneously build up, at this location, the stationary stress concentration. In figure 7(b), a concentration of fringes is seen to move along the weak plane at a very high speed. This fringe concentration represents the moving shear crack tip. Frame 7(c) features a discernable increase in fringe (and thus stress) intensity around the tip and, in addition, it features the formation of visible damage trailing behind the moving shear crack tip. The damage is confined to the upper side of the weak bond plane. In frames (d)–(f), the field of view is centred 63 mm ahead of the notch tip and, as a result, the initial notch is no longer visible. Figure 7(d) shows a crack entering the field of view from the left. The shape of the isochromatic fringes around this crack has changed dramatically, compared with its shape in the previous sequence. In frames 7(e) and (f), two lines radiating from the moving crack tip are clearly visible. These two lines are intense concentrations of fringes across which the isochromatic pattern changes abruptly and are clearly reminiscent of shock waves attached to the tips of objects moving supersonically in gases. These are clearly visible in the magnified pattern displayed in figure 8.

The abrupt changes in fringe density across the two lines are clear indications of the presence of shear stress discontinuities and the two lines are two travelling shear Mach waves emanating from the crack tip as this propagates along the interface. Their existence and inclination provides clear proof that the crack tip speed has indeed exceeded the shear wave speed of Homalite-100 and is well within the intersonic regime. The angle ξ, which the Mach waves make with the crack faces, is related to the crack speed through $\xi = \sin^{-1}(c_S/v)$ and can be seen by inspection to be close to 45°. Such an angle corresponds to a crack tip speed v close to the curious speed of $\sqrt{2}c_S$ that has been extensively discussed in section 2.2. In addition, a close look at figures 7(e) and (f) reveals isochromatic fringe patterns whose similarities indicate that the propagating crack at this stage may be approaching steady-state conditions. The insights obtained by visual inspection are confirmed by more accurate analysis of the experimental results. Typical crack tip speed histories for two identical experiments varying only in the position of the field of view are shown in figure 9. The crack tip speeds are determined using two methods. The first method involves fitting a second order polynominal to every three successive points in the crack length history and then differentiating it with respect to time in order to provide the speed of the mid-point. The results are displayed in figure 9(a). In the second method, the angles of inclination of the Mach waves to the crack faces are measured and the ratio v/c_S is obtained using the Mach angle formula discussed above (i.e. $v/c_S = (\sin\xi)^{-1}$). This method is limited to frames where the Mach waves are clearly visible. The results are displayed in figure 9(b). From figure 9(a) we see that, within experimental error, the initial crack speed is close to the shear wave speed of Homalite-100 beyond which it accelerates throughout the intersonic regime. The acceleration featured during this part of the process is of the order of $10^7 g$, where g is the acceleration of gravity. The maximum speed recorded is very close to the dynamic value of the dilatational wave speed of Homalite-100. After that point the crack tip decelerates gradually and ultimately reaches a steady-state speed that is slightly higher than $\sqrt{2}c_S$. This result is indeed consistent with the visual observation of Mach wave angles inclined at approximately 45° to the crack faces.

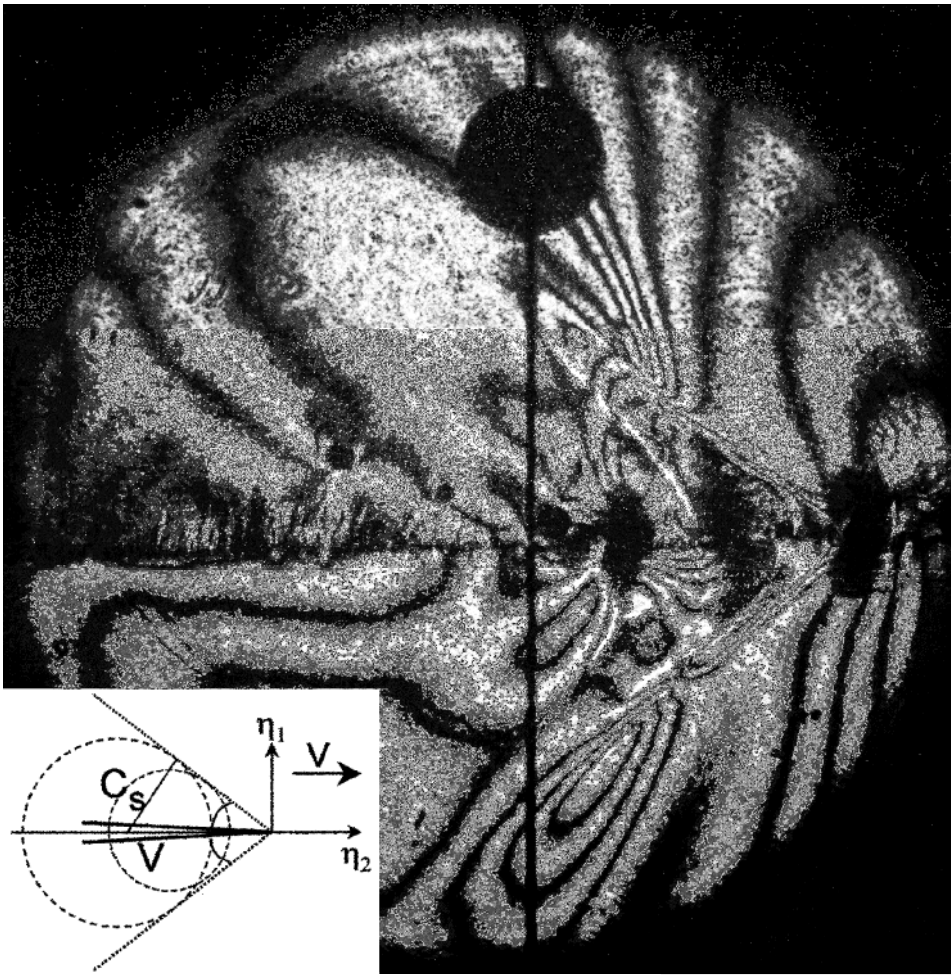

Figure 8. Enlarged view of the isochromatic fringe pattern around an intersonic shear crack moving along a weak plane in Homalite-100. A shear shock wave (Mach wave) is clearly visible.

The first experimental observations of intersonic rupture can now be integrated into the discussion of the early models of shear crack growth presented in section 2.1. To that effect, several points are appropriate.

The shear crack that started growing from the tip of the notch was 'born' intersonic and remained within the intersonic regime throughout our window of observation. Its ability to propagate at all speeds within this regime has provided the first unambiguous laboratory evidence that intersonic crack growth is a physical possibility; evidence that is consistent with the predictions of the early theoretical studies.

The crack was generated at the location of an artificially seeded singularity (stationary notch tip) whose purpose was to store energy that would induce intersonic growth. As a result, the crack was never subsonic and it never entered the forbidden crack tip speed regime between c_R and c_S. This in turn provides clear evidence of how the Burridge–Andrews mechanism can be circumvented.

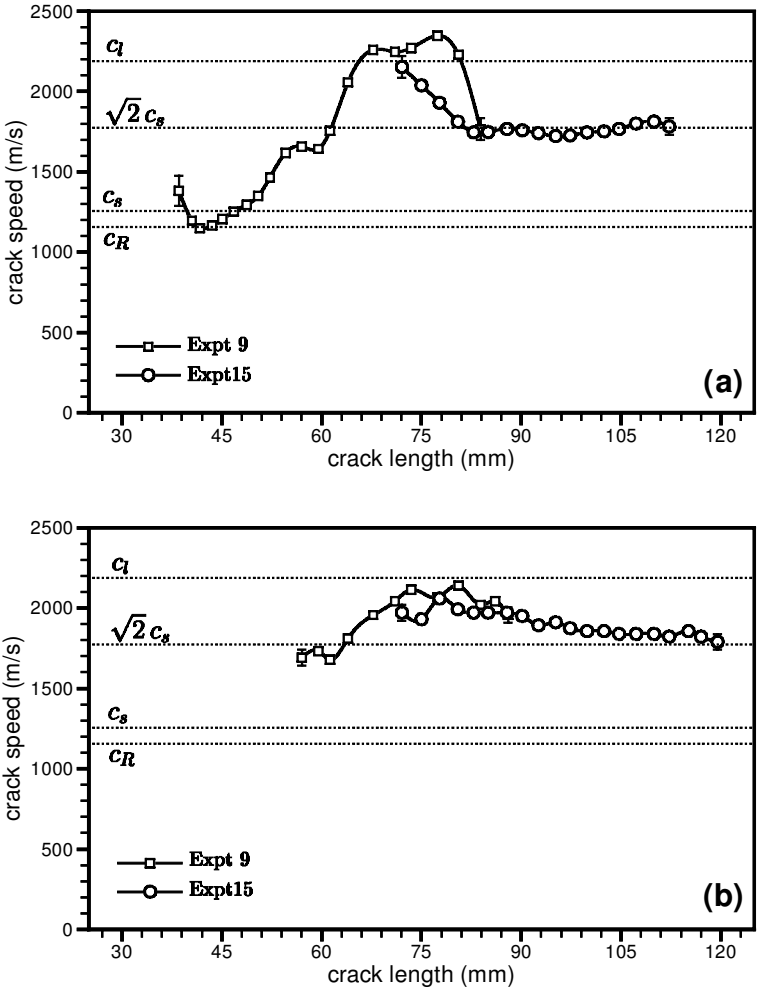

Figure 9. Shear crack tip histories. (a) Crack speed obtained by differentiation of the crack length record. (b) Crack speed inferred from Mach angle measurements.

The crack tip's rapid acceleration from c_S to c_ℓ and its subsequent slow deceleration to an almost steady-state value just above $\sqrt{2}c_S$ illustrates the special significance of this particular crack tip speed. It is noteworthy that the time of this deceleration is coincidental with the arrival of the first unloading waves, which signals the disassociation of the projectile from the impact area. This is equivalent to the end of the loading pulse. It is very interesting to note that although the crack tip is largely unloaded by the arrival of this information, it still persists in propagating at a steady-state speed close to $\sqrt{2}c_S$ instead of abruptly arresting as a subsonic crack would tend to do under similar circumstances. To comprehend this behaviour one should perhaps recall that the energy supply into the tip at this particular speed is very close to its maximum. This has been pointed out in relation to Freund and Broberg's works outlined in section 2.1. The only possible discrepancy with the predictions of the cohesive theories discussed by Broberg [45, 56] is related to the observation that the crack always tends to settle at a steady-state speed just above

rather than just below $\sqrt{2}c_S$. As we shall see in the following section, this discrepancy can be explained. In particular, Broberg considered the case of self-similar crack growth of a zero length crack whose two crack tips propagate symmetrically. In contrast to this model, our experimental situation involves the extension of a single crack tip that reaches nearly steady-state conditions as it expands. Therefore, a steady-state cohesive model of an intersonically moving semi-infinite rupture may be much more appropriate for detailed comparisons with the experimental results.

It is instructive to qualitatively compare the results of the experiments with the analytical predictions of Freund's singular steady-state solution of an intersonically moving shear crack described in section 2.1. The comparison can be achieved when the analytical expressions for the asymptotic stress field of such a crack, given here in equation (2.7), are substituted into equations (2.12), governing photoelasticity. By using the experimental values for the fringe constant of Homalite-100, a thickness equal to that of the specimen and a best fit for the value of the intersonic stress intensity factor K^*_{II} ($K^*_{II} = 2\,\mathrm{MPa\,m}^q$), a synthetic isochromatic fringe pattern is constructed. This pattern is shown in figure 10 and corresponds to a crack tip speed of $1.47c_S$. In this form, Freund's solution is directly comparable with the experimental isochromatic field shown in figure 8, which also corresponds to approxi-

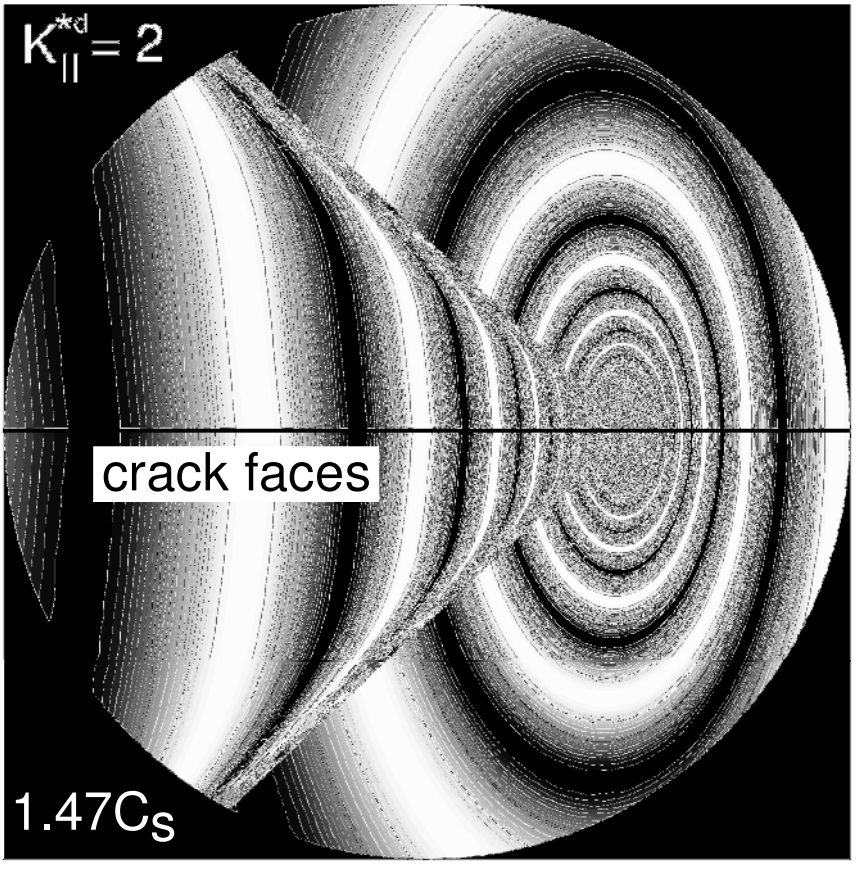

Figure 10. Synthetic isochromatic pattern constructed on the basis of Freund's 1979 singular solution [44] for an intersonically growing mode-II crack.

mately the same speed. The two patterns are in very good agreement with respect to the prediction of the two shear Mach waves, their inclination to the crack faces, and the overall qualitative shape of the fringes. However, ahead of the tip, the experimental fringe pattern is distorted by the stress field generated by the loading pulse. Behind the shock waves the experimental pattern is considerably more noisy than its theoretical counterpart. Possibly such a difference is due to the extensive frictional contact of the shear crack faces and the associated creation of tensile micocracks that result from this contact. Perhaps the most significant difference is in the structure of the Mach waves emitted from the tip. In the experiment, the Mach waves are not simply two sharp lines as they are in the theoretical solution. Instead, they seem to have some width and structure that is not modelled by the singular solution. This, in turn, suggests that an intersonic mode-II steady-state crack model incorporating a shear cohesive zone of finite extent, is required to model the structure of the Mach waves, as well as of the crack tip process zone. The incorporation of a shear cohesive zone will also provide a mechanism for modelling the creation of tensile microdamage trailing the shear crack tip.

A closer look at the crack faces, as these appear in figure 7(c), reveals the existence of damage created on the top side of the specimen as the shear crack tip ruptures the weak bond. Figure 11(b) shows a post-mortem photograph of the upper half of the specimen in a location near the notch tip. The area in the photograph

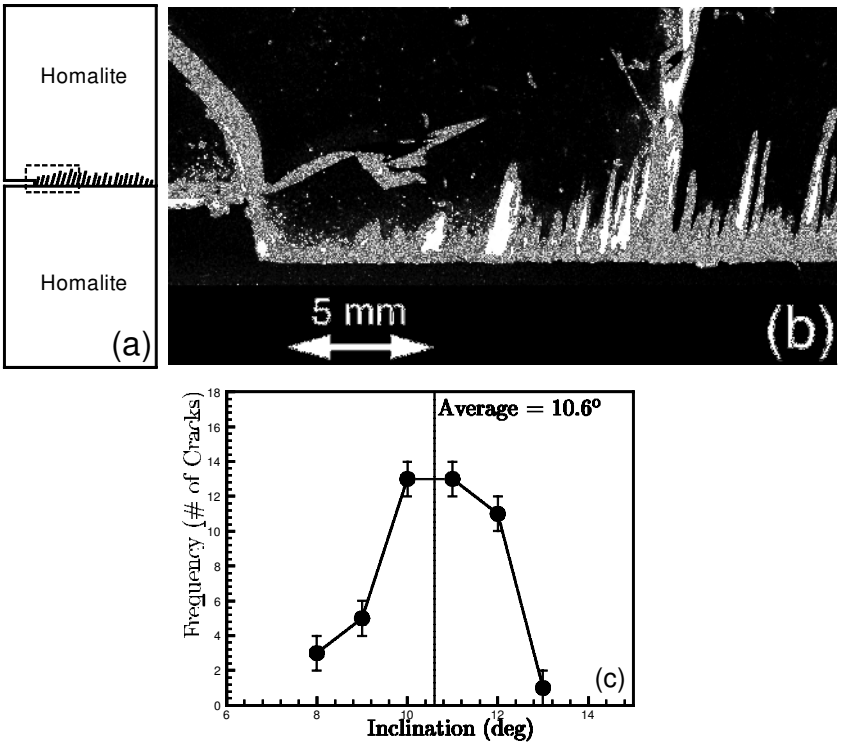

Figure 11. Mode-II microcracks formed on the tensile half of the specimen during intersonic shear rupture. (a) Schematic illustration of the specimen and the microcracks (not to scale). (b) Magnified post-mortem view of the specimen near the rupture path. (c) Microcrack inclination angle plotted versus frequency of occurrence.

corresponds to that enclosed by the dashed rectangle highlighted in figure 11(a). The photograph shows a series of short opening (mode-I) cracks, parallel to each other and steeply inclined to the main shear crack path. These secondary microcracks are observed all along the main crack path and are confined to the upper half only of the specimen. Their length varies from a few micrometres to a few millimetres. To study the statistical variation of the inclination angle of these cracks to the vertical, a number of broken specimens were assembled and inspected following each experiment. The results are shown in figure 11(c), which shows the variation of crack angle with frequency of occurrence (number of secondary cracks inclined at the same angle to the vertical). It is found that the angle of inclination varies from roughly 8° to 13° with an average value of approximately 10.6°. Within the measurement error of ±1°, no strong correlation was found between the secondary crack angle and the main shear crack tip speed. The initiation, propagation, and arrest of these cracks can also be observed in real time by scrutinizing the high-speed isochromatic images at the vicinity of the crack faces. A typical photograph illustrating this phenomenon is shown in figure 12(a). A series of symmetric shadow spots mark the location of the

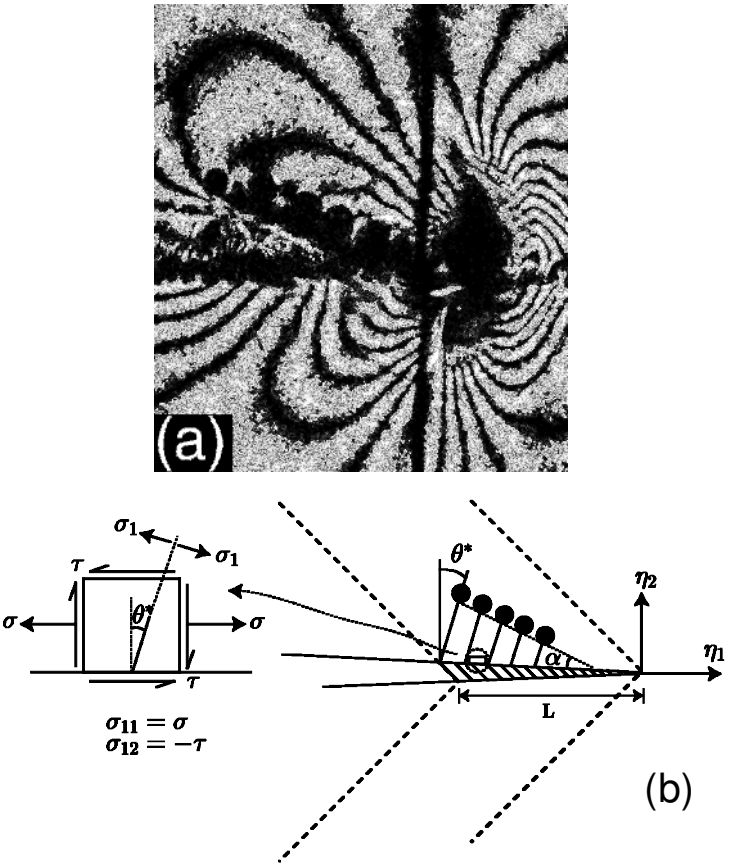

Figure 12. The mechanism of tensile microcrack formation. (a) An isochromatic image showing the location of the microcracks in relation to the main shear rupture. (b) An illustration of the stress state on the shear crack faces, providing an explanation of the microcrack's forward inclination.

tips of these growing mode-I microcracks as they propagate a finite distance into the upper half of the specimen. As indicated in figure 12(b), the centres of these shadow spots fall on to a straight line inclined at an angle $\alpha \approx 23^\circ$ to the crack faces. The initial speed of these microcracks can now be estimated by: (*i*) using α, (*ii*) using the inclination θ^* of these cracks to the vertical, and (*iii*) knowing the speed of the main shear crack. The cracks are found to be subsonic and their average speed was approximately $0.6c_S$. The symmetric nature of the shadow spots is a clear indication of the tensile (mode-I) nature of the microcracks. By extending the line passing through their tips (centres of the shadow spots), it can be seen readily that these cracks nucleate at a small distance behind the main shear rupture. Hence, the formation of these cracks is not akin to the typical branching phenomenon (see section 1), which involves branches or kinks emanating directly ahead of the moving crack tip. In fact, to explain the present phenomenon, the stress state just behind an intersonically moving crack at locations adjacent to the cracks faces should be considered.

Examination of Freund's intersonic singular solution at the appropriate locations (see figure 12(b)) reveals that the direct stress σ_{ij} acting parallel to the crack faces is indeed tensile on the top half of the specimen and is compressive on the bottom half. This explains why the opening microcracks are observed in the tensile half only of the specimen. However, Freund's analysis involves the assumption of traction free crack faces, an assumption inconsistent with the existence of the inclination angle that the microcracks make with the vertical. Specifically, this inclination can be explained only in terms of the presence of a more complex stress state at the immediate vicinity of the shear crack faces. As has already been seen above, it is likely that the crack faces are in contact and subsequently are undergoing frictional sliding resulting in a biaxial stress state at their initiation site. However, most of these cracks seem to originate only a couple of millimetres behind the main crack tip and in the absence of overall static normal compression. As a result, a simple way to include frictional stress at the microcrack initiation site is to introduce a shear cohesive stress zone of finite size translating with the main crack tip. Indeed, in the following section we shall introduce a rate dependent line cohesive zone at the intersonic tip to explain the inclination of these secondary cracks to the vertical. Figure 12(b) shows an illustration of the cohesive region near the shear crack tip, which explains our interpretation as to the origin and directivity of the secondary tensile cracks. The main intersonic shear crack is propagating with a line cohesive zone of length L in front of it. The secondary microcracks originate on the top of the cohesive surface. The stress state at that location is two-dimensional. It features a tensile direct stress $\sigma_{ij} = \sigma$ parallel to the interface, as well as a shear stress $\sigma_{12} = -\tau$ equal to the local value of the cohesive tractions resisting shear rupture $(\sigma > 0, \tau > 0)$. With such biaxial state of stress, the maximum tensile principal stress σ_1 acts on a plane (dashed line) that is inclined at a positive angle θ^* to the vertical which is consistent with the observed orientation of the microcracks. The driving force leading to the growth of these cracks is provided by the near tip field of the intersonic rupture. As the intersonic crack moves further away from the initiation site of a particular microcrack, the driving force acting on it falls. This leads to its eventual arrest a few millimetres away from the decohered shear crack faces.

2.3. *The velocity weakening model of dynamic shear rupture*

In an attempt to introduce some structure into the tip of a dynamically growing shear crack, the following section discusses the results of a rate sensitive cohesive zone analysis [58]. This mode-II crack is confined to propagate steadily along a straight line simulating the weak bond between two homogeneous and isotropic half spaces. The crack can propagate in either the subRayleigh or the intersonic regime. Growth at the 'forbidden' speed regime, however, is not considered.

As shown in figure 13, a shear cohesive zone of length L is located ahead of the crack tip and moves with it at speed v. A shear cohesive zone is a line ahead of the tip within which the shear traction decays from some initial value (the initial bond strength necessary to initiate slip) to zero. The intention of this section is to show how an appropriate choice of a cohesive zone model may reconcile some of the inconsistencies observed when classical models of shear rupture are compared with the experiments. These inconsistencies include issues relating to the finite structure of Mach waves, the formation of secondary tensile microfractures trailing the shear crack tip, as well as issues pertaining to crack tip stability and to the identification of favourable crack tip speed regimes. Cohesive zones of the slip weakening type have been used extensively in the past to model shear ruptures on earthquake faults [48–50]. Slip-weakening and slip-rate (or velocity) weakening models are extensions of cohesive zone models introduced initially on the one hand for tensile cracks by Dugdale [59], to model plastic yielding in ductile materials, and on the other hand by Barenblatt [60] to model interatomic cohesion in brittle solids. A slip-weakening and a slip-rate-weakening law relates the shear strength of a cohesive surface to the local slip or to the local slip rate, respectively. Ahead of a propagating rupture the strength decays from some relatively high peak value to zero as the physical rupture tip decoheres the cohesive surface. For shear ruptures on fault planes, cohesive forces result from non-uniform frictional sliding occurring immediately behind the rupture front. According to the elastodynamic shear crack model, as the rupture front approaches a material particle along its path, the particle experiences a sudden jump in slip rate, which then decays rapidly behind the rupture front. Consequently, the frictional strength of the fault is assumed to decay behind the rupture front over a characteristic slip distance. Slip-weakening laws assume that the strength decay depends on the local slip only. Rate and state dependent friction laws, however,

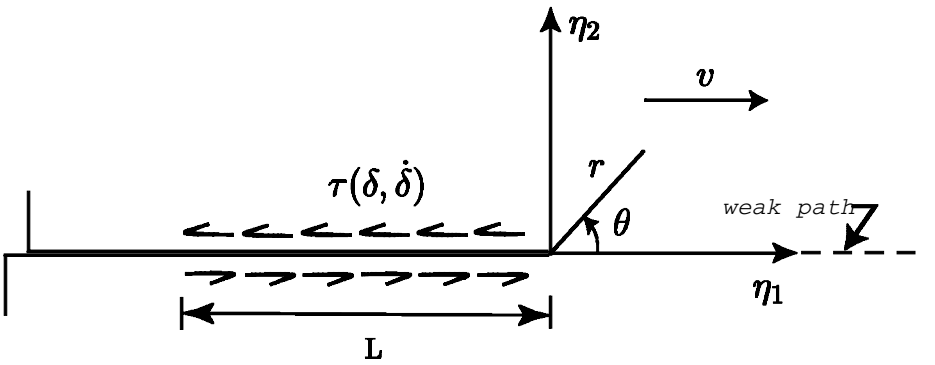

Figure 13. Schematic illustration of the shear cohesive zone and the coordinate system at the tip of the growing shear crack along a weak path.

indicate that frictional strength should also depend strongly on the local slip rate. Specifically, based on experimental data featuring sliding at moderate rates, Ruina [61], Rice and Ruina [62], and Kilgore *et al.* [63] proposed that the sliding friction, apart from being proportional to the normal traction, is also a nonlinear function of slip rate as well as of a number of internal variables that describe the local 'state' of the sliding surface [31, 37].

As was mentioned above, intersonic crack growth in our laboratory specimens was accompanied by crack face contact and sliding. Such evidence is provided by the forward inclination of the microfractures originating at the crack faces. The slip rate at this location is expected to be large, ranging from $1\,\mathrm{m\,s^{-1}}$ to $10\,\mathrm{m\,s^{-1}}$. The limited data available on dynamic sliding at such high slip rates [64–66] also show that the steady-state frictional stress drops with increasing slip rate. The above dynamic friction experiment motivated our use of a velocity weakening shear cohesive law. In that law, the dependence of sliding friction on the local 'state' was neglected.

Rate dependent cohesive relations have been used in the past for modelling subsonic mode-I crack growth in elastic–viscoplastic material behaviour by Glennie [67] and by Freund and Lee [68]. In these studies, however, the cohesive law models a rate strengthening behaviour, which is characteristic of metallic solids. This in turn provides a very different mechanism of crack tip dissipation from the one of interest to the present study. The simple rate dependent cohesive law employed here relates the cohesive shear traction τ at any point within the cohesive zone to the local slip rate $\dot{\delta}$, and is given by:

$$\tau(\dot{\delta}) = \tau_0 \left[1 + \beta \frac{\mu|\dot{\delta}|}{2\tau_0 c_S} \right], \quad \beta \leq 0. \tag{2.13}$$

In the above functional form, the parameter τ_0 represents the quasi-static cohesive strength of the weak path, $\dot{\delta}$ is the difference between the horizontal components of the particle velocities above and below a sliding portion of the interface. The parameter β is a dimensionless rate parameter and is referred to here as the velocity weakening parameter. β is non-positive and, as a result, the law described by equation (2.13) represents either a bond whose strength remains constant with sliding rate ($\beta = 0$), or a law whose strength decreases linearly with sliding rate ($\beta < 0$). A schematic illustration describing the dependence of τ on δ and on $\dot{\delta}$ is shown in figure 14. The form of the law in equation (2.13) is the same as that employed by Glenniel [67] and Freund and Lee [68] in their study of subsonic mode-I crack growth. The only difference is in the sign of β which in their case was taken to be a non-negative constant. The special case of $\beta = 0$ results in a Dugdale type of cohesive zone [59].

The steady-state rupture problem described above is analytically tractable both in the subRayleigh regime and in the intersonic crack tip regime [58]. Expressions for the stress displacement and particle velocity fields have been obtained, but will not be reproduced here. Instead, the presentation will take the form of a discussion of the main results as long as these pertain to the understanding of the experimental observations presented in section 2.2. The normalized shear stress distribution $\sigma_{12}(\eta_1)/\tau_0$ along the crack or bond plane, $\eta_2 = 0$, is displayed in figure 15. Figure 15(a) shows the effect of different levels of β for a fixed intersonic speed $v = 1.47 c_S$, while figure 15(b) represents the crack plane shear stress distribution for different intersonic speeds at a fixed $\beta = -0.4$. The choice of $\beta = -0.4$ is not random. Its

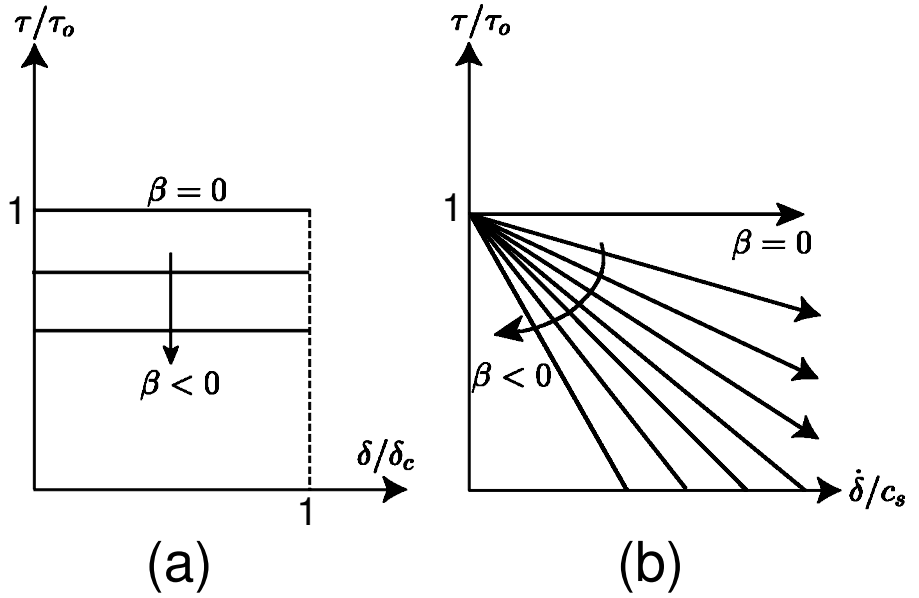

Figure 14. The dependence of the shear strength of the bond on (a) slip and (b) slip rate assumed by the cohesive zone model [58].

significance will become clear at the end of this section. Since the horizontal distance along the bond line has been normalized by the length of the cohesive zone, the location of the tip of the cohesive zone is at the origin, while the physical crack tip lies at -1.

Both figures 15(a) and (b) have some common characteristics. As a stationary point along the bond is approached, the shear stress rises steeply and reaches the maximum value τ_0 at $\eta_1/L = 0$. Subsequently, this particle is processed by the cohesive zone and sliding commences; the stress drops to zero at $\eta_1/L = -1$ which is the physical crack tip. The figures show that either a lower β or a faster speed results in a faster decay of the cohesive shear tractions. Unlike Freund's singular solution, we find that σ_{12} is bounded all along the crack plane. Far ahead of the tip ($\eta_1 \gg L$), the singular solution for a sharp, structureless, crack is, however, recovered.

Figure 16 displays the crack plane variation of the direct-stress component σ_{11} acting parallel to the crack faces. Because of mode-II antisymmetry the values of σ_{11} just above and just below the bond line (crack line) are equal and opposite. With respect to the orientation of the experiments, the top side of the crack faces experiences a tensile σ_{11}, which is responsible for the generation of the tensile microcracks. The bottom side experiences a compressive σ_{11} of equal magnitude.

The variation shown in figure 16 corresponds to the bottom side. The effect of β and of the speed are displayed in figures 16(a) and (b), respectively. In all cases, material particles above and below the bond experience zero direct stress until the arrival of the cohesive zone tip. When the cohesive zone arrives, the magnitude of the direct stresses (tensile stress above, compressive below) increases to a maximum value at $\eta_1/L = -1$, which is the location of the physical crack tip. After this the magnitude of the horizontal direct stresses slowly decreases to zero along the newly created traction free surfaces of the rupture. At this point it is worth noting that the

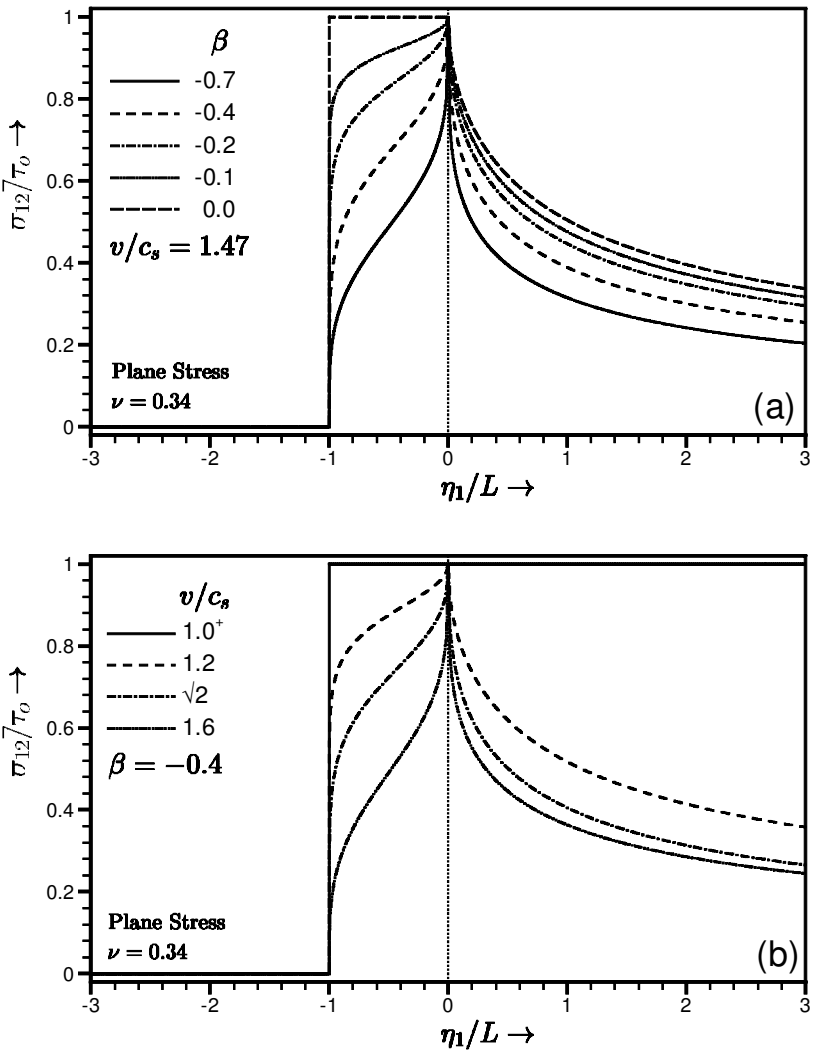

Figure 15. The spatial distribution of the shear stress σ_{12} along the rupture plane (bond line). (a) Dependence on velocity weakening parameter β. (b) Dependence on rupture speed.

maximum value of the direct stress is bounded for all negative values of β. On the other hand, for $\beta = 0$, σ_{11} becomes singular at the physical crack tip. The value of $\beta = 0$ corresponds to the special case of a rate insensitive bond strength and a Dugdale type of cohesive zone.

The distribution of the normalized sliding rate (slip rate) $\dot{\delta}_1/c_S$ is shown in figure 17. This distribution shown in the figure covers only the cohesive zone area. The analytical expressions presented in [58] show that $\dot{\delta}_1$ has the form:

$$\frac{\dot{\delta}_1}{c_S} = \frac{\tau_0}{\mu} f\left(\frac{\eta_1}{L}, v, \beta\right). \tag{2.14}$$

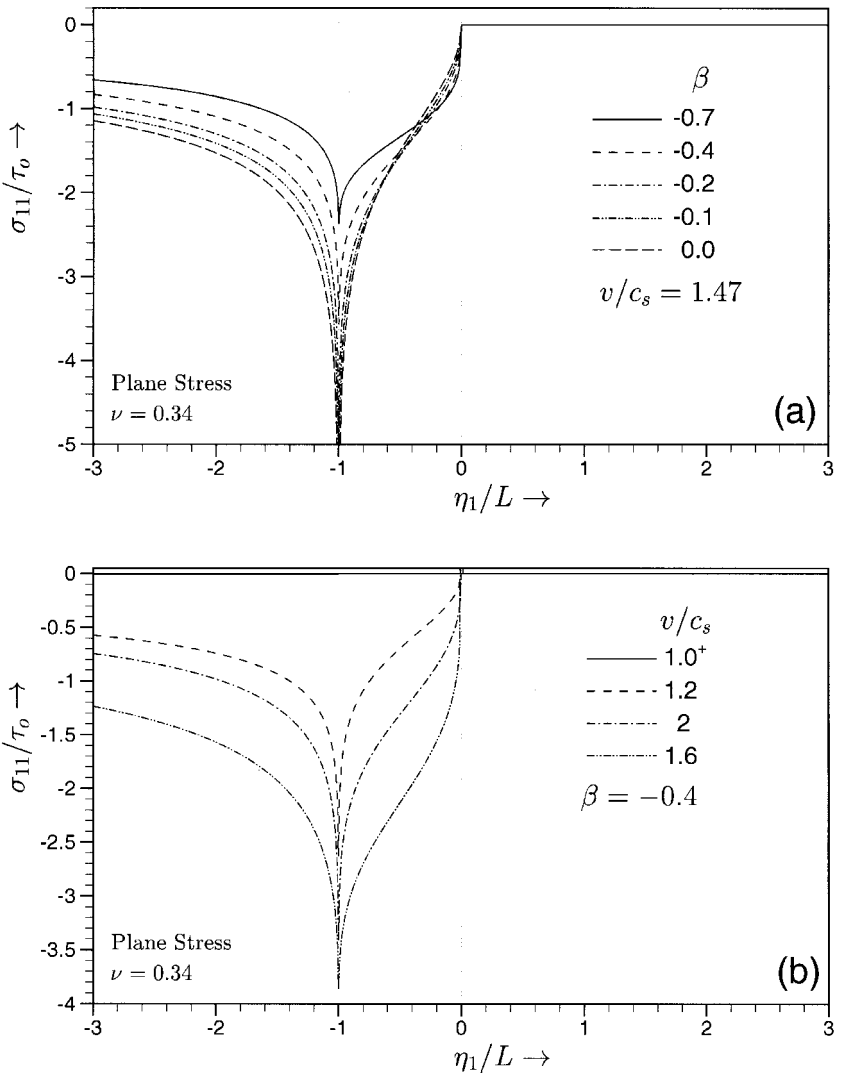

Figure 16. The spatial distribution of the direct stress σ_{11} along the rupture plane (σ_{11} acts parallel to the direction of shear crack growth). (a) Dependence on β. (b) Dependence on rupture speed.

In the above expression τ_0 is the quasi-static bond strength, μ is the shear modulus, and $f(.,.,.)$ is a complicated function of position within the cohesive zone, rupture speed, and β, respectively.

Figures 17(a), and (b) examine the dependence of the distribution of $\dot{\delta}_1/c_S$ on v and on β. The value of μ/τ_0 used is 136. This is equal to the ratio of the shear modulus of Homalite (1.9 GPa), to the quasi-static shear strength of the Homalite–Homalite bond of our experiments (14 MPa). For strictly negative values of β, $\dot{\delta}_1$ is non-singular and increases monotonically from 0 at the tip of the cohesive zone to a finite, bounded maximum at the physical crack tip. This maximum is the slip rate at which, according to the model, the cohesive shear strength vanishes. Only for the

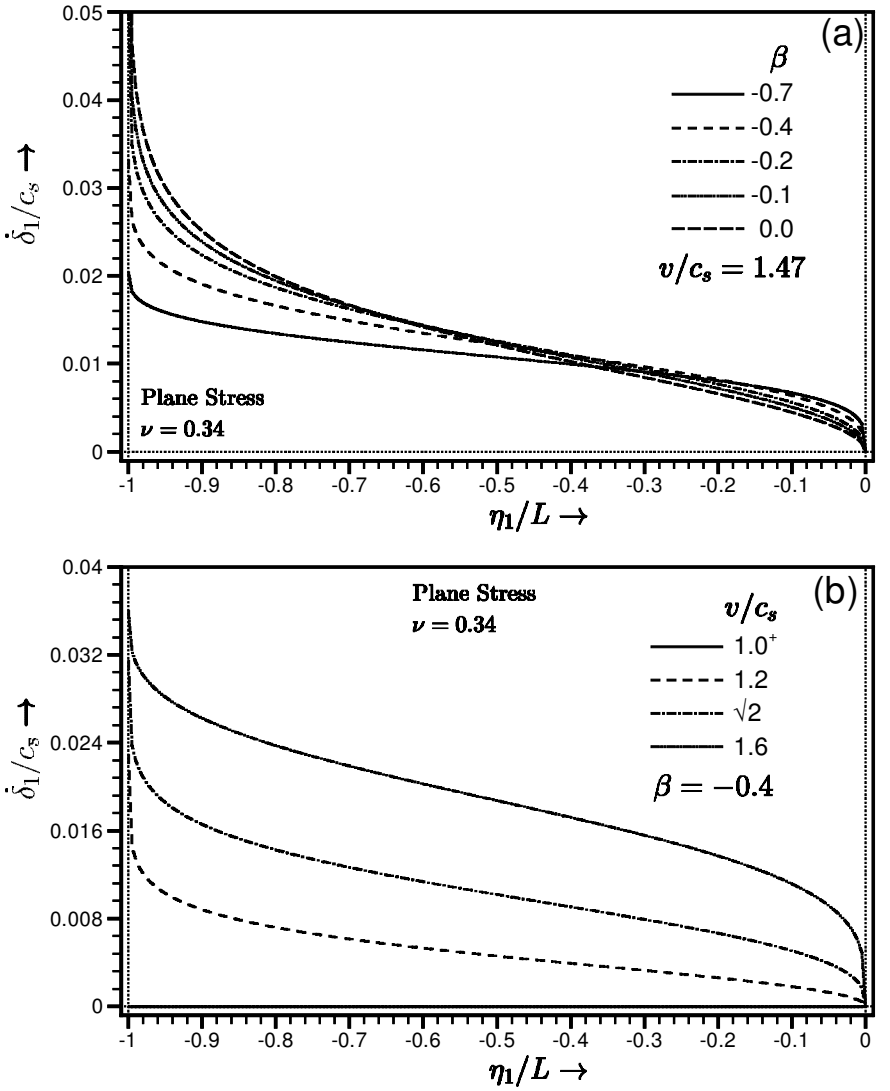

Figure 17. The normalized variation of the slip rate within the shear cohesive zone. (a) Dependence on β. (b) Dependence on rupture speed.

Dugdale type of cohesive zone ($\beta = 0$), does $\dot{\delta}_1$ become unbounded at the physical crack tip. This singularity in $\dot{\delta}_1$, as well as in the direct stress component σ_{11} described above, is an indication of the shortcomings of assuming a constant bond strength while it makes the case of $\beta = 0$ physically unattractive. The effect of β on $\dot{\delta}_1$ is found to be rather small, though a bit more pronounced than in the subRayleigh case [58], not shown here. It should be noted that $\dot{\delta}_1 = 0$ everywhere in the cohesive zone either as $v \rightleftarrows c_S$ or as $v \rightleftarrows c_R$. However, it is strongly influenced by v at all other intersonic speeds. For the bonded Homalite/Homalite material system used in the experiments this corresponds to 1–4% c_S (c_S for Homalite is 1255 m s^{-1}) resulting in average slip rates ranging between 12 m s^{-1} and 50 m s^{-1}. According to the equation

(2.14), $\dot{\delta}_1/c_S$ scales linearly with τ_0/μ and, as a result, if a different material bond system is to be considered, so would the plots of figure 17. In particular, by taking the shear modulus of crustal rock to be 30 GPa and the quasi-static strength of a crustal fault to be approximately equal to 20 MPa (weak fault model [23, 24]), the ratio of μ/τ_0 becomes 1500, which is roughly 90 times higher than the value for the Homalite/Homalite system. The implication is that the resulting normalized slip rates for a crustal fault system would be 90 times lower than those corresponding to Homalite/Homalite properties. This results in $\dot{\delta}_1/c_S$ values between 0.01% and 0.044% of c_S (c_S of crustal rock at a depth of 5 km is approximately 3460 m s^{-1}) or values of $\dot{\delta}_1$ ranging from 0.3 m s^{-1} to 1.52 m s^{-1}. Note that these slip rates are obtained by assuming a very low value of the 'local' strength of the fault. Such a low value corresponds to a situation close to what geophysicists surmise to exist along an active fault such as the San Andreas Fault [24]. Indeed, the resulting slip rates calculated above are compatible to averaged field measurements that have been reported in the geophysics literature [22, 23]. For the other extreme cases of a strong fault model, fault strength has been assumed to be as high as 100 MPa [69, 70], or even 200 MPa [24, 71]. Assuming a strength of 100 MPa, a similar calculation results in sliding rates $15\,\mathrm{m\,s^{-1}} < \dot{\delta}_1 < 63\,\mathrm{m\,s^{-1}}$ As stated by Ben-Zion [72], these values are much higher than what is assumed in seismology, but they are not necessarily unrealistic. Indeed, surface slip velocities of over 10 m s^{-1} may have occurred during the 1990 Luzon earthquake in the Philippines, as has been estimated by Yomogida and Nakata [73], and from surface data and eyewitness accounts. In addition, Ben-Zion's own calculations feature slip rates ranging from 15 m s^{-1} to 30 m s^{-1} [72]. Finally, it should be noted that the bonded Homalite/Homalite experiments, described above, feature a ratio of shear modulus to bond strength $\mu/\tau_0 = 136$ that would correspond to a fault strength of approximately 200 MPa in an equivalent crustal fault system (a system with the same ratio of μ/τ_0).

Further investigation of the solution discussed above requires the determination of the cohesive zone length L that is expected to depend on rupture speed v, fault strength τ_0, and some measure of the applied load. The solution is asymptotic and it also changes nature from the subsonic to the intersonic regime. As a result, there is no unique amplitude factor such as the 'far-field' stress intensity factor that allows for the construction of a single 'small-scale yielding' type of argument covering the entire velocity range of interest. To circumvent this, Samudrala *et al.* [58] chose a stress measure σ_{12}^{D} to represent the driving force of the crack. The shear stress σ_{12}^{D} was defined as the remote stress on the crack plane ($\eta_2 = 0$) acting at a distance $\eta_1 = D$ ahead of the advancing crack tip. The arbitrary distance D should be large enough ($D \gg L$) so that at the point along the bond the singular solution [2, 44], either subsonic or intersonic, still applies. In addition, the physical requirement that the stresses remain bounded at the front of the cohesive zone was imposed. This is a common characteristic of all cohesive zone models [60, 61] and in the present case results in the establishment of a functional relationship between L and the parameters σ_{12}^{D}/τ_0, v and β for the entire admissible speed range. This relationship is reported in [58]. The determination of L allows for the calculation of the dynamic energy release rate G or the energy flux into the cohesive zone per unit rupture advance along the bond, per unit thickness. This is defined as:

$$G = 2\int_0^{-1} \sigma_{12}(\eta_1, \eta_2 \rightleftarrows 0^+) u_{1,1}(\eta_1, \eta_2 \rightleftarrows 0^+)\, \mathrm{d}\eta_1. \tag{2.14}$$

In the above expression, σ_{12} and $u_{1,1}$ are the shear tractions and displacement gradients acting along the upper faces of the cohesive zone. The resulting variation in G with speed is obtained analytically in [58] and is displayed here in figure 18 for only the intersonic regime and for only the value of $\beta = -0.4$. G is normalized by the constant G_0 which is the energy release rate associated with a quasi-statically propagating mode-II crack subjected to the same far-field load σ_{12}^{D}. The normalizing constant G_0 is given by:

$$G_0 = \frac{\pi(\kappa+1)}{4}\frac{D(\sigma_{12}^{\mathrm{D}})^2}{\mu}, \tag{2.15}$$

where $\kappa = 3 - 4\nu$ for plane strain and $\kappa = (3-\nu)/(1+\nu)$ for plane stress.

As seen from figure 18, the dynamic energy release rate (energy flux into the tip) is finite throughout the intersonic regime except at speeds close to c_{S} and c_ℓ. Hence, based on the requirement of a positive energy flux, the entire intersonic regime is admissible for mode-II crack growth. The variation in G/G_0 for intersonic speeds depends strongly on the shear strength of the fault plane τ_0 through the ratio $\sigma_{12}^{\mathrm{D}}/\tau_0$. For a given value of σ_{12}^{D} as $\tau_0 \rightleftarrows \infty$, the structureless singular solution [44] is recovered and the variation exhibits a well-defined finite spike centred around $v = \sqrt{2}c_{\mathrm{S}}$. In most other speeds, G/G_0 is very close to zero. For lower shear strengths the spike becomes considerably wider and has a maximum value at speeds always higher than $\sqrt{2}c_{\mathrm{S}}$. As $\tau_0 \rightleftarrows 0$ the peak eventually moves very close to the dilatational wave speed c_ℓ. In the discussion of Broberg's cohesive analysis [45, 56], involving a self-similar expansion of a shear rupture from initial zero length, the energy release

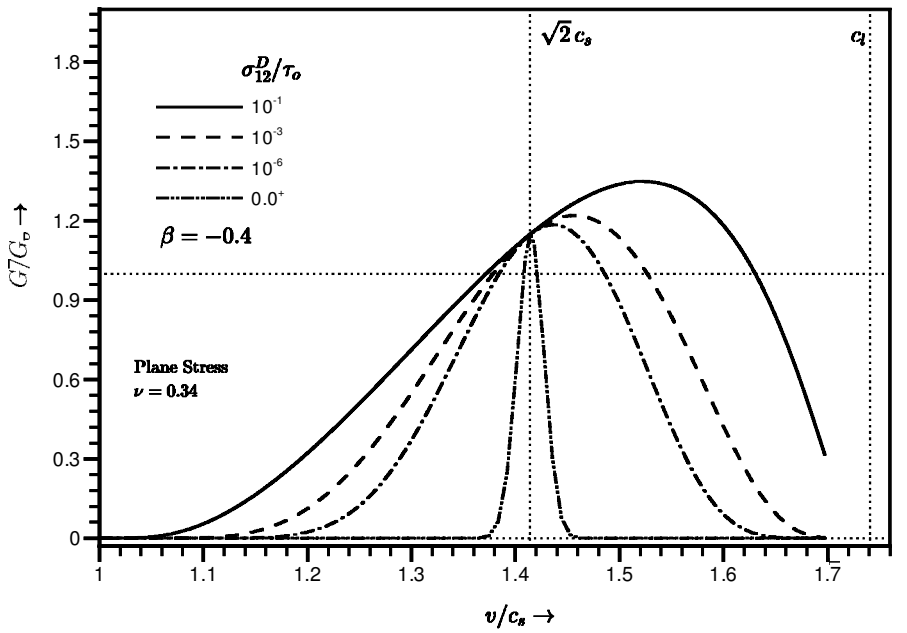

Figure 18. The normalized energy release rate as a function of intersonic rupture speed. The figure shows that the energy flux available to the tip has a maximum at or above $v = \sqrt{2}c_{\mathrm{S}}$.

rate was also found to be finite and positive throughout the intersonic regime. However, there was one important difference between Broberg's results and the results of the steady-state analysis presented in figure 18. The energy release rate G/G_0 for a self-similar crack featured a maximum, which always corresponds to a speed below rather than above $\sqrt{2}c_S$. The experiments described earlier feature speeds that approach $\sqrt{2}c_S$ from above, as the crack grows longer along the bond. This is perhaps to be expected since the steady-state model, which involves a semi-infinite crack, becomes increasingly relevant to the experiment as the crack slowly approaches steady-state conditions (see figure 9).

The variation in the energy flux with rupture speed provides strong hints regarding the possibility that an intersonic shear crack may favour propagation at a particular speed or a speed regime when it reaches steady-state conditions. However, this question cannot be conclusively answered before a rupture criterion is imposed to the analytical model. This may take the form of an energy balance argument. In such an approach, the energy supplied to the crack by the surrounding elastic field (energy flux G) per unit area of rupture is balanced by the critical energy G_C required to break the bond. Alternatively, it may take the form of a criterion requiring that sustained dynamic rupture, at any subRayleigh or intersonic speed, always occurs when the sliding displacement δ_t at the end of the cohesive zone reaches a critical value δ_t^C. In both cases, the critical values of G_C or δ_t^C introduce the notion of rupture resistance of the weak plane or interface into the continuum model either as a critical energy for failure or as a critical breakdown slip. Following the second approach [58], the relative sliding displacement δ_t at $\eta_1 = -L$ obtained by the velocity weakening model is required to obey

$$\delta_t = u_1(\eta_1 = -L, \eta_2 \rightleftarrows 0^+) - u_2(\eta_1 = -L, \eta_2 \rightleftarrows 0^{-1}) = \delta_t^C. \tag{2.16}$$

In the above relation, u_1 denotes a horizontal displacement component. The breakdown slip δ_t^C is a bond/sliding surface specific parameter. Whereas in the experiments this breakdown slip depends on the choice of bonding agent between the Homalite pieces, in the case of a crustal fault rupture it depends on conditions of surface sliding between crustal masses. Typical values of δ_t^C surmised in the geophysics literature are of the order of 10 cm [71]. For the Homalite/Homalite laboratory experiments it is estimated to be 20 μm. Equation (2.16) provides a relation between $(\sigma_{12}^D)_{dyn}^C$ (critical value at σ_{12}^D required to satisfy the critical crack tip sliding displacement criterion) and the crack tip speed. An example of this variation is shown in figure 19 and corresponds to a value of $\beta = -0.4$ (see discussion on microcracks explaining this choice of β). The critical shear stress $(\sigma_{12}^D)_{dyn}^C$ is normalised by its quasi-static counterpart, $(\sigma_{12}^D)_0 = \tau_0(4\mu\delta_t^C/(\kappa+1)\pi D\tau_0)^{1/2}$, and its speed variation is shown in both the subRayleigh and intersonic speed regimes.

As shown in figure 19, the critical level of far-field load required to sustain rupture in the subRayleigh case is a decreasing function of speed that drops to zero as $v \rightleftarrows c_R$. This case, in turn, can be interpreted as an unstable situation. Indeed, a small rupture acceleration, perhaps caused by local fault strength inhomogeneities, would result in a slightly increased rupture speed that requires less far-field load. As a result, more energy is available to the crack tip than is required to rupture the bond. Consequently, this can only lead to a further rupture acceleration all the way up to the Rayleigh wave speed of the material. For subRayleigh speeds the speed variation is independent of the static bond strength τ_0. As shown in [58] $(\sigma_{12}^D)_{dyn}^C$ still

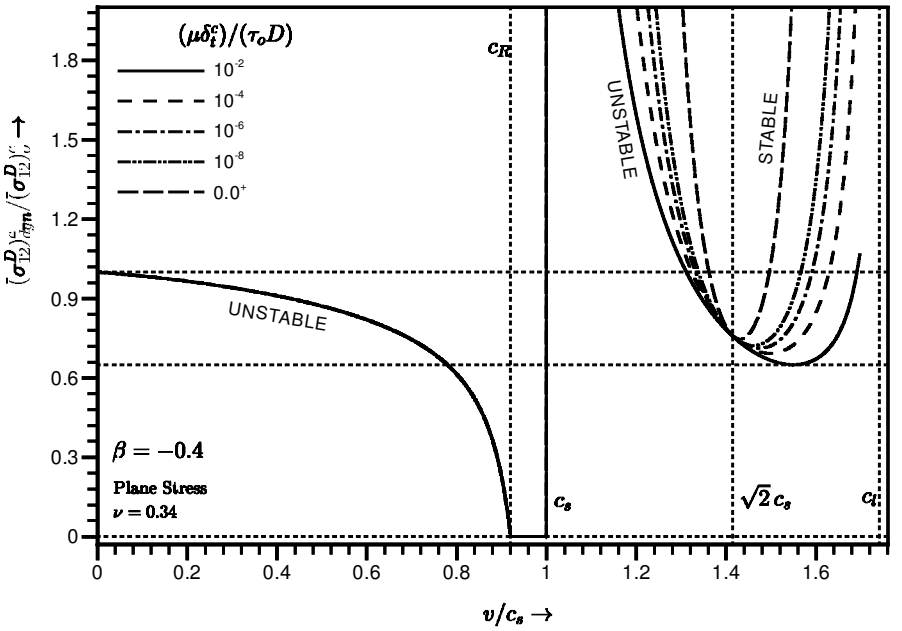

Figure 19. Dependence of the critical far-field shear stress (required to sustain dynamic rupture growth) on the rupture speed versus Stable and unstable speed regimes are indicated.

depends on β and lower β values tend to amplify the instability. For intersonic speeds, the variation is also a function of τ_0 through the parameter $(\mu\delta_t^C)/(\tau_0 D)$. This parameter can be thought of as a measure of the shear strength of the fracture plane. It is observed that the entire speed regime $c_S < v < \sqrt{2}c_S$ is unstable and the speed at which intersonic crack propagation becomes stable (rising branch of the U-shaped curves) depends on both τ_0 and β. For $\tau_0 \rightleftarrows 0$, almost the entire intersonic regime becomes unstable, indicating that ruptures on a plane of vanishing strength would propagate at a speed close to c_ℓ. On the other hand, for $\tau_0 \rightleftarrows \infty$ the onset of stability occurs at exactly $\sqrt{2}c_S$. This observation is consistent with the stability results obtained by Burridge *et al.* [55] and by Freund [44]. However, it should be emphasized that a slip-weakening rather than a slip-rate-weakening cohesive law was used in these studies.

It is important to note that figure 19 also shows the existence of a forbidden zone between the subRayleigh regime and the intersonic regime. Indeed, a crack that has unstably accelerated to c_R will find it difficult to transit to one of the U-shaped curves of the intersonic interval. In particular, the magnitude of the normalized driving stress required to propagate a crack at a speed just above c_S is unbounded, making shear-sonic crack growth practically impossible. For each value of the parameter $(\mu\delta_t^C)/(\tau_0 D)$, one can investigate the effect of the applied load in promoting subRayleigh crack growth, intersonic rupture growth, or both, by visualizing a horizontal line intersecting the various branches of figure 19. Three possible regimes are identified. If the normalized load is such that the horizontal line lies below the minimum of the U-shaped curve, then only subRayleigh crack growth is possible. However, if this level is increased up to the value of 1, then the horizontal line will

intersect both the subRayleigh and the intersonic branches. The rupture will first grow at a speed close to the first (subRayleigh) intersection point and then it will accelerate unstably to c_R. In this case, it is also conceivable that a rupture may initiate in either regime or it may even jump from subRayleigh to intersonic by utilizing the Burridge–Andrews mechanism. Finally, if the level is clearly above unity, only two intersonic intersections are possible. Here, a rupture could be 'born' intersonic at a level close to the first, lower speed, intersection with the U-shaped curve. It will then unstably accelerate to the minimum value and will remain there unless the driving force is increased. This minimum value is always higher than or equal to $\sqrt{2}c_S$.

Let us now turn our attention to the discussion of the tensile damage observed in the bonded Homalite/Homalite experiments. This secondary damage took the form of microcracks that nucleated at small distances (1–2 mm) behind the main intersonic rupture. A damage that was always confined to the upper half of the specimen. Remarkably, these cracks were all found to be almost parallel to each other with their angle of forward inclination θ^* varying between 8° and 13° to the normal of the weak plane.

As was argued in section 2.2, the driving force leading to microcrack initiation is provided by the near tip field associated with the main intersonic rupture. At this point, the near tip field of the velocity weakening cohesive zone model discussed above, will be used in conjunction with the maximum tensile principal stress criterion in order to study the nucleation of these microcracks. Here the purpose is to determine the feasibility of secondary crack initiation and, if possible, to extract some of the unknown model parameters describing the physical system used in the experiments. The maximum principal tensile stress at any point on the upper cohesive surface is given by

$$\sigma_1(-L < \eta_1 < 0, \eta_2 \rightleftarrows 0^+) = \frac{\sigma_{11}}{2} + \left(\left(\frac{\sigma_{11}}{2} \right)^2 + \sigma_{12}^2 \right)^{1/2}, \tag{2.17}$$

while the angle of inclination of the principal plane with the vertical (see figure 12(b)) is given by

$$\theta^*(-L < \eta_1 < 0, \eta_2 \rightleftarrows 0^+) = \frac{1}{2} \tan^{-1} \left(\frac{-2\sigma_{12}}{\sigma_{11}} \right). \tag{2.18}$$

For a given normalized rupture speed v/c_S and velocity weakening factor β, the variation in σ_1/τ_0 and θ^* can be obtained within the entire cohesive zone. This is achieved by substituting the normalized stresses σ_{11}/τ_0 and σ_{12}/τ_0, which appear in figures 15 and 16, into equations (2.17) and (2.18). These variations have been analytically obtained in [58] and will not be shown here. In assuming that the material obeys the maximum principal stress criterion for brittle fracture, a tensile microcrack would initiate at a point $\eta_1 = -L^*$ in the upper cohesive surface where the tensile principal stress reaches a critical level σ_u (i.e. $\sigma_1 = \sigma_u$). This critical stress level σ_u is the ultimate tensile strength of the homogeneous material, which for monolithic Homalite is equal to 35 MPa. The location L^*, where this criterion is first satisfied, corresponds to a particular value of the principal angle θ^*.

By using the procedure elaborated in [58], the functional dependence of θ^* on v/c_S, τ_u/τ_0, and β can be obtained. For a particular material system and bond strength, τ_u/τ_0 is fixed and can be measured in the laboratory. For the experiments

discussed above, this ratio is equal to 2.5, but the value of β, the velocity weakening parameter, is much more elusive. This is due to the scarcity of experimental information available in the literature on dynamic sliding. In fact, the nature of the velocity weakening behaviour at as high rates as those experienced within the cohesive zone is unknown. To provide a realistic first order estimate of β, the angle of inclination θ^* of the microcracks is plotted in figure 20 as a function of β. The effect of different intersonic speeds is also displayed. The ratio τ_u/τ_0 is taken to be equal to 2.5.

Figure 20 shows that a maximum angle of inclination of 21.8° is obtained for the rate insensitive case of $\beta = 0$ (Dugdale zone). For this case, the angle is independent of rupture speed. As β decreases, θ^* is monotonically reduced. For example, for $v = \sqrt{2}c_S$, the inclination reaches the experimentally observed average value of 11° at $\beta = -0.4$. However, at this value of β, the angle of inclination varies with the intersonic speed, from approximately 8° to 14.5°. The predicted variation is very close to the statistical variation reported in figure 11(c). Therefore $\beta = -0.4$ is an optimal estimate for the conditions that prevail in the Homalite/Homalite experiments.

Having established the optimal value of the velocity weakening parameter β, the cohesive zone solution can be used to construct 'synthetic' isochromatic patterns. A direct visual comparison of the model with the experiment is now possible. Figure 21 shows two such synthetic photoelasticity patterns corresponding to two intersonic rupture speeds and to identical material properties. The details leading to their construction can be found in [58]. In both figures, we can see that the presence of a cohesive zone gives a finite width to the Mach waves and it reveals the existence of a distinctive fringe structure. Such a structure is shown magnified on the right of each figure. In figure 21(a), the rupture speed is equal to $1.2c_S$ and the cohesive zone size is

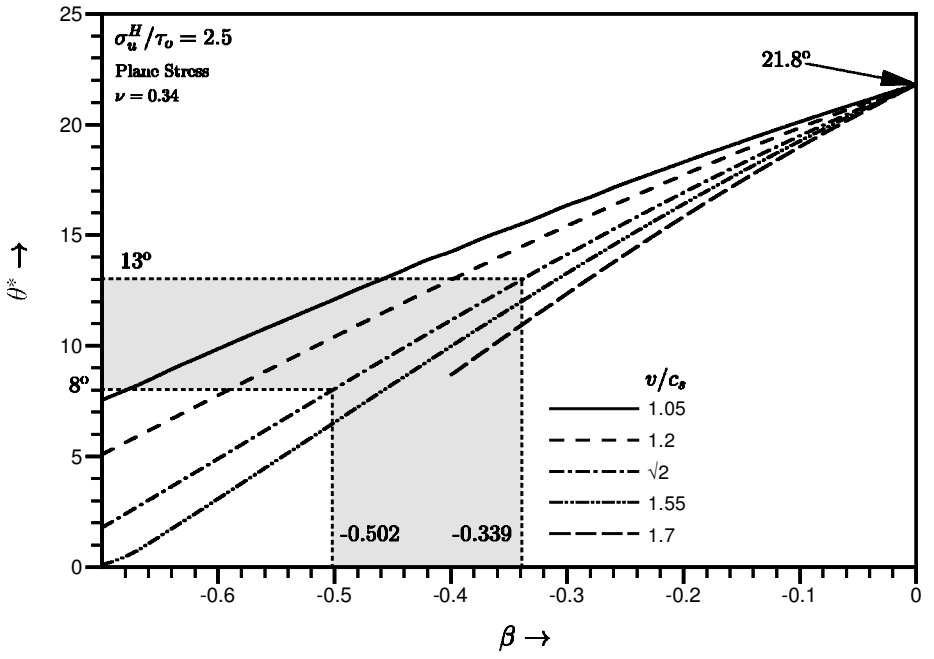

Figure 20. Inclination angle of microcracks to the vertical, plotted as a function of the slip rate weakening parameter β.

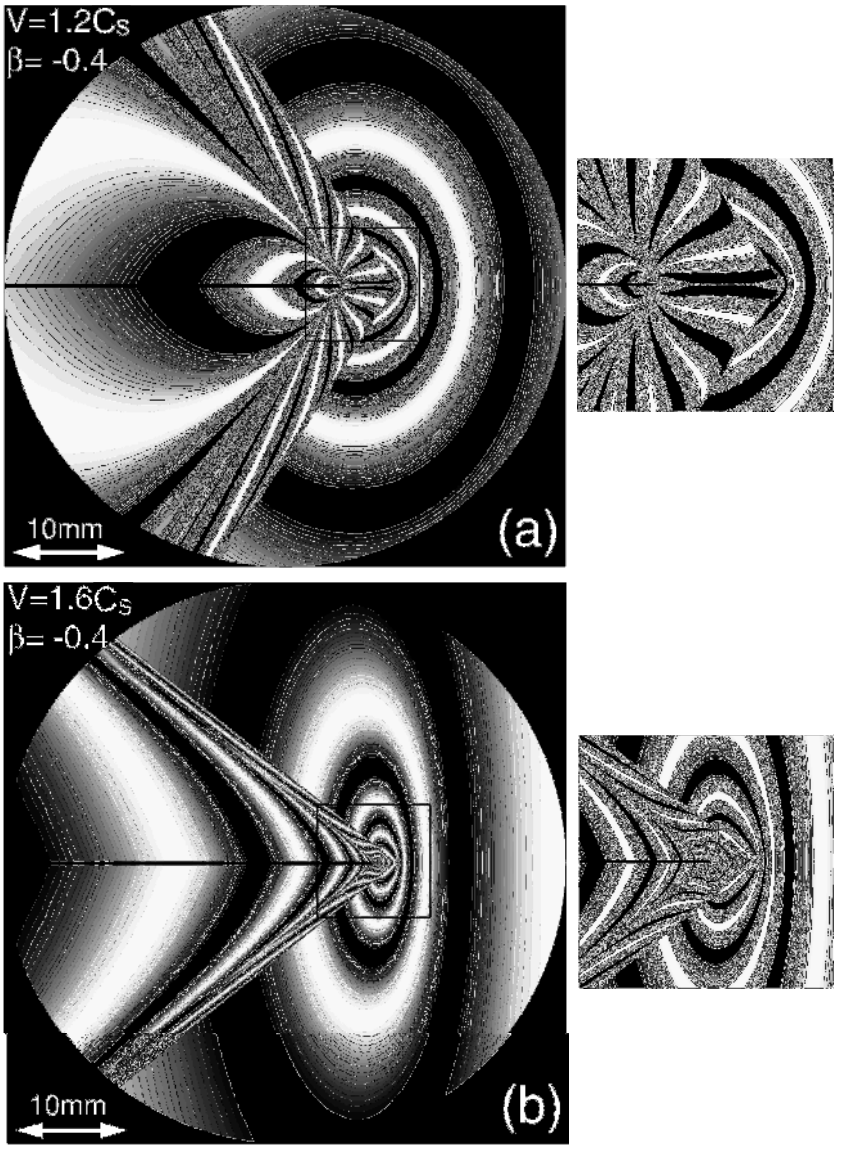

Figure 21. Synthetic isochromatic patterns constructed using the steady state velocity weakening cohesive zone model of reference [58].

5 mm. In figure 21(b), the rupture speed is equal to $1.6c_S$ and the cohesive zone size has dropped to almost 2.6 mm. The inclination of the Mach waves, as well as the shapes of the isochromatic fringes behind the Mach lines, are noticeably different.

3. Field evidence of intersonic fault rupture

The review so far has hinted at several crucial points. Firstly, and most significantly, the review strongly suggests that the experimental, as well as the theoretical paradigms allow for the possibility that shear rupture may, in fact,

become intersonic. Secondly, it suggests that although certainty of such a phenomenon cannot be attained, the experimental paradigm should be expanded to include seismological field studies. Thirdly, the conventional wisdom in seismology, which speaks of crustal ruptures that can propagate only at subRayleigh speeds between $0.75c_R$ and $0.95c_R$, may have to be revised.

Indeed, the process of rupture is rather irregular owing to the heterogeneities of fault strength. As a result, local intersonic bursts of rupture speed cannot be excluded in view of the indirectness of seismological measurements. Evidence of the existence of such 'bursts' is generally averaged out by the lack of resolution in the inversion process. In fact, in a few cases, clear evidence does exist that ruptures are propagating at supershear speeds over substantial parts of a fault. One such case is the 1979 Imperial Valley earthquake in California analysed by Archuleta [38]. His results have clear support from observations reported by Spudich and Cranswick [74]. In this particular event, the reported length of intersonic rupture was sufficiently large that the inference of the speed was not greatly affected by the averaging nature of the inversion process.

In some other earthquake events, such as the 1992 Landers earthquake, Hernandez *et al.* [40] and Olsen *et al.* [39] reported that rupture may have locally exceeded the shear wave speed over fault patches that were only a few kilometres in length. The evidence here is not as conclusive as it is in the Imperial Valley earthquake, since rupture speed over such small distance ranges is poorly resolved. The most recent and perhaps the most conclusive evidence of intersonic rupture propagation comes from the 1999 Izmit and Düzce earthquakes in Turkey.

3.1. *The Izmit and Düzce earthquakes*

The Izmit earthquake occurred on 17 August, 1999 and ruptured a long segment of the North Anatolian fault. According to Toksöz *et al.* [75], its surface rupture extended from east to west and over a length of approximately 120 km. This event was recently analysed by Bouchon *et al.* [42, 43]. The Düzce earthquake occurred three months later and extended the rupture zone of the Izmit earthquake by 40 km to the east. A discussion of this event was also presented by Bouchon *et al.* [43]. Figure 22 illustrates the segment of the fault along which the rupture propagated during the Izmit earthquake. The red star located along the fault line is the estimated position of the hypocentre. To the left of the figure, the triangle marked 'ARC' indicates the location of one of the recording stations. This station is located 55 km to the west of the hypocentre. Another station, also indicated by a triangle and marked 'SKR', is located 40 km east of the hypocentre. The fault, which is vertically dipping, is 150 km long and, as indicated by the red line in the figure, it trends almost east–west [43]. The nearly symmetric location of the two ground stations with respect to the hypocentre is fortuitous. Indeed, one would expect that because of this symmetry the east–west ground motion recorded at the two sites would be comparable. Obviously, this could have been the case, provided that the slip propagated self-similarly from the hypocentre outwards.

The horizontal ground accelerations at the two sites (ARC to the west and SKR to the east) are shown on the lower part of figure 22. To the west, the arrival of the dilatational (P) and shear wave (S) trains can be clearly identified. As expected in a classically subRayleigh rupture event, the fast moving dilatational wave emitted from the hypocentre arrives first. Then the slower shear waves were recorded. Soon after the arrival of the shear waves, strong ground shaking commences following the

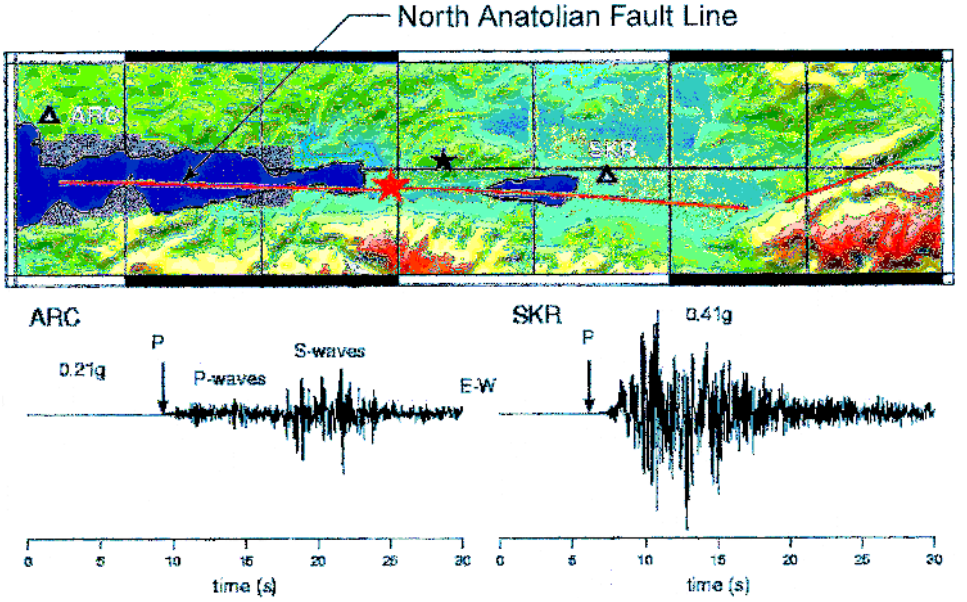

Figure 22. (Top) Map showing the hypocentre (⋆) of the Izmit earthquake, the ruptured segment of the North Anatolian Fault, and two recording locations (ARC and SKR). (Bottom) The ground acceleration records (figure modified from Bouchon *et al.* [43]).

arrival of the rupture front, which usually propagates at a large fraction of the shear wave speed. There is nothing unusual about this record and, indeed, a full inversion confirms that the rupture propagated to the west with a speed 3000 m s^{-1}, which was very close to the Rayleigh wave speed of the upper crust.

An astonishing result, however, was reflected in the SKR record. In this record, the two wave trains seem to be mixed together and, surprisingly, strong ground shaking commences only 1.8 s after the arrival of the dilatational P wave. This constitutes a strong indication that the rupture arrived at the vicinity of SKR well before the arrival of the S wave that was generated at the hypocentre [42, 43]. Indeed, under normal circumstances, this shear wave would arrive at SKR at a time approximately 4.5 s later than the arrival of the P wave. If such an interpretation is indeed correct, the strong ground motion observed at SKR results from shear wave induced excitations associated with the passage of the shear shock waves (shear Mach lines) that radiate from an intersonically moving rupture tip. In fact, this would be consistent with the observation that when the acceleration records are integrated, the maximum resulting ground velocities are approximately 0.82 m s^{-1}, which is 4.5 times greater than in ARC. Since most of the seismic energy released in earthquakes is radiated in the form of shear waves, the two dramatically different records show that the ruptures extended to the west and to the east have drastically different speeds. To the west, the rupture propagated close to the classical Rayleigh wave speed allowing for the clear separation of P and S waves. To the east, however, the rupture grew intersonically and it did so as it produced strong Mach wave induced shaking at SKR. This happened before the expected arrival of the normal S wave. The rupture speed to the east was initially directly inferred from the S–P time on the SKR record. As shown by Ellsworth and Celebi [41] and by Bouchon *et al.*

[43], the average speed thus calculated was $4700\,\mathrm{m\,s^{-1}}$. Compensating for the fact that the station was located a few kilometres from the fault and that it really records the inclined shear shock waves of the rupture (see figure 8), Bouchon *et al.* [42] calculated a speed in the range of $4800\,\mathrm{m\,s^{-1}}$ to $4900\,\mathrm{m\,s^{-1}}$. Consistent with this range of values, inversion of the entire records predicts speeds in the range between $4700\,\mathrm{m\,s^{-1}}$ and $4900\,\mathrm{m\,s^{-1}}$. In addition, use of these rupture speeds in the modelling led to accurate prediction of SKR records. What is perhaps even more remarkable about this inference is the observation that this speed is very close to the curious speed of $\sqrt{2}c_S$ whose significance we have been discussing throughout the present article. Finally, it is worth noting that the east running segment over which rupture propagated at supershear speeds makes a remarkably linear surface scar, often no more than a metre wide. This is seen in the field and has been discussed by Michel and Avouac [76]. The thus implied simple planar morphology of the fault may have contributed to the establishment of uninterrupted intersonic rupture growth for nearly 50 km. In contrast, to the west the rupture entered the more complex faulting system of the Marmara Sea whose complex morphology may have slowed down its growth.

Three months after the Izmit earthquake, the Düzce earthquake took place and once again featured intersonic eastward and subRayleigh westward ruptures. To the east, the estimated average speed was $4300\,\mathrm{m\,s^{-1}}$, while to the west the rupture speed was $3000\,\mathrm{m\,s^{-1}}$. It is perhaps unnecessary to overemphasize the connection between this remarkable field evidence and the results of the experiments together with the theory presented in sections 2.1–2.3. However, it may be informative at this point to refer once again to figure 19, which discusses the issue of stability of shear crack growth along a fault in relation to the velocity weakening cohesive model. The figure clearly shows that at certain levels of normalized applied load, both subRayleigh and intersonic crack growth may be possible. This can be seen by drawing a horizontal line across the curve at a vertical height slightly above 0.7. As discussed in section 2.3, this line would intersect the unstable subRayleigh branch at a speed close to c_R producing, as a result, a classical subRayleigh rupture. This rupture will perhaps accelerate up to c_R because of the unstable nature of the branch. The horizontal line would also generally intersect the intersonic branch at two points. Depending on the material properties and fault strength, the intersonic crack would first propagate at the speed of the first intersection with the U-shaped curve and will subsequently settle to its minimum value as steady state is achieved. This minimum is always slightly above $\sqrt{2}c_S$, its exact location depending on the fault strength. So following this scenario the possibility that an earthquake event may feature concurrent subRayleigh and intersonic growth is realistic. By emphasizing a similar line of thought, the same fault may subsequently host purely subsonic ruptures (after-shocks) provided that the far-field stress has been sufficiently relaxed so that only subsonic intersections are possible.

3.2. *Field evidence of tensile microcracking*

We shall finish this section with a short discussion of more circumstantial field evidence of the existence of secondary damage processes of the type observed in the laboratory studies described in section 2.2. One should recall that the dynamic experiments revealed the formation of secondary tensile microcracks trailing the main shear rupture. As shown in figures 11 and 12 these microcracks were highly

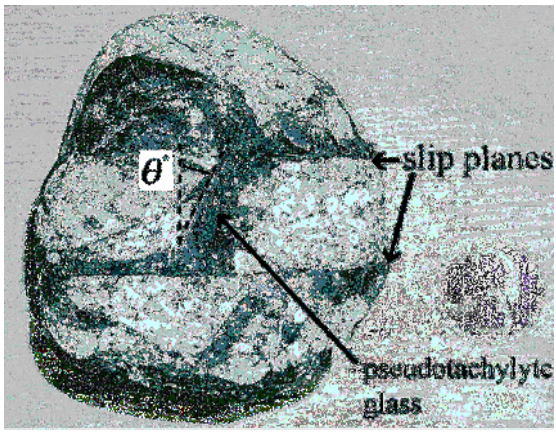

Figure 23. A rock piece from an exhumed fault located in the Outer Hebrides thrust zone in Scotland. Horizontal slip planes and opened secondary tensile cracks are visible. The black material within the opened cracks is pseudotachylyte. (Courtesy of S. Das, Oxford University [77].)

periodic and were forwardly inclined at an angle θ^* to the vertical of the slip plane. The statistical variation of θ^*, shown in figure 11, reveals a range of angles between 8° and 14°. The velocity weakening model of section 2.3 is capable of predicting this phenomenon and explains the angle variation in terms of variations in intersonic crack tip speeds (see figure 20).

Figure 23 is a photograph of a weathered piece of rock curved out of an ancient exhumed fault in the Outer Hebrides thrust zone in Scotland. It was sent to the author by S. Das of Oxford University who was aware of his interests in intersonic shear rupture [77]. The two horizontal planes visible in this picture appear to be slip planes whose thickness is very small and is of the order of 1 mm. The dark bands, inclined to the right, seem to be gaps resulting from secondary tensile cracking of the type described above. These gaps are filled with a black substance called 'pseudotachylyte' which, according to Sibson [78], is a glassy, amorphous solid. As discussed by Scholz [22], the appearance of natural pseudotachylyte is a clear indication of adiabatic frictional melting induced along the thin fault lines during dynamic rupture. As a result, there is strong evidence that the observed inclined tensile cracks are formed as part of a dynamic process. In fact, the most plausible scenario states that the molten material generated during frictional sliding gets ejected into the gaps formed by the secondary tensile cracks as these open up behind the propagating main rupture. As the molten material enters into the gaps it rapidly cools and solidifies forming the amorphous pseudotachylyte glass.

Very clear evidence of the existence of a periodic array of tensile microcracks inclined at a steep angle to a slip direction is shown in figure 24. The series of photographs shown in this figure were taken in August 2001 during the author's visit to the island of Skopelos in Greece. Figure 24(a) clearly shows a now exposed slip plane of an uplifted ancient fault that has been subjected to continuous erosion by air and water. The circled area is magnified in figures 24(b)–(d). These reveal the existence of multiple slip planes, all parallel to the exposed fault plane that is visible

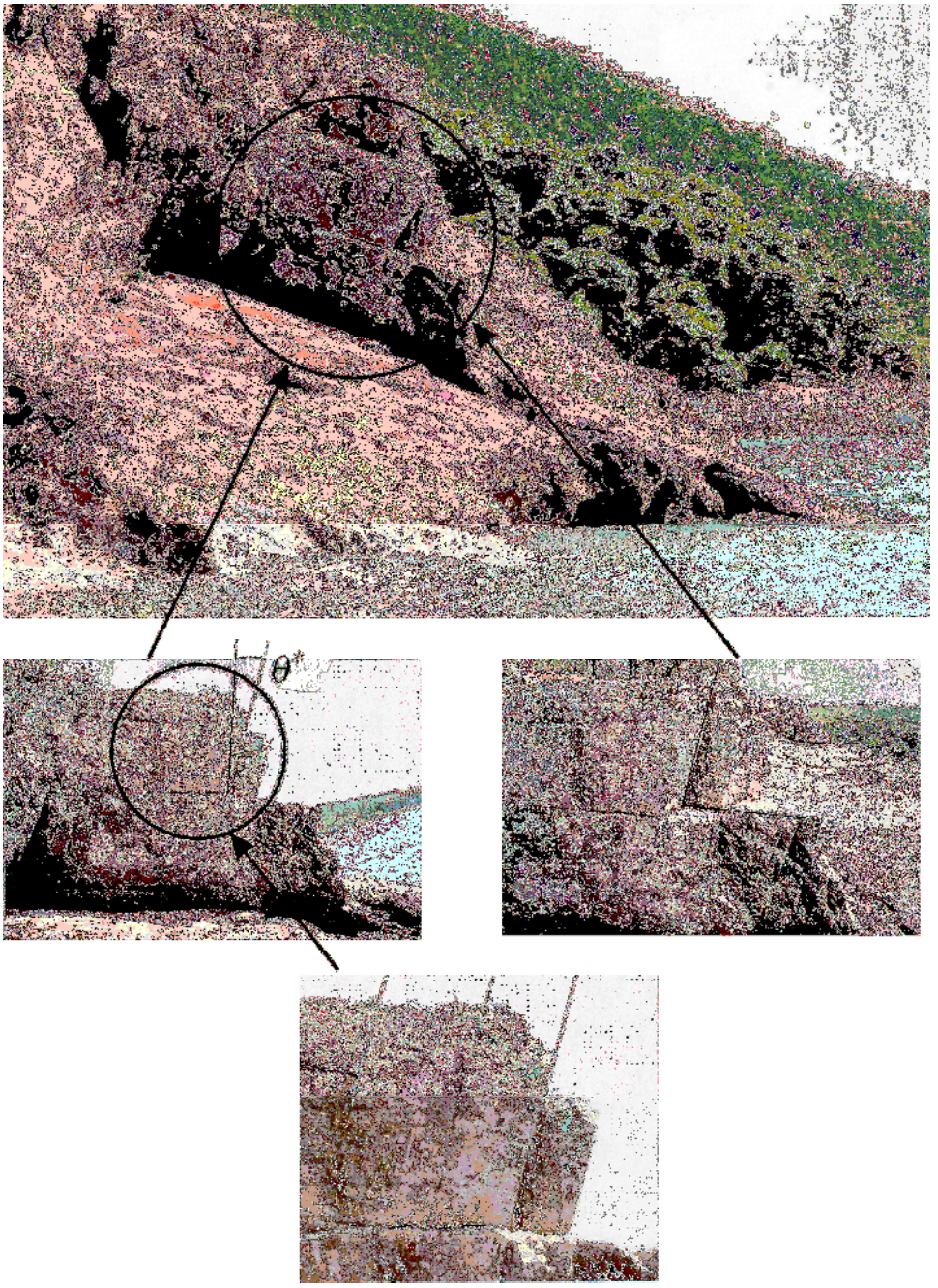

Figure 24. An uplifted and exposed ancient fault plane in the island of Skopelos, Greece. (a) Global view, (b), (c) magnified view of exposed tensile fracture surfaces, (d) periodic array of parallel tensile cracks inclined at shallow angles θ^* to the vertical.

in 24(a). The three magnifications also reveal the presence of a very periodic array of tensile microcracks that are inclined at an angle θ^* of the vertical to the slip plane. The tensile nature of these cracks is evident from recently exposed fracture surfaces shown in figure 24(c). The angle of inclination varies between 9° and 12°. This is consistent with the experimental results displayed in figure 11 and with the analytical predictions of figure 20. Finally, visual inspection of the base of the circled structure in figure 24(a) revealed remaining evidence of the presence of pseudotachylyte glass as a testimony of the dynamic origins of the failure process.

Visual field evidence of damage presented in this last section is not meant to provide conclusive proof of the existence of intersonic shear rupture processes in the earth's crust. Instead, our purpose is only to demonstrate that intersonic processes discovered under highly controlled laboratory conditions and analysed with models of intersonic shear rupture are capable of qualitatively predicting ancient rock damage of the type still visible in the field. Moreover, it should be emphasized that tensile cracking is a common occurrence in the earth's crusts and has been attributed to a variety of static and dynamic deformation and crack branching mechanisms (see Sagy *et al.* [79] and Poliakov *et al.* [80]).

4. Recent continuum and atomistic models of intersonic shear rupture

We conclude our discussion of intersonic shear rupture of bonded identical isotropic solids by briefly reviewing some recent important analytical and numerical contributions of significance to the dynamic rupture literature. Using a newly developed cohesive element methodology in conjunction with the finite element method, Needleman [81] simulated the Homalite/Homalite experiments described earlier. He conducted a highly systematic study of the parameter space of relevance to the intersonic rupture phenomenon. In particular, his work examined the effect of shear strength, of fracture energy, and of projectile impulse duration on the subRayleigh to intersonic transition. If the projectile pulse duration is not cut off, the shear rupture propagates at c_R provided that the bond strength remains high enough to prevent intersonic growth. If the bond strength is lowered, the rupture, after spending some limited time at c_R, accelerates to a constant intersonic speed above $\sqrt{2}c_S$. As the bond strength becomes even weaker, the rupture approaches the dilatational wave speed of the solid. The transition from Rayleigh to intersonic speed is found to involve the Burridge–Andrews mechanism. When the duration of the pulse is cut off, the intersonic crack decelerates to $\sqrt{2}c_S$ and after a while it becomes subRayleigh then abruptly arrests. Needleman's numerical work has been crucial to our understanding of the intersonic shear rupture phenomenon.

Using a spectral boundary element method, Geubelle and Kubair [82] studied the problem of transient initiation and growth of a mixed-mode crack propagating along a straight-line path under the action of asymmetric far-field loading. Their work employs the use of a quasi-linear rate independent cohesive failure model, which couples the normal and the shear cohesive failure modes. Their work examines the loading and bond strength conditions under which mode-II and mixed-mode crack growth can occur in either the subRayleigh or the intersonic speed regimes. For the purely mode-II case and for the low values of bond toughness, their results show that subRayleigh crack propagation is possible only for moderate values of the shear loading. For higher values of bond toughness no subRayleigh regime is observed and what is only possible is intersonic growth.

For the mixed-mode case, Geubelle and Kubair found that the higher the shear component of the applied load, the lower the load level required to achieve intersonic crack propagation. For subRayleigh mixed-mode crack growth both opening and sliding displacements are observed at the cohesive zone. However, for intersonic crack growth only sliding displacements appear near the growing tip and opening displacements appear only outside the cohesive zone. This is a remarkable observation since it links local shear failure to intersonic conditions even when the far-field loading is not purely asymmetric.

Abraham and Gao [83] performed the first atomistic simulation of shear rupture along a weak interface. This interface was between two harmonic crystals and characterized by a Lennard-Jones potential. Their simulations showed that a shear dominated crack, or atomistic rupture, accelerates to speed c_R soon after initiation. At that point, the crack promotes the nucleation of an intersonic microcrack that travels at speed c_ℓ, in accordance with the Burridge–Andrews mechanism.

A visual demonstration of the nucleation of the secondary microrupture in front of the primary Rayleigh crack has been illustrated by F. Abraham and H. Gao [83] and is displayed in figure 25. Figure 25(a) shows the primary rupture and it also illustrates in front of it, along the bond, a small decohered line, which is indicated by an arrow. Initially, the microrupture propagates at approximately the shear wave speed. Shortly thereafter, the two ruptures join up and the combination accelerates through the intersonic regime as it is evidenced by the two inclined Mach waves attached to the tip. When the simulation involves bonded harmonic crystals, which mimic the linear elastic behaviour, the recorded terminal speed is c_ℓ. When the applied far-field strains are subsequently relaxed, the crack decelerates to $\sqrt{2}c_S$ in a manner similar to that observed in the Homalite/Homalite experiments of section 2.2.

The possibility of supersonic crack growth was investigated in [83] and also in a more recent, three-dimensional simulation involving bonded unharmonic crystals by Abraham [84]. In this study the local wave speeds at the highly strained crack tip region are higher than those of the unstrained bulk solid. This is due to the nature of the specific unharmonic potential used in the study. Consequently, the crack is able to propagate supersonically with respect to the 'linearized' wave speeds (unstrained limit) of the crystal. However, with respect to the wave speeds of the highly strained crack tip region, the crack is still p-sonic. Figure 26 shows the acceleration process of the shear crack past the intersonic regime.

The well-formed set of inclined lines seen in figures 26(a) and (b) correspond to the shear shock waves. Since the crack speed is very close to the dilatational wave speed (figure 26(b)) a second set of lines signals the imminent development of a dilatational or pressure shock wave front. This process is completed in figure 26(c).

The clear observation of the subRayleigh to intersonic transition, as well as the reappearance of the curious speed of $\sqrt{2}c_S$ in an atomistic setting, is extremely significant. Indeed, the scale at which the atomistic calculation is performed is six orders of magnitude smaller than the laboratory experiments and 11 orders of magnitude smaller than the crustal fault rupture events. Yet, the main features observed under laboratory situations and those predicted by continuum theory are still preserved to a remarkable level of detail. To demonstrate that point conclusively, Gao *et al*. [85] compared the atomistic calculations with continuum level

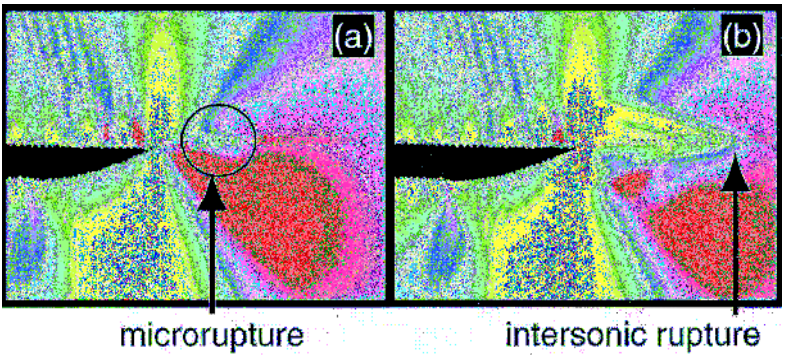

Figure 25. The first atomistic view of the 'Burridge–Andrews mechanism' responsible for subRayleigh to supershear transition (courtesy of F. Abraham, IBM, and H. Gao, Max Planck Institute [83]).

analysis thus demonstrating the magnificent predictive power of continuum mechanics over a variety of length scales.

Finally, the most recent analytical contributions to the subject of intersonic crack growth include the work by Huang and Gao [86] and by Antipov and Willis [87]. These workers obtained the fundamental solution of a transient intersonic mode-II crack propagating in an elastic and a viscoelastic solid, respectively.

Our discussion will be incomplete if we fail to point out that the intersonic motion of other shear dominated processes, such as dislocations and twins, have clear similarities to shear rupture. In fact, Eshelby [88] and Weertman [89] early on showed that radiation free intersonic motion of a glide dislocation in an isotropic solid is possible at a steady-state speed of $\sqrt{2}c_S$. Indeed, many authors refer to this radiation free speed as the 'Eshelby' speed. Furthermore, Weertman showed that no such critical speed exists for climb dislocations. Such observations are indeed consistent with the arguments presented in the present review. It is true that an intersonically propagating mode-II crack can be constructed by the superposition of a continuous array of glide dislocations, whereas a mode-I crack can be considered as a superposition of an array of climb dislocations. To make this connection, a unified continuum mechanics treatment of both intersonic cracks and dislocations was developed by Gao *et al.* [90]. More recently, a study of intersonic glide dislocations within the framework of discrete atomistic models was reported by Gumbsch and Gao [91]. Finally, the possibility of 'supersonic' growth of dislocations was discussed analytically by Rosakis [92]. In this study, the classical Peierls model was modified to account for drag and for higher gradient effects and was used to demonstrate that the presence of higher gradients allows for the possibility of supersonic dislocation motion. The model was then used to examine regimes of stable and unstable dislocation motion and to compare the analytical predictions with the atomistic calculations of Gumbsch and Gao. The intersonic growth of mechanical twins was discussed by Rosakis and Tsai [93] and their intersonic behaviour was related to the experimentally observed phenomenon of 'twin-cry' (acoustic emission associated with the presence of shear shock waves at growing twin tips).

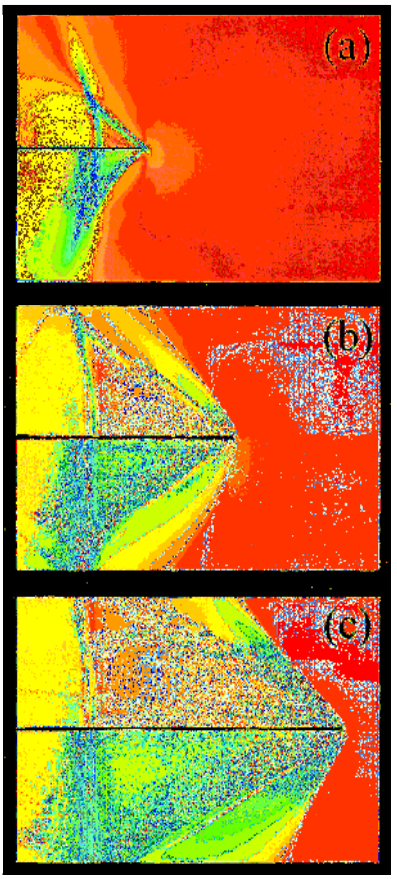

Figure 26. A shear crack rupturing a 'Lennard-Jones' weak interface joining two unharmonic bcc crystals. The crack accelerates through the intersonic regime and eventually becomes supersonic (courtesy of F. Abraham [84]).

5. Rupture of constitutively homogeneous systems containing weak planes: anisotropic materials

Our discussion so far has concentrated on constitutively homogeneous and isotropic solids that also contain weak paths along which shear ruptures may be trapped and may propagate dynamically. We have demonstrated that such ruptures may attain intersonic speeds and may propagate as fast as the dilatational wave speed of the isotropic material. We have investigated issues of crack tip stability and have shown that certain multiples of the isotropic wave speeds delineate the boundaries of acceptability of stable intersonic shear rupture. In this section, we extend our discussion to the study of dynamic rupture in simple anisotropic materials also containing preferable rupture paths. In particular, we shall discuss recent experiments by Coker and Rosakis [94], who studied dynamic rupture of thick unidirectional fibre reinforced composite plates subjected to impact loading.

Dynamic crack growth along weak planes is a predominant mode of failure in all types of structural composite materials, as well as in most layered graded or sandwich structures. With increasing demand for specialized, lightweight, and

high-strength structures, the failure mechanisms encountered in such composites have been receiving increased attention from the engineering community. The particular case of a unidirectional graphite fibre, polymer matrix composite that will be discussed here represents perhaps the simplest case of a truly anisotropic material of some practical significance. When viewed 'macroscopically', the details of the fibre dimension and local properties become invisible and a homogenized constitutive description may be adopted. Through this homogenization, the composite material appears as 'anisotropic' but is still considered constitutively homogeneous and features drastically different stiffness and wave speed along different directions. In addition to introducing wave speed anisotropy, the fibres have another effect. They also feature weak crack paths along their interface with the matrix. These paths are lines along which the fracture resistance of the solid is drastically lower than in any other direction. As a result, the solid can be viewed as inhomogeneous regarding its resistance to fracture in much the same way the bonded Homalite/Homalite plates were viewed earlier.

Figure 27 shows the geometry of the composite plates used in the fracture experiments. It also displays micrographs of the fibre microstructure corresponding to two areas within the plate thickness. Unidirectional composites of the type shown in figure 27 are modelled by a very simple anisotropic constitutive law and are known as 'transversely isotropic' materials. The details of their constitutive description are given in [94] together with the values of various physical properties of the particular material under consideration. The particular type of material anisotropy introduced by the fibres results in different bulk wave speeds of

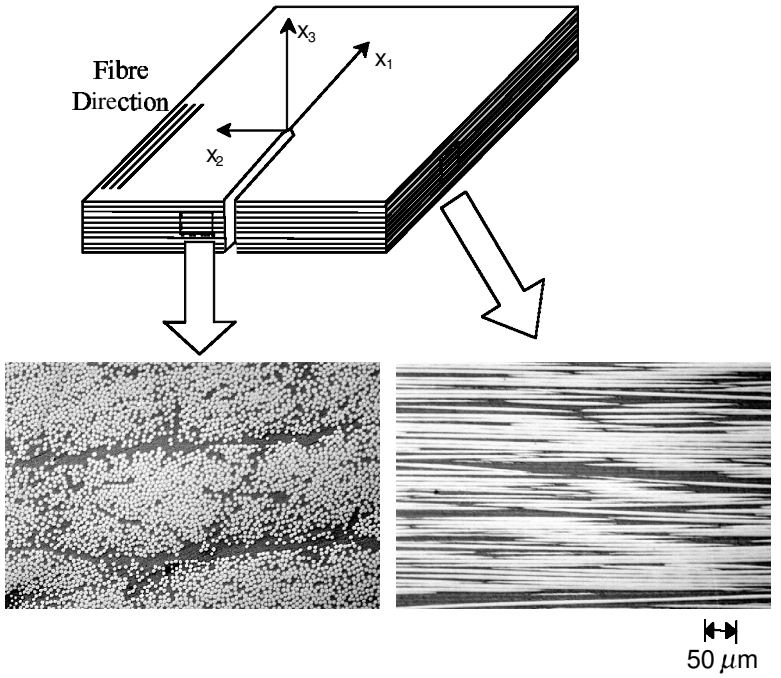

Figure 27. View of a thick composite plate containing a notch. The micrographs provide cross-sectional views of the microstructure of the unidirectional graphite–epoxy material.

dilatational waves travelling along the two principal directions of anisotropy. The shear wave speed, however, is independent of direction. The dilatational wave speed c_ℓ^{II} along the direction of the fibres is $7500\,\mathrm{m\,s^{-1}}$, the dilatational speed $c_\ell^{\perp}$ perpendicular to the fibres is $2700\,\mathrm{m\,s^{-1}}$, while the shear wave speed c_{S} is $1550\,\mathrm{m\,s^{-1}}$. It should be noted that $c_\ell^{\perp}$ is only slightly higher than that of the polymer matrix, while c_ℓ^{II} is slightly lower than that of the graphite fibres. Also, $c_\ell^{\mathrm{II}} = 2.8c_\ell^{\perp}$. The Rayleigh speed $c_{\mathrm{R}}^{\mathrm{II}}$ of surface waves propagating parallel to the fibres on the surface of a transversely isotropic half space of the same material considered in [94] is $c_{\mathrm{R}}^{\mathrm{II}} = 0.99c_{\mathrm{S}} = 1548\,\mathrm{m\,s^{-1}}$. Plates of the type shown in figure 27 were subjected to impact loading through a projectile fired by a gas gun at speed varying from $10\,\mathrm{m\,s^{-1}}$ to $57\,\mathrm{m\,s^{-1}}$. A schematic diagram of the experimental arrangement is shown in figure 28.

The plates were impacted at the plate's edge opposite the initial notch. When the projectile impacted the plate along the specimen centre line, the resulting stress waves loaded the initial notch symmetrically and the resulting failure was in the form of a growing mode-I crack. When the specimen was hit below the centre line, the loading of the notch was shear dominated and the resulting failure proceeded in the form of a mode-II crack. In both cases, the existence of weak fibre–matrix interfaces forced the crack to grow directly ahead of the notch tip along the horizontal centre line. In order to record the history of crack growth, the method of coherent gradient sensing (CGS) [10], was used in a reflection arrangement and in conjunction with high-speed photography (2×10^6 frames $\mathrm{s^{-1}}$). The fringe patterns visible in the images that follow are contours of equal out-of-plane surface displacement gradient, $\partial u_3/\partial x_1$. They are intimately related to the stress state near the propagating crack tip and their shape and size reflects the nature and the intensity of the near tip singularity.

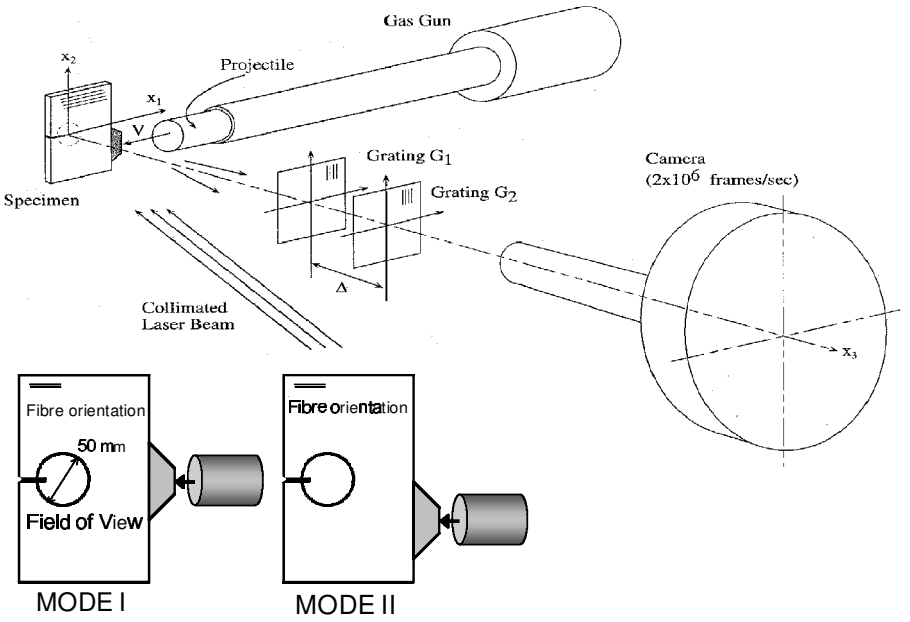

Figure 28. Diagram of the high-speed photography experimental set-up and the optical method of CGS shown in a reflection arrangement.

5.1. *Symmetric crack growth along the fibres*

Symmetric, mode-I, crack tip deformations were obtained by impacting the specimen symmetrically along the notch line as described earlier. Three images from a sequence of CGS interferograms, corresponding to mode-I crack initiation and growth, are shown in figure 29 for the highest impact speed of $57\,\mathrm{m\,s^{-1}}$. Images of this type allow for the measurement of crack tip speed and for the estimation of dynamic fracture parameters.

The images in figure 29 show that for the symmetric loading case, the resulting mode-I cracks propagate dynamically along the fibres, ahead of the initial notch tip, and attain very high speeds without displaying any tendency to branch. The crack tip speed histories of three mode-I experiments corresponding to three different projectile impact speeds are shown in figure 30. As the impact speed is gradually increased so is the speed of the resulting mode-I cracks. However, there is a critical level of impact speed beyond which changes in crack tip speed are no longer achievable. In fact, as discussed in [94], the mode-I cracks seem unable to ever exceed the Rayleigh wave speed of the composite (horizontal line) irrespectively of the far-field energy available to it through impact loading. This phenomenon is very consistent with the discussion presented in section 1.2. It is analogous to the behaviour of dynamic mode-I cracks in bonded isotropic solids [15] and shows that $c_{\mathrm{R}}^{\mathrm{II}}$ is still the limiting speed of the transversely isotropic solid in the presence of preferable crack paths along the fibres.

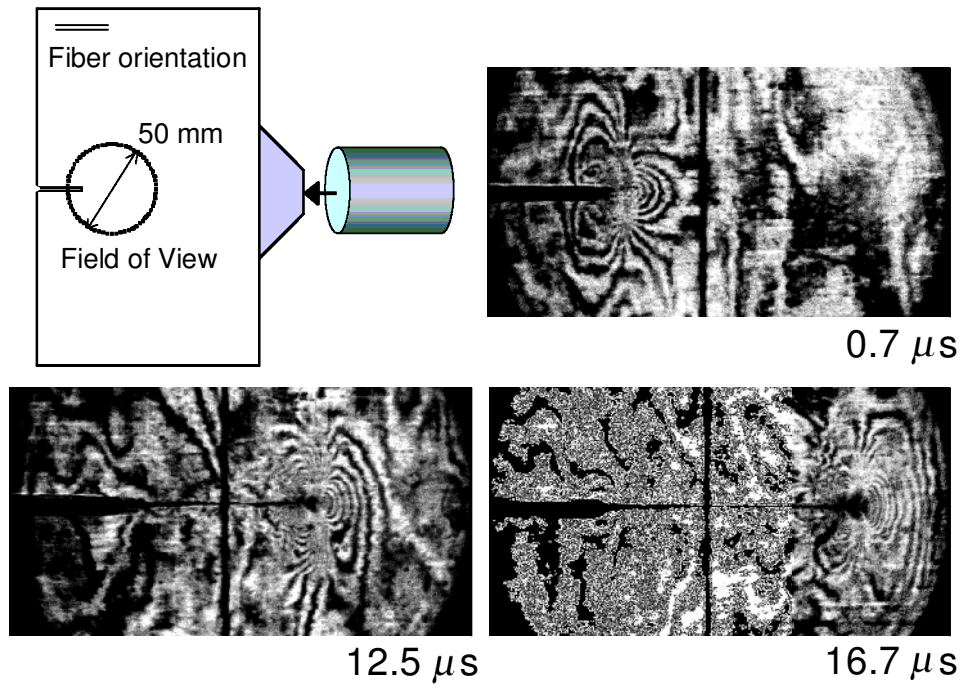

Figure 29. CGS interferograms illustrating the process of initiation (from a notch) and dynamic growth (along the horizontal fibres) of a mode-I crack in a unidirectional composite plate.

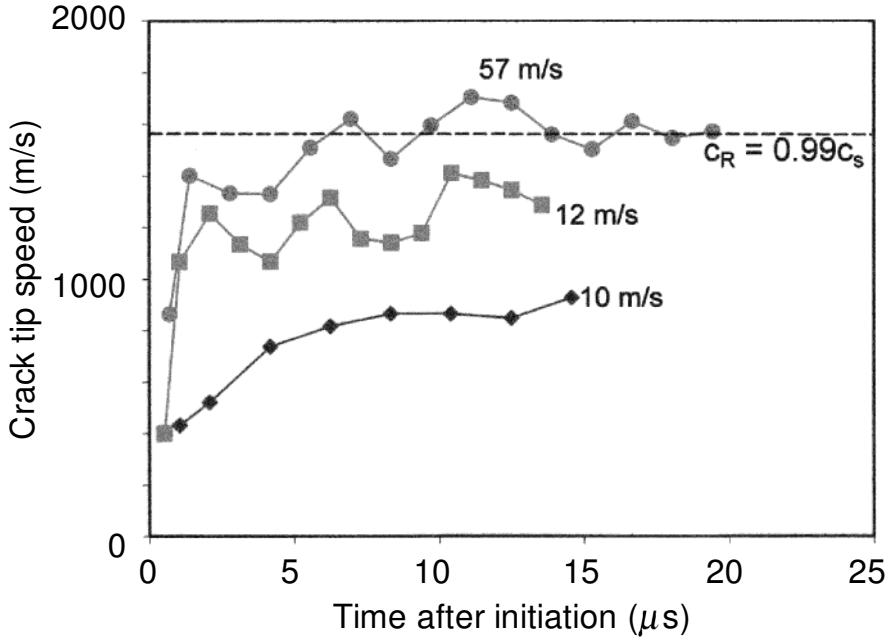

Figure 30. Mode-I crack tip speed histories. As the impact speed increases the crack tip speed reaches but never exceeds c_R.

5.2. *Shear rupture along the fibres*

In the asymmetrically loaded experiments, the impact wave compression propagates from one end of the plate to the other (side of the notch), and just below the notch, is being reflected as a tensile wave. This reflection loads the notch in a predominately shear mode, inducing dynamic shear rupture. Figure 31 is a sequence of four CGS interferograms and illustrates the crack initiation and shear crack growth process. Figure 31(a) shows the mode-II fringe pattern that has developed around the notch as it is loaded by the arriving wave. As the crack initiates and grows along the straight-line fibres, the nature of this fringe pattern changes significantly. The fringes are pulled back and are elongated. The rounded fringe loops change to a triangular wedge, which is bounded by lines of highly concentrated fringes emerging from the rupture tip at a well-defined angle. Eventually these lines broaden into more parallel line structures (see figures 31(c) and (d)), which intercept the rupture faces a few millimetres behind the propagating rupture front.

The observed structures are indeed reminiscent of the isochromatic images presented earlier in figure 7 and 8 in relation to intersonic rupture in bonded isotropic Homalite/Homalite plates. A major difference, however, is that the images presented in figure 31 are obtained by reflection of light from the specularly reflective surface of the composite plate. Also, the absolute magnitude of the maximum observed crack tip speed is unprecedented and approached $7500\,\mathrm{m\,s^{-1}}$, which is approximately 3.4 times greater than those observed during intersonic shear rupture of the Homalite/Homalite system. Finally, one should note that the clear formation of double shock waves, visible in the photographs, provides clear evidence that

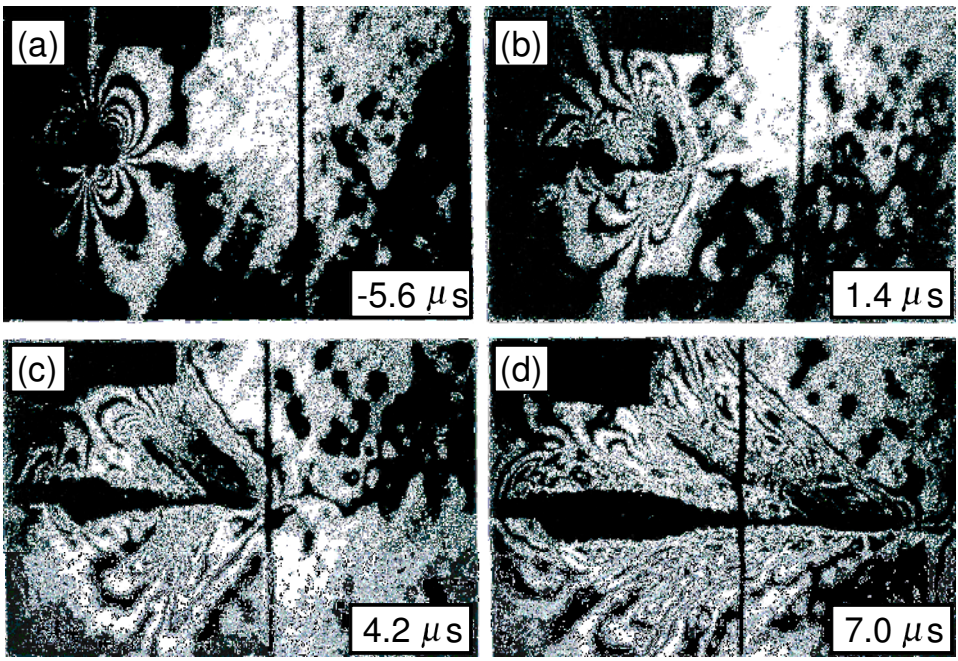

Figure 31. A shear rupture propagating intersonically along the fibres of a unidirectional composite plate. The high-speed images are obtained in a reflection arrangement through CGS interferometry. Fringe patterns correspond to contours of the surface slope component along the horizontal.

dynamic large-scale frictional contact takes place on a scale much higher than in the Homalite/Homalite system.

Figure 32 collectively displays the speed histories of three different shear rupture (mode-II) experiments. For comparison purposes, the speed history of the fastest recorded mode-I crack in the same material system is also shown. The general trends for the shear dominated ruptures is to initiate within the intersonic regime, to accelerate up to 7500 m s^{-1}, which is the dilatational wave speed along the fibres, and to then oscillate between this speed and another speed, v_C. The speed v_C is well defined in the experiments and is equal to 6500 m s^{-1}. This phenomenon is highly repeatable and suggests that v_C may have some special significance worth of theoretical scrutiny. How exaggerated and unprecedented this maximum mode-II crack tip speed really is can only be appreciated by comparison to the mode-I case. As shown at the bottom of figure 32, the classical mode-I opening cracks never exceed $v = c_R^{II} = 1548$ m s^{-1}, a speed which is roughly five times smaller than their shear rupture counterparts.

Let us now turn our attention to the speed v_C. Its significance became apparent through the theoretical work of Huang *et al.* [95] and Gao *et al.* [90]. They investigated the asymptotic nature of intersonic shear ruptures propagating along a predetermined straight path in orthotropic solids. As is evident from these investigations, the energy flux into the rupture tip vanishes at all speeds within the intersonic regime with the exception of $v = v_C$. At this speed, the energy flux is finite

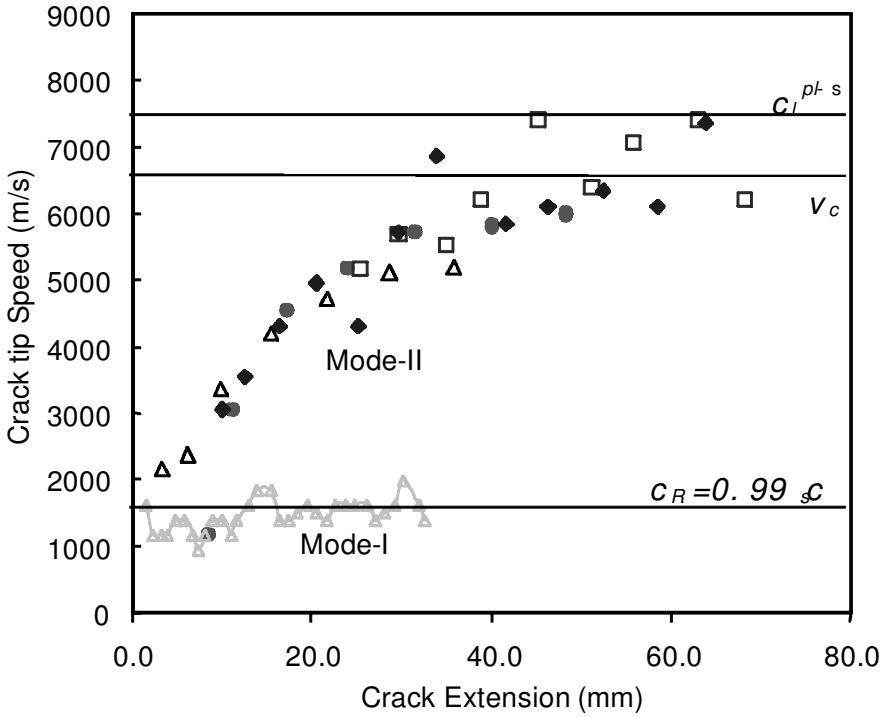

Figure 32. (◆, □, ●), Mode-II rupture speeds as a function of crack tip position. The speed history of a mode-I crack in the same composite material is also shown for comparison. Maximum speeds as high as 7.5 km s^{-1} were recorded.

and positive, and the near tip deformation field resumes its original subsonic, square root singular, and radiation free nature. In particular, for a transversely isotropic solid, this critical speed is given by

$$v_C = \left(\frac{c_{11}c_{22} - c_{12}^2}{c_{66}(c_{12} + c_{22})} \right)^{1/2} c_S = \left(\frac{E_{11}}{\mu_{12}(1 + \nu_{12})} \right)^{1/2} c_S, \tag{5.1}$$

where c_{ij}, E_{11}, and μ_{12} are the anisotropic elastic moduli, ν_{12} is an anisotropic Poisson's ratio, and c_S is the shear wave speed. Exact definitions for E_{11}, μ_{12}, ν_{12} and c_S can be found in [94] together with their measured values for the fibre reinforced composite of the experiments. By using these values the speed v_C is calculated and it is found to be equal to 6600 m s^{-1}. Moreover, this value is very close to the level identified experimentally as the lower bound of the oscillations discussed in relation to figure 32.

At this point it is important to note that for the case of isotropic materials the factor multiplying c_S in equation (5.1) becomes equal to $\sqrt{2}$ and the critical speed reduces to $v_C = \sqrt{2}c_S$. This is indeed the familiar speed that has consistently appeared in relation to the intersonic shear rupture of isotropic solids discussed throughout this article. Its physical importance and meaning is derived by the same energetic and stability arguments that have been discussed throughout section 2. In fact, as has also been shown by Gao *et al*. [90], the existence of radiation free

transonic states for both dislocations and cracks can be demonstrated in relation to a much wider class of anisotropic solids. Recently, Barnett and Zimmerman [96], making use of the Stroh formulation, have completed an exhaustive analysis of intersonic motion of point defects in general anisotropic materials and have presented a most general discussion of radiation free conditions.

The importance of using cohesive zone models to study intersonic rupture in orthotropic solids was once again emphasized by Broberg [97]. His analytical work shows that introducing cohesive structure into the crack tip removes the pathology of predicting zero energy flux into the intersonic crack tip. In fact, the cohesive zone model ensures the existence of a finite and positive energy flux throughout the intersonic regime. In a manner analogous to the isotropic cohesive models of section 2, the energy flux has a distinct maximum value at a speed close, but not equal, to the critical speed v_C. Finally, cohesive theories have recently been used in conjunction with elaborate numerical schemes to study intersonic rupture. Noteworthy are Hwang and Geubelle's [98] contributions, which employed a spectral scheme to model mixed-mode failure of orthotropic materials. This work outlines the role of far-field mixity in determining favourable crack tip speed regimes. For the case of shear dominated crack growth, their speed history predictions are in excellent agreement with the results of figure 32.

5.3. *Frictional contact and hot spot formation*

In connection with the CGS interferograms of figure 31, it was mentioned that a double shock wave structure appears near the tip of the intersonically growing rupture. Figure 33 displays a magnified view of the near tip area for a crack growing at approximately $5800\,\mathrm{m\,s^{-1}}$. One should observe the existence of a band that intersects the rupture plane in a 5 mm wide area trailing the crack tip. The band's boundaries are shear shock waves. The existence of this particular band together with the appearance of a 'noisy' structure along the rupture is suggestive of non-uniform contact and frictional sliding in these locations. To conclusively verify the existence of frictional contact and heat dissipation during intersonic crack growth, a high-speed infrared camera was used to record the transient temperature field at a

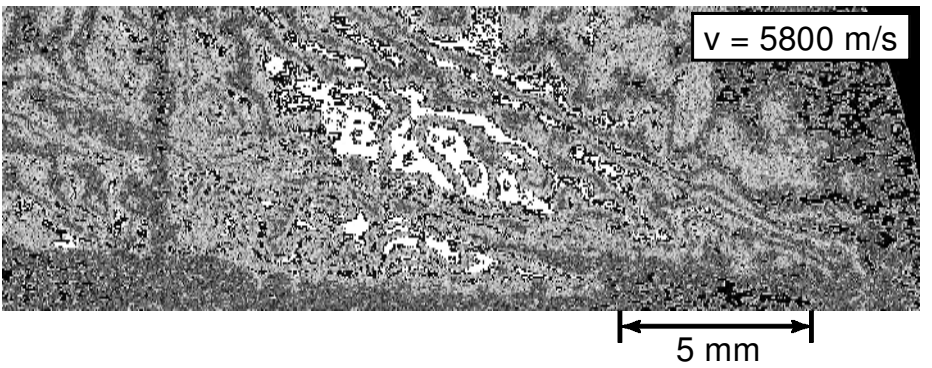

Figure 33. A close-up view of the near tip vicinity of an intersonically moving crack in a unidirectional composite. The double shock wave structure is an indication of multiple contacts.

small fixed location near the rupture faces. This camera is capable of acquiring full-field images of temperature at a rate of 10^6 frames per second with a system rise time of 750 ns [99]. It was focused in a small fixed area 100 μm × 100 μm, situated a few millimetres ahead of the notch field along the predetermined shear rupture path. This area is indicated in figure 34(a).

Figures 34(b)–(f) show contours of constant temperature elevation corresponding to different times after impact. In figure 34(b) the shear crack tip can be seen to enter the measurement field of view from the left. In figure 34(c) the crack has already left this field of view and the camera records increasing temperature elevations at the shear crack faces. The only explanation for the observed continuous increase in temperature is the meeting of the rupture faces resulting in frictional sliding and contact.

Behind the rupture tip, one can now observe the formation of areas of localized 'flash-heating' that provide direct evidence of the non-uniformity of the dynamic sliding process. These localized 'hot spots' are very transient and are seen to suddenly flare up or to jump around as the process goes on. Initially, the temperature increase is most likely due to non-uniform asperity sliding at the crack faces, which demonstrates itself by means of 'hot spot' creation. At later times the temperature distribution widens and becomes a substantially more uniform band of high temperature as shear deformation spreads to adjacent layers of fibres.

The existence of non-uniform, highly transient sliding processes trailing the tip of an intersonic shear rupture have recently been verified numerically by Yu *et al.* [100]. In this calculation the unidirectional composite plates used by Coker and Rosakis [94] were modelled in three dimensions by means of finite elements. Material failure was allowed to proceed by satisfying a local decohesion law that was embedded in the boundaries between elements. The possibility of frictional contact was also taken

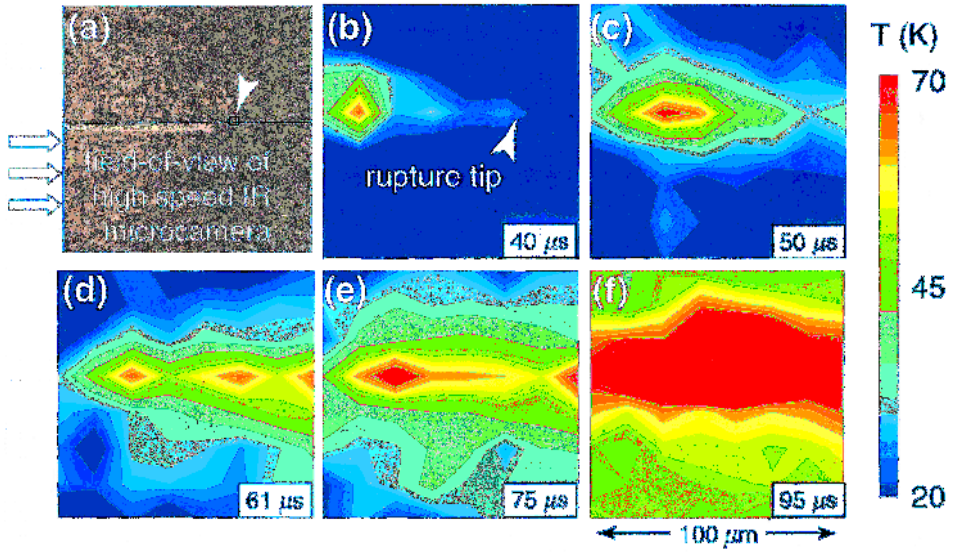

Figure 34. High-speed infrared images of hot spot formation due to non-uniform contact and sliding behind an intersonically moving shear crack.

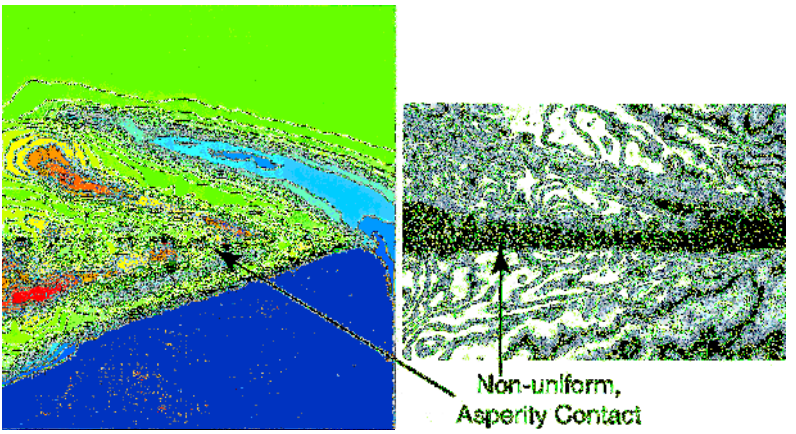

Figure 35. Numerical prediction and experimental fringes. Both parts of the figure illustrate the complex shock wave structure near the rupture tip. Asperity contact is suggested.

into account while local temperature increases resulting from frictional dissipation were calculated at the appropriate locations.

Figure 35 provides a qualitative comparison of the numerical predictions with the experimental CGS fringe patterns. The calculation displays a clear shock wave and band structures very similar to the experiments, and it clearly predicts the existence of non-uniform sliding and the generation of frictional hot spots behind the growing rupture tip [100].

6. Rupture of inhomogeneous systems: highly dissimilar bimaterials

The review so far has exclusively concentrated on the discussion of intersonic shear rupture of constitutively homogeneous systems (isotropic or orthotropic) containing preferable shear crack growth paths or weak fault planes. Regarding their failure strength, such systems are still inhomogeneous and can be thought of as a small subset of the much wider class of truly inhomogeneous bimaterials, a class that involves constituents of distinctly different mechanical behaviour.

The dynamic failure of inhomogeneous bimaterials is a much more complex phenomenon than that involved in the special cases discussed so far. The reasons for such complexity include the existence of, first of all, two distinct sets of waves, secondly, the presence of three distinct levels of fracture toughness (one for each constituent and one for the bond), and lastly, the extensive coupling between the shear and the normal traction distributions along the bond. The normal shear coupling that is responsible for the lack of clear fracture mode separation makes analysis of the interfacial crack growth problem considerably more difficult than in the cases discussed so far. Indeed, an in-plane crack on a dissimilar material interface generally experiences a mixed-mode deformation in the crack tip vicinity, even when the applied far-field loading possesses the symmetries of a pure mode. Under symmetric far-field loading, a bimaterial interface crack often opts, if possible, to kink off the interface and into one of the materials on either side and thus establishes, near the tip, pure mode-I conditions. However, if one of the phases has a higher fracture toughness than the other, an interface crack, under certain far-field mode

mixities, might prefer to propagate along the interface itself even though this interface may not be significantly weaker than both phases. Hence, the possibility of mixed-mode and in particular shear dominated crack propagation is much more pronounced along a dissimilar material interface than in homogeneous solids containing a weak interface. A common way to guarantee that a dynamic interfacial crack remains and grows along an interface, is to provide dynamic shear loading of the type that encourages the crack tip to kink into the bimaterial constituent of higher fracture toughness. If this toughness is high enough, the crack is forced to follow the interface and it does so at very high speeds, which often become intersonic with respect to the weaker material constituent. An example of such a behaviour is illustrated in figure 36.

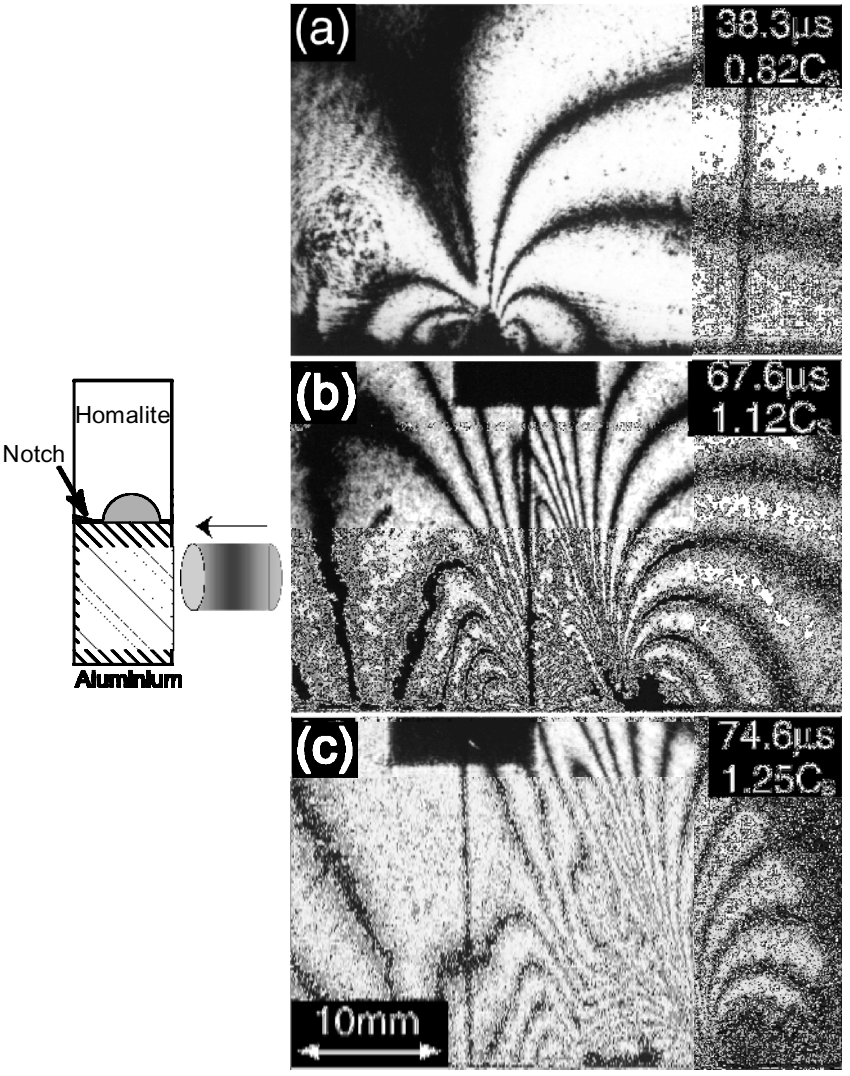

Figure 36. An interfacial crack rupturing the bond between Homalite and aluminium. (a) Subsonic growth phase. (b) and (c) Intersonic crack growth phase.

The experiment described in figure 36 involves a bimaterial specimen constructed by bonding a Homalite-100 plate on to an aluminium plate. The fracture toughness of the polymeric bond is almost as high as that of Homalite, but significantly smaller than that of aluminium. At the same time, the wave speeds of aluminium are approximately two and a half times higher than those of Homalite. The plate is impacted by a projectile on the steel edge, located opposite an initial notch, which is placed along the bimaterial bond. The compressive stress waves travelling fast in the steel arrive in the specimen edge just below the notch tip and are being reflected as tensile waves. After reflection, the waves reach the tip of the notch and by loading it they initiate a crack which in turn grows into the interface. The nature of the loading is such that if the metal had substantially lower fracture toughness, the crack would kink into the bottom half of the specimen and thus would become locally mode-I. Its inability to do so confines it to grow dynamically into the interface as a predominately shear rupture [101]. Figure 36 illustrates the crack growth process. At a time of approximately 38 μs after impact, the crack is seen propagating subsonically at a speed that is close to the 80% of the shear wave speed of Homalite. The isochromatic fringe pattern features smooth fringes that are centred at the moving crack tip. Their nature is characteristic of subsonic shear dominated bimaterial rupture. Figures 36(b) and (c), however, present us with a very different story. The crack tip is shown to have accelerated well beyond c_S (Homalite) and the fringe patterns exhibit a dramatic change in structure. This new structure features intense, Mach type concentrations of fringes at multiple locations at and behind the moving crack tip. They are reminiscent in nature of the isochromatic patterns shown in figures 7 and 8 in relation to bonded Homalite/Homalite systems, and in figure 31 in relation to anisotropic composites. However, their structure is substantially more complicated, a structure that suggests the existence of a highly inhomogeneous crack face contact process that develops as a consequence of intense normal–shear coupling.

If one follows the chronological development of experimental research on dynamic rupture along interfaces, one would realize that the first observations of intersonically propagating cracks were made in connection with bimaterials. Indeed, those observations led to the discovery of intersonic failure in homogeneous bonded systems of the type described in section 2.2. It was initially presumed that intersonic rupture can be realized only in the presence of high bimaterial mismatch. Stress waves travelling faster in one of the constituent solids could, indeed, provide energy to the moving interfacial crack tip at fast enough rates to force it to become intersonic with respect to the more compliant (low wave speed) solid. Although this might seem a plausible interpretation, there is another factor that is of central importance in the attainment of intersonic speeds. That is the factor of the existence of a favourable or preferred crack path that traps a growing crack forcing it to assume a predominantly shear nature. As we have seen earlier, assuming such a shear nature is sufficient to attain intersonic conditions even in the absence of a wave speed mismatch.

Subsonic dynamic crack propagation along interface separating two dissimilar, homogeneous isotropic solids has been studied theoretically since the early 1970s. After a few theoretical investigations [102–105] interest in this area subsided owing to the complete absence of experimental observations. In the first systematic experimental study of dynamic crack propagation along a bimaterial interface, Tippur and Rosakis [106] observed interfacial cracks along poly(methyl methacrylate) (PMMA)–Al interfaces propagating at speeds close to 80% of the Rayleigh wave

speed of PMMA (c_R^{PMMA}) and featuring unprecedented accelerations as high as $10^8 g$. In contrast, cracks in homogeneous (monolithic) PMMA rarely exceed 35% of c_R^{PMMA} before branching into multiple cracks. The observations that a PMMA–Al interface can sustain much higher crack speeds spurred a renewal of interest in dynamic crack propagation along bimaterial interfaces. Motivated by the unusual results of the experiments, Yang *et al.* [107] obtained explicit expressions for the asymptotic stress field around a crack running subsonically (subsonically with respect to the constituent with lower wave speeds) along a bimaterial interface. Equipped with this analytical solution of Yang *et al.*, Lambros and Rosakis [108, 109] and Kavaturu and Shukla [110] analysed CGS and photoelastic experiments of subsonic interfacial crack growth and proposed propagation criteria for subsonic crack growth along bimaterial interfaces. Lambros and Rosakis [108] proposed that the crack face profile remains unchanged during subsonic interfacial crack propagation; whereas Kavaturu and Shukla [110] proposed that the crack face displacement components increase with crack speed according to a power law. An interesting feature exhibited by both these fracture criteria is that the dynamic fracture toughness decreases as the lower of the two Rayleigh wave speeds is approached. This behaviour is opposite to that observed in strictly homogeneous polymers and metals (in the absence of favourable crack paths) where, as the crack accelerates close to the onset of the branching instability, the dynamic fracture toughness is usually observed to increase sharply with crack speed.

The first experimental observations of intersonic crack growth in bimaterials were reported by Rosakis and co-workers [111–114] using CGS interferometry and were later confirmed by Singh and Shukla [115] using dynamic photoelasticity. It was demonstrated that for sufficiently high rates of loading, resulting in highly shear dominated conditions at the crack tip, interfacial crack tip speeds can exceed the shear wave speed of the more compliant material. The crack tip speeds could increase even more, provided that the impact speed of the loading projectile exceeded a certain level. Figure 37 shows the normalized variation of crack tip speed with time for five experiments corresponding to different projectile speeds. The bimaterial system is one of Homalite-100 bonded on steel. The time $t = 0$ corresponds to projectile impact at the specimen edge. The impact speeds are very low and range from $3\,\mathrm{m\,s^{-1}}$ to $28\,\mathrm{m\,s^{-1}}$. The wave speeds c_S, c_R, and c_ℓ shown in the figure are the wave speeds of Homalite. The wave speeds of the steel are approximately 2.6 times greater. These results are taken from a recent work by Samudrala and Rosakis [101] and they correspond to the experimental configuration shown in figure 36. As is evident from figure 37, the interfacial crack below a critical impact speed remains subsonic and attains speeds that are close to c_R. As the impact speed is increased, the cracks accelerate at levels between c_S and $\sqrt{2}c_S$ and remain there for a while until wave reflections from the boundary accelerate to levels close to c_ℓ.

Motivated by such observations of intersonic crack growth, Huang, Liu and Rosakis [116, 117] and Yu and Yang [118, 119] derived the asymptotic near tip fields for an intersonic crack on a bimaterial interface and showed that some of the features observed in the experimental fringe patterns are predicted by the analytical solution. More recently, Yu and Suo [120] obtained much more general solutions for the near tip fields around an interface crack propagating at a constant speed in orthotropic or transversely isotropic bimaterials.

As predicted analytically [116, 117], the stress field distribution around an intersonic crack on a bimaterial interface differs dramatically from that around a

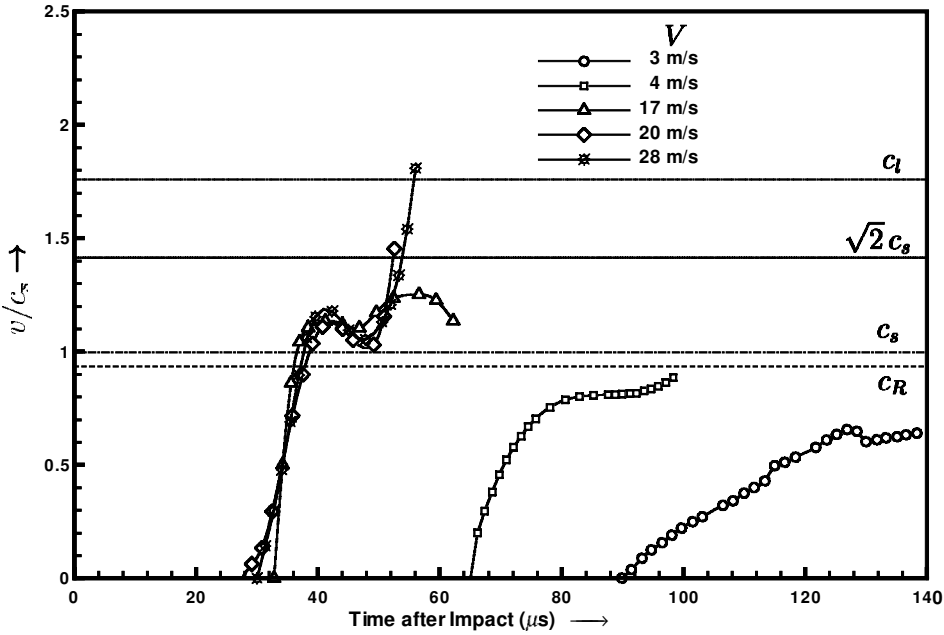

Figure 37. The effect of projectile impact speed on interfacial crack growth history. If the impact speed is high enough the crack can even become 'supersonic'.

subsonic interfacial crack. Since the crack speed has exceeded c_S, a shear Mach wave is expected to radiate from the intersonically moving tip in a similar way to an intersonic crack in a bonded homogeneous system. The Mach wave carries with it a strong shear stress discontinuity in the stress field. Such a Mach wave was first predicted by Liu *et al.* [116] on the basis of an elastic/rigid analysis of intersonic bimaterial rupture. This analysis modelled the metal constituent as rigid and the Homalite as an isotropic linear elastic solid. The predicted Mach wave in the Homalite half of a bimaterial was subsequently observed in the isochromatic fringe patterns recorded by Singh and Shukla [115]. In addition to the Mach wave radiating from the tip, they also observed a second Mach line parallel to the first one, which was radiating from a point located at a finite distance behind the growing crack tip. This observation was consistent with an earlier conjecture by Lambros and Rosakis [112] who proposed, on the basis of the shape of CGS interferograms, that an intersonic crack on a bimaterial interface propagates with a finite zone of crack face frictional contact behind it.

The observation of a second Mach line in the isochromatic fringes provided further evidence of finite contact and explained the finite separation distance between the two lobes of the CGS fringe pattern on either side of the intersonically moving crack tip [112]. The size of the contact zone was found to range between 2 mm and 10 mm and figure 36 illustrates its developmental sequence in a series of photographs. The presence of extended frictional contact highlighted the inability of the purely singular elastodynamic analyses to model intersonic rupture in bimaterials. To remedy this shortcoming, Huang *et al.* [121] and Wang *et al.* [122] obtained the near tip fields around intersonically propagating interfacial cracks with a finite zone

of crack face frictional contact trailing behind the crack tip. Their results compared qualitatively well with some of the observed behaviour and provided an accurate way to experimentally estimate the energy dissipated behind the moving rupture as a result of frictional contact [123].

At this point, it should be noted that the curious speed $\sqrt{2}c_S$ does not appear in bimaterial failure analysis as prominently as it does in the analysis of rupture of bonded identical solids. Indeed, the order of singularity for a crack propagating intersonically in a bimaterial interface is always smaller than 0.5 and radiation free conditions are not achieved at any speed. However, in models that involve elastic/rigid bimaterial idealizations, the speed $\sqrt{2}c_S$ reappears as a special case, acquires new physical meaning, and thus regains some of its significance. In particular, the early asymptotic elastic/rigid analysis by Liu *et al.* [116], in which the crack faces were assumed to be traction free, revealed an interesting contradiction. According to this model and depending on the sign of shear, the direction of rupture, and the crack tip speed, it was predicted that the crack faces develop interpenetration. For example, if the sign of shear is such that the compliant material moves in the direction of rupture, then crack face interpenetration is predicted for speeds in the range $\sqrt{2}c_S < v < c_\ell$. The crack faces are predicted to open if $c_S < v < \sqrt{2}c_S$. The situation is reversed when the sign of shear is also reversed. This prediction hints at the potential development of crack face contact at various speed intervals and is consistent with the experimental evidence presented by Lambros and Rosakis [112]. For cracks propagating at exactly $v = \sqrt{2}c_S$, however, the same analysis predicts the complete disappearance of the bothersome interpenetration irrespective of the sign of shear and the relative direction of rupture. In addition, the subsequent analytical work by Huang *et al.* [121] also exhibited special behaviour at $v = \sqrt{2}c_S$. This was the first analysis to properly account for the existence of a finite frictional contact zone at the crack faces. For crack growth at $v = \sqrt{2}c_S$, this analysis predicts the disappearance of all normal stresses at the contact zone and the solution becomes independent of the value of the friction coefficient or more generally independent of the nature of the friction law. Finally, the predicted frictional dissipation at the crack faces drops identically to zero, perhaps suggesting the crack's propensity to choose this growth speed as a means of minimizing the energy needed during intersonic bimaterial rupture. In conclusion, for large wave mismatch bimaterials, $\sqrt{2}c_S$ is the speed that delineates speed regimes of intersonic crack growth featuring crack face pressure release (or enhancement) arising from the bimaterial nature of the bond. This provides a new physical interpretation for this speed. This interpretation is different from the classical 'radiation-free' interpretation that the same speed has for 'homogeneous' interfaces.

Recently, numerical simulations of the phenomenon revealed an even more non-uniform and transient structure of crack face sliding which involved multiple sites of localized contact and stress field discontinuity behind the growing crack tip [124–126]. Experimental evidence of such behaviour is shown in figure 38. The figure demonstrates a highly unstable crack tip propagating in a Homalite–steel interface. The two photographs in figures 38(a) and (b) correspond to two different recording times and crack speeds and are extracted from the same experiment. The magnified views in the insets of the near tip region reveal at least three clearly visible Mach lines. As illustrated in 36(c), these lines, which originate from the crack tip and from the ends of the contact zone, form a 'wave packet' of sliding and contact. The transient nature of the process is revealed from the observation that these Mach lines

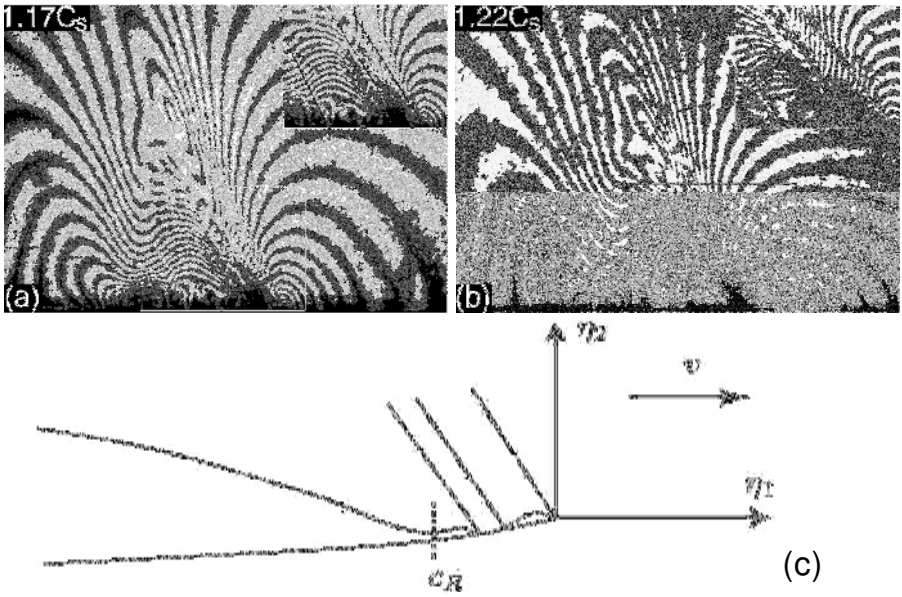

Figure 38. Multiple shock waves reveal the complex 'wave packet' nature of sliding and contact travelling behind the interfacial crack tip. Non-parallel shock lines imply a highly transient and unstable contact process.

are not parallel to each other. Specifically, the Mach lines delineate separate transient regions of contact and of opening whose lengths vary continuously with time.

The highly transient mechanisms governing the formation of crack face contact as the interfacial crack accelerates from subsonic to intersonic speeds are still rather obscure. Indeed, the effects of loading type (e.g. the sign of imposed shear), of the level of bimaterial mismatch and of confinement have never been investigated. Of particular interest to geophysicists is the case of rupture along bimaterial interfaces featuring small difference in shear wave speed (10–30%) [19, 72], a subject that is currently under investigation by the author and his co-workers. Another issue, which is perhaps related to recently developed geophysical theories of rupture, is the unambiguous observation of the 'wave packet' nature of sliding contact in bimaterials. This phenomenon is clearly reminiscent of the development of self-healing (Weertman [25, 127] or Heaton [26]) pulses along faults. The development of the elaborate models of describing such pulses has recently been critically discussed by Rice [19]. Finally, it should be noted that the normal to shear stress coupling that is introduced by the existence of bimaterial mismatch, or the complex nature of dynamic friction, are not the only two factors promoting pulse-like behaviour. Geometric effects such as fault heterogeneity (Beroza and Mikumo [128]) and the three-dimensional nature of fault rupture (Fukuyama and Madariaga [129]) may play a strong effect in the development of this mode of rupture and in the selection of rupture speeds (also see Rice [19]).

7. Concluding remarks

Extensive evidence of intersonic rupture processes which occur in a variety of material systems containing preferable rupture paths or faults have been presented in

this article. Laboratory studies, field observations, and theoretical and numerical models all strongly suggest that there are many underlying common elements in the physics governing shear decohesion. In particular it is clear that, irrespective of observational length scales and material systems, all intersonic shear ruptures involve common properties such as:

(a) single or multiple shock wave formation,
(b) large-scale, non-uniform, frictional contact and sliding,
(c) similar mechanisms of nucleation or of subsonic to intersonic transition,
(d) similar intervals of preferable rupture speed stability.

The above commonalities are characteristic properties of dynamic shear rupture and are only relevant to the study of failure in solids that contain preferable crack growth paths. In strictly homogeneous (monolithic) solids, however, shear crack growth is unattainable. In addition, tensile crack growth is purely subRayleigh.

Table 1 summarizes the maximum attainable crack tip speeds and illustrates the stable crack tip regimes in different material classes. Crack growth speed characteristics of both mode-I (tensile) cracks and mode-II (shear) cracks are compared in the table, as is crack growth behaviour between strictly homogeneous (monolithic) materials and constitutively homogeneous materials that have preferred crack paths or faults. Also compared is the crack speed behaviour of cracks in orthotropic and in bonded isotropic solids.

The case of inhomogeneous systems involving dissimilar bonded constituents, however, is not represented in the above table. For such systems, research has not yet provided us with a clear-cut picture of maximum attainable crack tip speeds and preferable speed stability regimes. Given the complexities involved in such systems, complexities due to the shear–normal traction coupling at the interface, it would not be surprising to conceive of the processes involved in the rupture of such systems as requiring a much more sophisticated level of analysis.

Table 1. Maximum attainable crack tip speed and stable crack tip regimes in different material classes. Only brittle solids are included.

	Homogeneous materials (homogeneity in elastic behaviour and homogeneity in fracture toughness)	Materials with preferred crack paths (homogeneity in elastic behaviour and inhomogeneity in fracture toughness (fault))	
Mode-I	Monolithic rock, ceramics, glass, brittle polymers	Orthotropic fibre composites	Bonded isotropic solids
Theory limit	c_R	c_R	c_R
Observed limit	$v_b \approx 0.35$–$0.5c_R$ (branching)	$\approx c_R$	$\approx c_R$
	stable steady state $0 < v < v_b$	Stable only at c_R	Stable only at c_R
Mode-II	Inaccessible (asymmetric loading results in crack kinking along a locally mode-I direction)	Maximum observed $c_L^{\parallel}$ Stable steady state $v > v_C$ $v_C = \left[\frac{E_1}{\mu_{12}(1+\nu_{12})}\right]^{1/2} c_S$	Maximum observed c_L Stable steady state $v > v_C$ $v_C = \sqrt{2}c_S$

The dynamic rupture phenomena discussed in this article have significant application in both engineering and geophysics. In the case of engineering, there is an increasing practical demand for specialized, lightweight, and high-strength structures. Such inhomogeneous structures include structural composites, bonded and sandwich structures, as well as layered or graded microelectronic components. Many such systems are composed of brittle constituents that are bonded together with weak interfaces, which are potential catastrophic failure sites and are designed for applications involving either anticipated or accidental impact loading. In the case of geophysics, on the other hand, there is an increasing scientific interest in the detailed understanding and analysis of the basic physical processes involved during the rupture of shallow crustal faults.

Acknowledgements

The author would like to thank the US Office of Naval Research (Grant #N00014-95-1-0453, Y.D.S. Rajapakse, Project Manager) for their consistent support of past and ongoing research at Caltech on dynamic failure mechanics. He also would like to acknowledge a series of very important interactions (and debates) with mentors and colleagues including L. B. Freund, J. Rice, A. Needleman, J. Achenbach, B. Broberg, J. R. Willis, W. G. Knauss, Y. Huang, H. Gao, Y. Ben-Zion, M. Bouchon, H. Kanamori, and T. Heaton, on the subject of this review. In addition, the author is very grateful to Shamita Das, Farid Abraham, and Huajian Gao for providing their own work that has enhanced the didactic quality of this review. It should also be pointed out that without the keen editorial eye of Dr I. Dimitracopoulou and the determination and resourcefulness of Ms D. Thobe and Dr D. M. Owen this article would never have been completed. Finally, the author is grateful to the two reviewers of this work who have provided highly constructive suggestions and detailed comments that have improved the flow and clarity of presentation.

References

[1] Achenbach, J. D., 1973, *Wave Propagation in Solids* (Amsterdam: North Holland).
[2] Freund, L. B., 1990, *Dynamic Fracture Mechanics* (Cambridge: Cambridge University Press).
[3] Ravi-Chandar, K., and Knauss, W. G., 1984, *Int. J. Fract.*, **26,** 65.
[4] Ravi-Chandar, K., and Knauss, W. G., 1984, *Int. J. Fract.*, **26,** 141.
[5] Ramulu, M., and Kobayashi, A. S., 1985, *Int. J. Fract.*, **27,** 187.
[6] Johnson, E., 1992, *Int. J. Fract.*, **55,** 47.
[7] Gao, H. J., 1993, *J. Mech. Phys. Solids*, **41,** 457.
[8] Fineberg, J., and Marder, M., 1999, *Phys. Rep.*, **313,** 2.
[9] Ravi-Chandar, K., and Knauss, W. G., 1999, *Comput. Sci. Engng.*, **5,** 24.
[10] Owen, D. M., Rosakis, A. J., and Johnson, W. L., 1998, Dynamic failure mechanisms in beryllium-bearing bulk metallic glasses, in *Proceedings of the Materials Research Society Symposium on Bulk Metallic Glasses*, Vol. 554 (Warrendale, PA: Materials Research Society), pp. 419–430.
[11] Rosakis, A. J., 1993, *Experimental Techniques in Fracture* (New York: VCH), chap. 10.
[12] Broberg, K. B., 1999, *Cracks and Fracture* (London: Academic).
[13] Broberg, K. B., 1989, *Int. J. Fract.*, **39,** 1.
[14] Broberg, K. B., 1996, *Mater. Sci.*, **32,** 80.
[15] Washabaugh, P. D., and Knauss, W. G., 1994, *Int. J. Fract.*, **65,** 97.
[16] Cotterell, B., and Rice, J. R., 1980, *Int. J. Fract.*, **16,** 155.

[17] Nemat-Nasser, S., and Horii, H., 1982, *J. geophys. Res.*, **87,** 6805.
[18] Hutchinson, J. W., and Suo, Z., 1992, *J. geophys. Res.*, **77,** 3796.
[19] Rice, J. R., 2001, New perspectives on crack and fault dynamics in *Mechanics for a New Millennium: Proceedings of the 20th International Congress of Theoretical and Applied Mechanics*, edited by H. Aref and J. W. Phillips (Dordrecht: Kluwer), pp. 1–23.
[20] Das, S., 1985, *Int. J. Fract.*, **27,** 263.
[21] Dmowska, R., and Rice, J. R., 1986, *Continuum Theories in Solid Earth Physics* (Amsterdam: Elsevier), pp.1881–1902.
[22] Scholz, C. H., 1990, *The Mechanics of Earthquakes and Faulting* (Cambridge: Cambridge University Press).
[23] Kanamori, H., and Brodsky, E., 2000, *Phys. Today*, **54,** 34.
[24] Kanamori, H., 1994, *Annu. Rev. earth planet. Sci.*, **22,** 207.
[25] Weertman, J., 1980, *J. geophys. Res.*, **85,** 1455.
[26] Heaton, T. H., 1990, *Phys. earth planet. Sci.*, **64,** 1.
[27] Andrews, D. J., and Ben-Zion, Y., 1997, *J. geophys. Res.*, **102,** 553.
[28] Adams, G. C., 1995, *J. appl. Mech.*, **62,** 867.
[29] Adams, G. C., 1998, *J. appl. Mech.*, **65,** 470.
[30] Ben-Zion, Y., and Andrews, D. J., 1998, *Bull. seismol. Soc. Am.*, **88,** 1085.
[31] Ranjith, K., and Rice, J. R., 2001, *J. Mech. Phys. Solids*, **49,** 341.
[32] Nielsen, S. B., and Carlson, J. M., 2002, *Bull. seismol. Soc. Am.*, in press.
[33] Cochard, A., and Madariaga, R., 1996, *J. geophys. Res.*, **101,** 25321.
[34] Beeler, N. M., and Tullis, T. E., 1996, *Bull. seismol. Soc. Am.*, **86,** 1130.
[35] Zheng, G., and Rice, J. R., 1998, *Bull. seismol. Soc. Am.*, **88,** 1466.
[36] Perrin, G., Rice, J. R., and Zheng, G., *J. Mech. Phys. Solids*, **43,** 1461.
[37] Rice, J. R., Lapusta, N., and Ranjith, K., 2001, *J. Mech. Phys. Solids*, **49,** 1865.
[38] Archuleta, R. J., 1984, *J. geophys. Res.*, **89,** 4559.
[39] Olsen, K. B., Madariaga, R., and Archuleta, R. J., 1997, *Science*, **278,** 834.
[40] Hernandez, B., Cotton, F., and Campillo, M., 1999, *J. geophys. Res.*, **104,** 13 083.
[41] Ellsworth, W. L., and Celebi, M., 1999, Near field displacement time histories of the M7.4 Kocaeli (Izmit) Turkey earthquake of August 17, 1999, in *Proceedings of the American Geophysical Union Fall Meeting*, Vol. 80 (Washington DC: American Geophysical Union), p. F648.
[42] Bouchon, M., Toksoz, N., Karabulut, H., Bouin, M. P., Dietrich, M., Aktar, M., and Edie, M., 2000, *Geophys. Res. Lett.*, **27,** 3013.
[43] Bouchon, M., Bouin, M. P., Karabulut, H., Toksoz, N., Dietrich, M., and Rosakis, A. J., 2001, *Geophys. Res. Lett.*, **28,** 2723.
[44] Freund, L. B., 1979, *J. geophys. Res.*, **84,** 2199.
[45] Broberg, K. B., 1995, *Ach. Mech.*, **47,** 859.
[46] Broberg, K. B., 1996, *Mater. Sci.*, **32,** 80.
[47] Broberg, K. B., 1999, *Fatigue Fract. Engng. Mat.*, **22,** 17.
[48] Burridge, R., 1973, *Geophys. J. Royal astronom.*, **35,** 439.
[49] Andrews, D. J., 1976, *J. geophys. Res.*, **81,** 5679.
[50] Ida, Y., 1972, *J. geophys. Res.*, **77,** 3796.
[51] Palmer, A. C., and Rice, J. R., 1973, *Proc. Royal Soc. Lond.*, **A332,** 527.
[52] Das, S., and Aki, K., 1977, *Geophys. J. Royal Astro. Soc.*, **50,** 643.
[53] Day, S. M., 1982, *Bull. seismol. Soc. Am.*, **72,** 1881.
[54] Johnson, E., 1990, *Geophys. J. Int.*, **101,** 125.
[55] Burridge, R., Conn, G., and Freund, L. B., 1979, *J. geophys. Res.*, **85,** 2210.
[56] Broberg, K. B., 1994, *Geophys. J. Int.*, **119,** 706.
[57] Rosakis, A. J., Samudrala, O., and Coker, D., 1999, *Science*, **284,** 1337.
[58] Samudrala, O., Huang, Y., and Rosakis, A. J., 2001, *J. geophys. Res.* (in press).
[59] Dugdale, D. S., 1960, *J. Mech. Phys. Solids*, **8,** 100.
[60] Barenblatt, G. I., 1962, *Adv. appl. Mech.*, **7,** 55.
[61] Ruina, A., 1983, *J. geophys. Res.*, **88,** 10359.
[62] Rice, J. R., and Ruina, A., 1983, *J. appl. Mech.*, **50,** 343.
[63] Kilgore, B. D., Blanpied, M. L., and Dietrich, J. H., 1993, *Geophys. Res. Lett.*, **20,** 903.

[64] Prakash, V., and Clifton, R. J., 1993, Pressure-shear plate impact measurement of dynamic friction for high speed machining applications in *Proceedings of the 7th International Congress of Experimental Mechanics* (Bethel, Connecticut: Society for Experimental Mechanics) pp. 568–596.
[65] Prakash, V., and Clifton, R. J., 1993, *Experimental Techniques in the Dynamics of Deformable Solids* (New York: American Society of Mechanical Engineers), pp. 33–44.
[66] Prakash, V., 1998, *J. Tribol.–T ASME*, **120,** 97.
[67] Glennie, E. B., 1971, *J. Mech. Phys. Solids*, **19,** 255.
[68] Freund, L. B., and Lee, Y. J., 1990, *Int. J. Fract.*, **42,** 261.
[69] Rice, J. R., 1980, The mechanics of earthquake rupture, in *Proceedings of the International School of Physics 'Enrico Fermi'*, Vol. 78 (Amsterdam: IOS), pp. 555–649.
[70] Brune, J. N., 1970, *J. geophys. Res.*, **75,** 4997.
[71] Harris, R. A., and Day, S. M., 1993, *J. geophys. Res.*, **98,** 4461.
[72] Ben-Zion, Y., 2001, *J. Mech. Phys. Solids*, **49,** 2209.
[73] Yomogida, K., and Nakata, T., 1994, *Geophys. Res. Lett.*, **17,** 1799.
[74] Spudich, P., and Cranswick, E., 1984, *Bull. seismol. Soc. Am.*, **74,** 2083.
[75] Toksöz, M. N., Reilinger, R. E., Doll, C. G., Barka, A. A., and Yacin, N., 1999, *Seismol. Res. Lett.*, **70,** 669.
[76] Michel, R., and Avouac, J. P., 2002, *J. Geophys. Res* (in press).
[77] Das, S., 1999, Personal communication.
[78] Sibson, R. H., 1975, *Geophys. J. Royal astronom. Soc.*, **43,** 66.
[79] Sagy, A., Reches, Z., and Roman, I., 2001, *J. struct. Geol.*, **23,** 1223.
[80] Poliakov, A., Dmowska, R., and Rice, J. R., 2002, *J. geophys. Res.* (in press).
[81] Needleman, A., 1999, *J. Mech. Phys. Solids*, **66,** 847.
[82] Geubelle, P. H., and Kubair, D. V., 2001, *J. Mech. Phys. Solids*, **49,** 571.
[83] Abraham, F. F., and Gao, H. J., 2000, *Phys. Rev. Lett.*, **84,** 3113.
[84] Abraham, F. F., 2001, *J. Mech. Phys. Solids*, **49,** 2095.
[85] Gao, H. J., Huang, Y., and Abraham, F. F., 2001, *J. Mech. Phys. Solids*, **49,** 2113.
[86] Huang, Y., and Gao, H. J., 2001, *J. appl. Mech.*, **68,** 169.
[87] Antipov, Y. A., and Willis, J. R., 2001, Transient loading of a rapidly-advancing crack in a viscoelastic medium, Mathematics Reprint # 01/06, The University of Bath, UK.
[88] Eshelby, J. D., 1949, *Proc. Royal Soc. Lond.*, **A62,** 307.
[89] Weertman, J., 1969, *Mathematical Theory of Dislocations* (New York: American Society of Mechanical Engineering), p. 178.
[90] Gao, H. J., Huang, Y., Gumbsch, P., and Rosakis, A. J., 1999, *J. Mech. Phys. Solids*, **47,** 1941.
[91] Gumbsch, P., and Gao, H. J., 1999, *Science*, **283,** 965.
[92] Rosakis, P., 2001, *Phys. Rev. Lett.*, **86,** 95.
[93] Rosakis, P., and Tsai, H. Y., *Int. J. Solids Struct.*, **32,** 2711.
[94] Coker, D., and Rosakis, A. J., 2001, *Phil. Mag.* A, **81,** 571.
[95] Huang, Y., Wang, W., Liu, C., and Rosakis, A. J., 1999, *J. Mech. Phys. Solids*, **47,** 1893.
[96] Barnett, D. M., and Zimmerman, J. A., 2000, Non-radiating dislocations in uniform supersonic motion in anisotropic linear elastic solids, in *Proceedings of the 6th International Conference on Integral Methods in Science and Engineering (IMSE 2000)* (Boston, MA: Birkhäuser), Chap. 7, pp. 45–50.
[97] Broberg, K. B., 1999, *Int. J. Fract.*, **99,** 1.
[98] Hwang, C., and Geubelle, P. H., 2000, *CMES–Comp. Model Engng. Sci.*, **4,** 45.
[99] Zehnder, A. T., Guduru, P. R., Rosakis, A. J., and Ravichandran, G., 2000, *Rev. Sci. Instrum.*, **71,** 3762.
[100] Yu, C., Pandolfi, A., Ortiz, M., Coker, D., and Rosakis, A. J., 2001, *Int. J. Solids Struct.* (submitted).
[101] Samudrala, O., and Rosakis, A.J., 2001, *Engng. Fract. Mech.* (in press).
[102] Goldstein, R. V., 1967, *Appl. Math.* Mech., **31,** 496.
[103] Willis, J. R., 1971, *J. Mech. Phys. Solids*, **19,** 353.
[104] Brock, L. M., and Achenbach, J. D., 1973, *Int. J. Solids Struct.*, **9,** 53.

[105] ATKINSON, C., 1977, *Mechanics of Fracture–Elastodynamic Problems*, Vol. 4 (Groningen: Noordhoft), p. 213.
[106] TIPPUR, H. V., and ROSAKIS, A. J., 1991, *Experi. Mech.*, **31,** 243.
[107] YANG, W., SUO, Z., and SHIH, C. F., 1991, *Proc. Royal Soc. Lond.*, **A433,** 679.
[108] LAMBROS, J., and ROSAKIS, A. J., 1995, *Proc. Royal Soc. Lond.*, **A451,** 711.
[109] LAMBROS, J., and ROSAKIS, A. J., 1995, *Int. J. Solids Struct.*, **32,** 2677.
[110] KAVATURU, M., and SHUKLA, A, 1998, *J. appl. Mech.*, **65,** 293.
[111] LIU, C., LAMBROS, J., and ROSAKIS, A. J., 1993, *J. Mech. Phys. Solids*, **41,** 1857.
[112] LAMBROS, J., and ROSAKIS, A. J., 1995, *J. Mech. Phys. Solids*, **43,** 169.
[113] SINGH, R. P., LAMBROS, J., SHUKLA, A., and ROSAKIS, A. J., 1997, *Proc. Royal Soc. Lond.*, **A453,** 2649.
[114] ROSAKIS, A. J., SAMUDRALA, O., SINGH, R. P., and SHUKLA, A., 1998, *J. Mech. Phys. Solids*, **46,** 1789.
[115] SINGH, R. P., and SHUKLA, A., 1996, *J. appl. Mech.*, **63,** 919.
[116] LIU, C., HUANG, Y., and ROSAKIS, A. J., 1995, *J. Mech. Phys. Solids*, **43,** 189.
[117] HUANG, Y., LIU, C., and ROSAKIS, A. J., 1996, *Int. J. Solids Struct.*, **33,** 2625.
[118] YU, H. H., and YANG, W., 1994, *J. Mech. Phys. Solids*, **42,** 1789.
[119] YU, H. H., and YANG, W., 1995, *J. Mech. Phys. Solids*, **43,** 207.
[120] YU, H. H., and SUO, Z., 2000, *Proc. Royal. Soc. Lond.*, **A456,** 223.
[121] HUANG, Y., WANG, W., LIU, C., and ROSAKIS, A. J., 1998, *J. Mech. Phys. Solids*, **46,** 2233.
[122] WANG, W., HUANG, Y., ROSAKIS, A. J., and LIU, C., 1998, *Engng. Fract. Mech.*, **61,** 471.
[123] KAVATURU, M., SHUKLA, A., and ROSAKIS, A. J., 1998, *Experi. Mech.*, **38,** 218.
[124] XU, X. P., and NEEDLEMAN, A., 1996, *Int. J. Fract.*, **74,** 289.
[125] BREITENFELD, M. S., and GEUBELLE, P. H., 1998, *Int. J. Fract.*, **93,** 13.
[126] NEEDLEMAN, A., and ROSAKIS, A. J., 1999, *J. Mech. Phys. Solids*, **47,** 2411.
[127] WEERTMAN, J., and WEERTMAN, J. R., 1980, *Dislocations in Solids*, Vol. 3, (Amsterdam: North-Holland), chap. 8.
[128] BEROZA, G. C., and MIKUMO, T., 1996, *J. geophys. Res.*, **101,** 22.
[129] FUKUYAMA, E., and MADARIAGA, R., 2000, *Pure appl. Geophys.*, **157,** 1957.